Use Authorization

In presenting this thesis in partial fulfillment of the requirements for an advanced degree at Idaho State University, I agree that the library shall make it freely available for inspection. I further state that permission for extensive copying of my thesis for scholarly purposes may be granted by the Dean of Graduate School, the Dean of my academic division, or the University Librarian. It is understood that any copying or publication of this thesis for financial gain shall not be allowed without my written permission.

Signature ___________________________

Date___________________________

Smart Grocery Packaging System with Novel Rotary Grasping Mechanism and Multi-Interface Shelf

by

Safal Lama

A thesis

submitted in partial fulfillment

of the requirements for the degree of

Master of Science in the Department of Mechanical Engineering

Idaho State University

Summer 2023

Committee Approval

To the Graduate Faculty:

The members of the committee appointed to examine the thesis of Safal Lama find it satisfactory and recommend that it be accepted.

Dr. Taher Deemyad

Major Advisor

Dr. Anish Sebastian

Committee Member

Dr. Arya Ebrahimpour

Graduate Faculty Representative

Acknowledgments

I want to express my gratitude to all those who have played a part in contributing to my thesis project, whether directly or indirectly. I especially want to thank my advisor, Dr. Taher Deemyad, an assistant professor in the Mechanical Engineering Department at Idaho State University's College of Science and Engineering. His expert guidance, patience, and support have been invaluable throughout this challenging innovation process. His guidance and constructive criticism have played a crucial role in shaping the project and keeping me motivated. I am also grateful to my colleagues, Michael Crump and Kyler Bingham, who provided me with all the resources they could, particularly when it came to tackling design and prototyping issues. Finally, I would like to express my immense appreciation to the Graduate School of Idaho State University for providing me with the resources and support needed to achieve my project goal.

Additionally, I want to express my gratitude to my family for their love and unwavering inspiration. I want to extend sincere thanks to my parents, Sunil Lama and Gita Maya Lama, as well as my brother, Sameer Lama, for their selfless efforts in shaping me into the person I am today. Additionally, I want to acknowledge my friends, Prasis Timilsena and Kiran Pandey, for their unwavering support throughout this journey, which provided me with the strength to carry on.

In conclusion, I am thankful to everyone who played a part in bringing this project to fruition. Your contributions were priceless and unconditional in helping me achieve this goal.

TABLE OF CONTENTS

List of Figures vii

List of Tables x

Abstract xi

Chapter 1: Introduction 1

1.1 Background and Motivation 1

1.2 Thesis Goals 3

1.3 Problem Statement and Scope 4

1.4 Thesis Structure 5

Chapter 2: Literature Review 6

2.1 Importance of Universal Grasping Tools 6

2.2 Novel Grippers and Designs Based on Different Applications 8

2.3 Review on Smart Shopping 14

Chapter 3: Robot Kinematics and Grasping 16

3.1 Introduction to Kinematics 16

3.1.1 Linkage Analysis 20

3.1.2 Linkage Synthesis 22

Chapter 4: Novel Rotary Grasping Mechanism 24

4.1 Parts and Specification of the Mechanism 24
4.1.1 Mechanical Advantage 29
4.1.2 Material Selection 30
4.1.3 Electrical Components 32
4.2 Kinematic Analysis 35
4.3 Force Analysis 37
4.4 Stress Analysis 42
4.5 Motion Analysis 44
Chapter 5: Smart Shelf with Load Cells and Touchscreen Interface 47
5.1 Parts and Specification of the Mechanism 48
5.1.1 Mechanical Component – Load Cell 49
5.1.2 Material Selection 52
5.1.3 Electrical Components 52
5.2 Touchscreen Interface 55
Chapter 6: Results, Discussions, and Conclusions 57
6.1 Robotic Arm Path Planning for Efficient Task Execution 59
6.2 Weight Data Extraction and Display 63
References 65
Appendices 71
Appendix A: Motor control code for Arduino 71

Appendix B: Arduino code for smart shelf 72

Appendix C: MATLAB code for calculating determinant of Jacobian 77

Appendix D: Drawing for gripper parts. 81

Appendix E: Drawing parts for Smart Shelf parts 92

Appendix F: Load cell product specification used 101

Appendix G: Figures of Grippers from review papers 102

Appendix H: Figures of Kinematic Background 105

Appendix I: Figures from novel grasping mechanism design 108

Appendix J: Stress and motion study results' figure for mechanism parts 113

Appendix K: Figures from Smart shelf design process 116

Appendix L: Figures from Smart shelf design process 117

Appendix M: CAD and real-life figures of the prototype 120

Appendix N: Figures from robotic path planning for task execution 121

Appendix O: Figure of working smart shelf. 123

Appendix P: Tables from design process 124

Appendix Q: Table of determinant calculation 127

List of Figures

Figure 1: Kinematics of a single soft finger and the soft gripper exhibition deformation under different air pressure [12] 8

Figure 2: Prototype of the space debris removal gripper [13] 9

Figure 3: Closed (left) and Open (Right) state of the cable-driven mechanical gripper. 10

Figure 4: Meshed pin array gripper mechanism [15] 11

Figure 5: Grasp experiment on different objects [15] 12

Figure 6: Gripper design (left), and inspiration from pole climbing technique (right) [1] 13

Figure 7: Rigid body in the reference frame 18

Figure 8: Joints and their Degrees of freedoms 19

Figure 9: 3-DOF SPM 2-RPU&SPR over-constrained mechanism [27] 20

Figure 10: Kinematic sketch of 3-DOF SPM 2-RPU&SPR over-constrained mechanism [27] .. 21

Figure 11: Conventional 4-bar linkage 22

Figure 12: Exploded view of the assembly with part number 26

Figure 13: Shutter CAD model referencing TABLE I 28

Figure 14: Electric circuit diagram [32][33][34][35] 33

Figure 15: General study of motion (side views).. 35

Figure 16: Kinematic sketch of the mechanism.. 37

Figure 17: Speed (rpm) vs Torque (N-mm) chart for the motor [29]. 38

Figure 18: Tangential angle between curve path and motor rotation path. 39

Figure 19: Soft finger & forces related. 41

Figure 20: FEA static analysis of the part TOP. 43

Figure 21: Topology study of the part TOP.. 43

Figure 22: Improved TOP considering analytical studies.. 44

Figure 23: Visual representation of the motion study for non-constrained vertical motion of the curved plate.. 45

Figure 24: Motion study results for the torque required to actuate the system............................ 45

Figure 25: Parts assembly (Exploded view) 49

Figure 26: Load cell [38] 50

Figure 27: Strain gauge load cell setup [39] 51

Figure 28: Actual load cell setup 51

Figure 29: HX711 Amplifier [40].. 52

Figure 30: Electrical circuit diagram (only one of the load cells (#1) is shown instead of eight in total) [41][42] 53

Figure 31: Home screen of the touchscreen interface 55

Figure 32: Prototype of the smart shelf 56

Figure 33: Whole design assembly (Excluding electronics and actuation system). 58

Figure 34: Actual prototype attached to the robotic arm. 58

Figure 35: Five cases of singularity for a serial 6-DOF robotic manipulator 60

Figure 36: Robotic-arm joint and links breakdown for D-H parameter. 62

Figure 37: Grasping (a) a tomato, (b) a guava, and (c) a hand-sanitizer bottle (all bottom view of the gripper) 63

Figure 38: Smart shelf displaying the weight of the hand sanitizer bottle 64

List of Tables

TABLE I: Designed Parts with Dimensions and Part Numbers (O = outer, R = radius, T = Thickness, H = Heigh; In detail in Appendix D 27

TABLE II: Material Properties Comparison.. 31

TABLE III: Electrical Components 32

TABLE IV: Parts, Dimensions, Part Numbers, and Quantities; In detail in Appendix E 48

TABLE V: Electronics, their Quantities, and Sources 53

TABLE VI: Determinant (Det.) & Rank of the Jacobian from MATLAB® 62

Smart Grocery Packaging System with Novel Rotary Grasping Mechanism and Multi-Interface Shelf

Thesis Abstract – Idaho State University (2023)

This thesis introduces a groundbreaking mechanism that, in contrast to many contemporary innovations, prioritizes simplicity alongside novelty. It unveils a novel gripper mechanism, integrated into a grocery packaging system, equipped with an open-loop system and a touchscreen interface within a smart shelf. The gripper prototype features a stepper motor for actuation and a thoughtfully crafted one-third circular pattern, facilitating both the force-closed and the form-closed grasping of objects with a diameter of five to nine centimeters. Importantly, this design can be easily adapted to cater to various applications, ensuring versatility and broad applicability across industries such as food, beverage, and grocery markets. The accompanying shelf enhances the customer experience through an engaging interface. Rigorously developed, analyzed, and tested through CAD software and in conjunction with a commercial industrial robotic arm, this gripping innovation promises to deliver sophisticated simplicity, scalability, and multifaceted utility to the relevant industries.

Keywords: Minimum Actuation; Scalability; Novel Gripper; Spring Mechanism; Stepper Motor; Shutter Design; Load Cells; Machine Learning; Grocery Packaging; Human Machine Interface; Form Closure; Force Closure; Touch Screen Interface

Chapter 1: Introduction

1.1 Background and Motivation

"The day science begins to study non-physical phenomena, it will make more progress in one decade than in all the previous centuries of its existence."

Nikola Tesla

(July 10, 1856 – January 7, 1943)

Human civilization has evolved as an example of a perfect machine. Things have been rejected, corrected, developed, presented, and repeat. The process has improved over time. Fortunately, civilization changed but their discoveries remain. Lifestyle, education, and abilities get better every day like a complete machine learning model. While every machine is invented out of necessity or luxury, almost all of them are inspired by some natural phenomena. For instance, the idea of a belt-pushing gripper design is inspired by the human pole climbing technique [1].

Humans are machines with complex artificial intelligence and learning abilities. While most of the abilities are governed by the brain via neural networks throughout the body, execution requires different physical body parts such as hands, legs, and many more. Human beings operate almost exactly like machines. What separates is the learning ability and artificial intelligence "till now". Throughout the development of civilization, humans have learned via suffering, failure, and sometimes coincidence. To compare, the brain is like a microcontroller/controller of a machine, wires can be perceived as a neural network that sends and receives signals, sensory organs are the feedback sensors, and physical organs are the mechanical components of a machine.

One of the most important organs to humans is the hands. Its primary functions include grasping. With the ability to learn and control the movement of muscles, humans have achieved the upper place in the survival chart. Brachiation in our primates, where hands are used to grasp and swing like a pendulum [2] for locomotion, keeps them safe from fierce ground threats. Experimental studies have revealed three manipulative abilities that are considered unique to humans such as precise handling, forceful precision grasping, and power squeezing [2]. These abilities represent every human activity that brought safety, prosperity, and luxury to human civilization.

With the evolving civilization, human has made their life easier with their knowledge and abilities, resulting in the industrial revolution. The development of machines led to the idea of eliminating repetitive actions for efficient production. After almost 100 years of Industrial and Manufacturing evolution, we are now entering the Robots Revolution [3]. It is believed to have the potential to radically transform employment and organizations [4], resulting in the most competitive playground for the world's great researchers and engineers. In recent years, military robots have shifted from the realm of science fiction to the reality [5]. As a result, robotic manipulators have become one of the most sought-after areas for scientists as an applicable and useful tool for various purposes [6].

Different systems are developed in search of better efficiency and results. There are millions of things or objects that we may see and use throughout our lifetime. Just a little probability that they are not mass-produced in a factory. Industry 4.0 has led the demand for novel designs to increase in every machine. The technology push in industrial practice refers to mechanization and automation, digitalization and networking, and miniaturization [7]. With the wide range of opportunities to reduce repetitive actions and to bring facilities to consumers, there have been many lives-changing inventions. For instance, mass production of motor vehicles brought costs down to make them affordable to millions of less-earning consumers. Similarly, the application of smart image processing offered improved accuracy in the rejection of defective products, robotic bartenders serving drinks in the bar, and many more.

Many production lines rely on robots that are equipped with specific end-of-arm tools to handle repetitive tasks. Some robots are less sophisticated and can only perform programmed tasks, while others are highly advanced with features like feedback communication and response systems. As consumer outlets increasingly adopt smart technologies, customized and precise services become more readily available to customers. These smart systems are not only necessary but also provide a fascinating experience. From life-changing inventions to small details, competition drives constant improvement in everything around us.

1.2 Thesis Goals

This thesis aims to create an intelligent packaging system for groceries and an innovative rotary end-of-arm mechanism that requires minimal degrees of freedom (D.O.F) and feedback sensors.

A motion conversion-based design is created for a new rotary mechanism to meet the goal. This design is inspired by the shutter mechanism found in cameras. To enhance the user experience, a smart shelf with load cells and communication capabilities through an image processing system is designed and added to the system. Additionally, a touchscreen-based human-machine interface (HMI) is introduced to enable users to select their desired groceries and weight.

The whole system was designed and tested for its mobility and strength using computer-aided design (CAD) software.

1.3 Problem Statement and Scope

In the United States, the grocery and convenience store industry is worth $818.6 billion [8] and serves millions of consumers with various products and services. However, shopping for groceries can be tiring and time-consuming, from pushing carts to weighing items to staying within a budget. While some supermarket chains have adopted smart shopping technology, others remain conventional. There is still a need for technology to make grocery shopping even smarter, given the variety of items available in stores.

This project involves designing a smart grocery packaging system using a new rotary gripper mechanism and a smart platform for grocery items. While the focus may seem narrow, the system has scalability and flexibility that allows for future expansion. The platform provides consumers with item descriptions to make informed choices and the rotary mechanism facilitates the pick and place of items.

The initial challenge of this project involves creating a new mechanism that can be easily adjusted to fit different applications and requires only a few control systems. This task requires careful planning and the incorporation of innovative mechanical components, such as compression springs. Once the design is complete, it will undergo analysis to ensure its effectiveness, strength, and mobility. Finally, the brain of the system is designed, a smart shelf with a digital communication interface.

To overcome the problems and meet the goals, Chapters 2, 3, and 4 will explain the background knowledge and resources that were used.

1.4 Thesis Structure

The structure of the thesis is presented in the flowchart below.

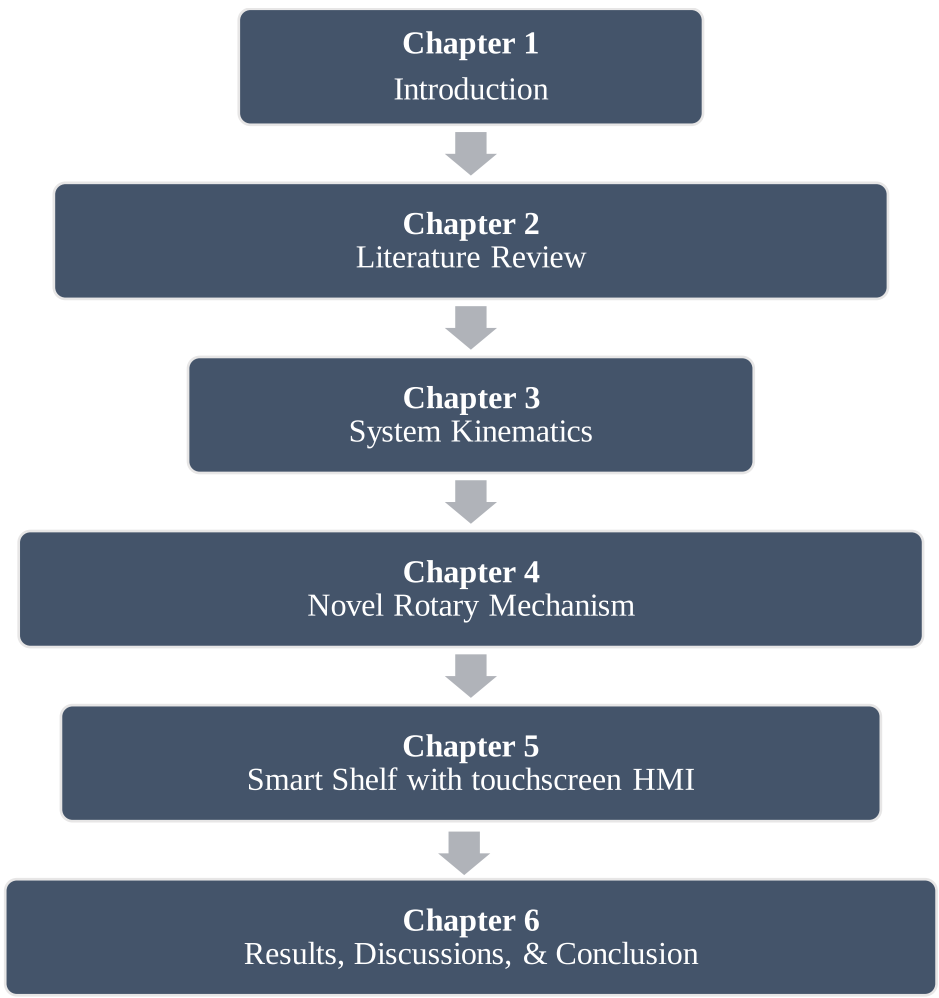

Chapter 2: Literature Review

In the literature review section, we will explore previous research on novel grasping mechanisms and touchscreen-based human-machine interfaces. This will include different models, kinematic mechanisms, their pros and cons, and their various applications. Since this is a popular topic, there have been numerous studies in this area, leading to significant technological progress.

2.1 Importance of Universal Grasping Tools

Robotic grippers are one of the most essential components of a robotic manipulator [9]. They are the difference-making factor in the whole robotic manipulation process. To understand the importance of robotic grasping tools, we need to understand the importance of the industrial robot [10] especially for Industry 4.0. Industrial robots in general, are the robots that are planted in manufacturing facilities that are programmable to perform desired tasks. For instance, robots in shipping facilities, are programmed to pick up and place packages on desired delivery lines with the help of high-speed image processing. For Industry 4.0, collaborative industrial robots have been the most suitable one. When it's collaborative, it is equipped with novel components most of the time. Otherwise, there is not much human and robot collaboration. Every other company is moving towards automation whether software-based or hardware. For this reason, the knowledge of robotic applications is already a vital element in this age of cutting-edge technology. While comparatively newer manufacturing facilities are already using huge numbers of robots, older and bigger companies are pouring millions to doing the same. On the other hand, robotic application has grown into the medical field too. One of the most famous is robotics in surgery. Vision-based surgery can be viewed as a robotic CAD-CAM system where diagnostic images from (CT, NMR, US, etc.) are used for off-line planning and robots can be used to make precision cutting, drilling, or similar tasks [11]. Not only for the surgery, but robotics in rehabilitation serves the primary objective to fully or partially restore the disabled user's manipulative functions typically by placing the robot arm between the user and the environment [11]. More importantly, space exploration is widely dependent on robotics and grasping tools to navigate and collect samples from different planets remotely. It remains an interesting topic of interest how vast robotic applications are.

With the growing application, growth in variety is obvious. Let's take a car manufacturer as an example. With billions of dollars invested, the company would want to set up a plant that can manufacture a maximum number of their models. It would be better if they can produce three or four models rather than just one. The company would now seek novel machines that are capable to adjust as per the need and application. The concept of a novel grasping mechanism rose out of this necessity accordingly in every field. Several design research has been performed and presented over the years to claim the novelty of end-effectors. As a result, there have been researchers working to achieve novelty via different types of grippers such as mechanical grippers, sensory feedback grippers, multiple-fingered grippers, vacuum grippers, adhesive grippers, clamp grippers, roller grippers, the air hand gripper, inchworm gripper [9].

Novel grippers are end-of-arm tools that are designed to grasp objects of unfamiliar shapes and sizes. The design of such a gripper is challenging and imposes several problems due to the differences in target object properties. Most current designs are aimed to look and work like humans' multi-fingered hands [9]. It is typical to assume that human hands are one of the most novel grasping mechanisms out there but designing such a mechanism gets complex with force sensing, image processing, joint controls, and so on.

2.2 Novel Grippers and Designs Based on Different Applications

Recently, the design and fabrication of a soft robotic gripper have attracted growing attention from researchers as it has promising features, such as being lightweight, inexpensive, easily fabricated, and easy to control [12]. The soft gripper is actuated using the pneumatic pressure in the fingers, typically decreased/negative pressure to bend outwards, atmospheric pressure to remain neutral, and increased/positive pressure to bend inward to grasp the object [12], as depicted in the figure below. In the research paper, the authors/researchers have presented their design of a pneumatic four-fingered soft gripper with a tunable effective finger length [12]. While the ability to adjust the pressure offers a great deal in grasping force application as per the target object, it allows the user to grasp the object of a wide variety.

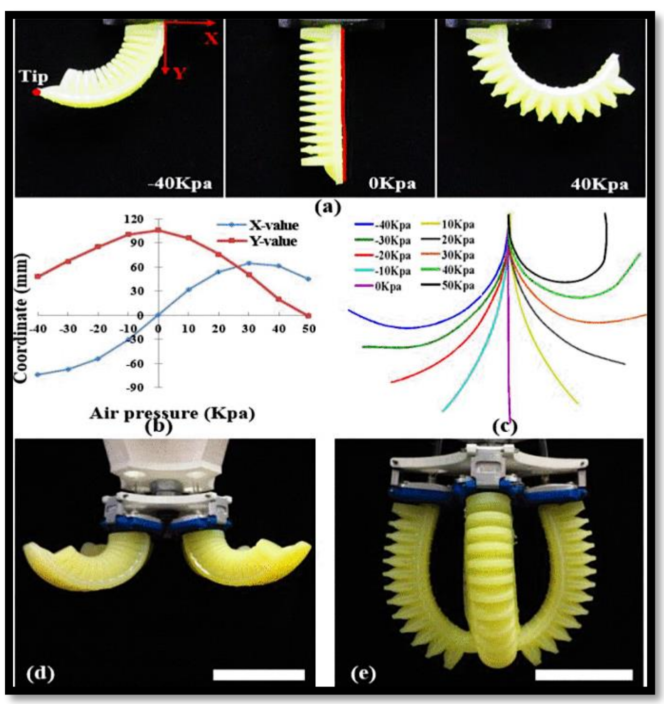

Figure 1: Kinematics of a single soft finger and the soft gripper exhibition deformation under different air pressure [12]

Researchers in 2018 proposed a novel mechanical gripper device for the capture of targets in space such as an aluminum honeycomb panel that covers the major areas of satellites for thermal insulation [13]. The main purpose of the design was to capture the aluminum honeycomb panel of non-cooperative satellites. It is claimed to have great significance for satellite service and space debris removal. Researchers performed the non-vertical piercing experiment on the gripper to find that it can withstand the destructive force greater than 1000N [13]. According to the authors (2018), the gripper can complete the whole process of grasping and releasing the object in four main stages. They are spring compression, preparatory phase, target grasping, and target release. The first stage begins with a motor rotating the screw. It will eventually have the tray mesh with the spring moving up while compressing the spring. In this position, the claw-like structures are open and ready to go to the preparatory phase. After the preparatory phase is complete the switch mechanism lets go of that spring causing the claws to close to grab the object. Finally, the compression phase comes in again as a release phase [13].

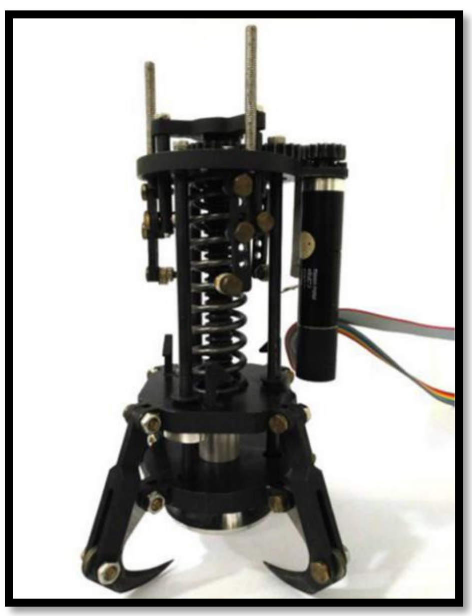

Figure 2: Prototype of the space debris removal gripper [13]

Along with the pneumatic and spring-based systems, one of the most interesting systems is the cable-driven one. Researchers, most of the time use cables in their mechanisms for distinct and specific motions. While soft gripers are trying to become a synonym with novel grippers, Zhang, Cheng, and Yue claimed that much effort has not been paid to the research on mechanical grippers [14]. Cable-driven mechanisms are widely used in the biomedical industries for their versatility in copying human hands. Lots of prosthetic hands follow the concept of the design. It has more effective gripper manipulation than other mechanical structures. The paper proposes a similar cable-driven mechanism for different complex manipulations as shown in the figure below.

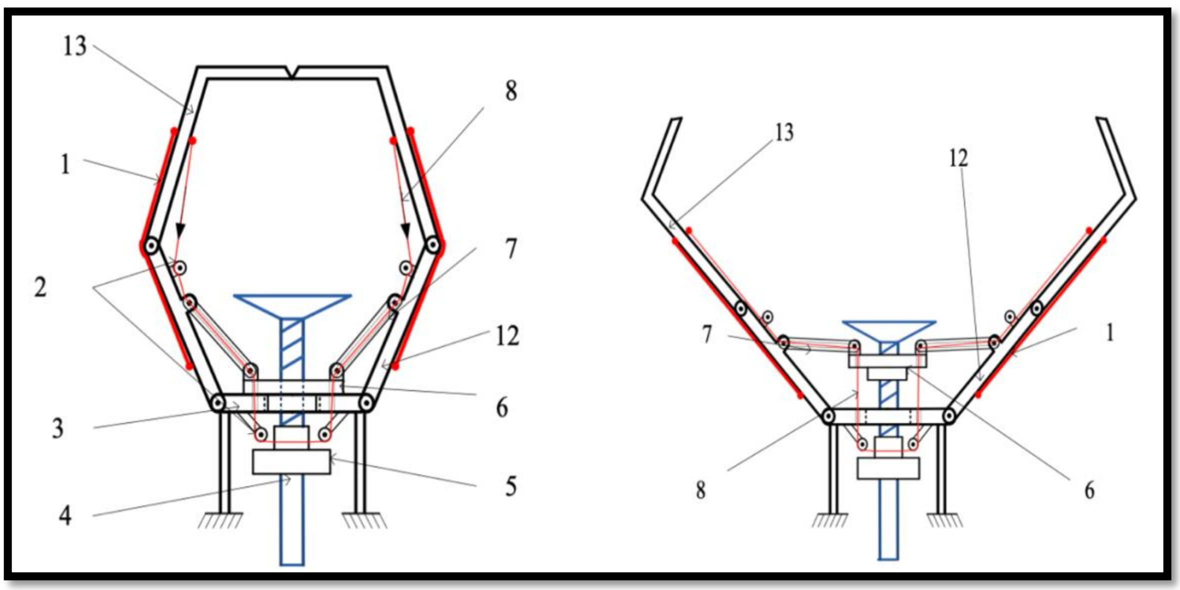

Figure 3: Closed (left) and Open (Right) state of the cable-driven mechanical gripper.

Even though the design consists of small parts and implications of thin wires, the working process is simple. Needless to say, the complex design made the working mechanism simpler. Like lots of grippers, this also calls for the action of rotation of the screw using a motor. The rotation causes the linearly vertical (up and down) motion of those central rods which eventually causes the cables to stretch and loosen. The kinematic analysis is done to make sure the design works perfectly under certain parameters.

Mo and Zhang (2019) in [15], introduced the novel gripper to challenge the universal grasp capability by presenting a design based on meshed pin array. The proposed design is not of the usual kind, but it is fascinating. The design is inspired by a popular executive toy patented by Ward Fleming in 1987 [15]. The concept is taking an imprint of the object to finally close the object for grasping. The proposed design in [15] is based on the meshed pin array actuated on top with spring columns as depicted in the picture below.

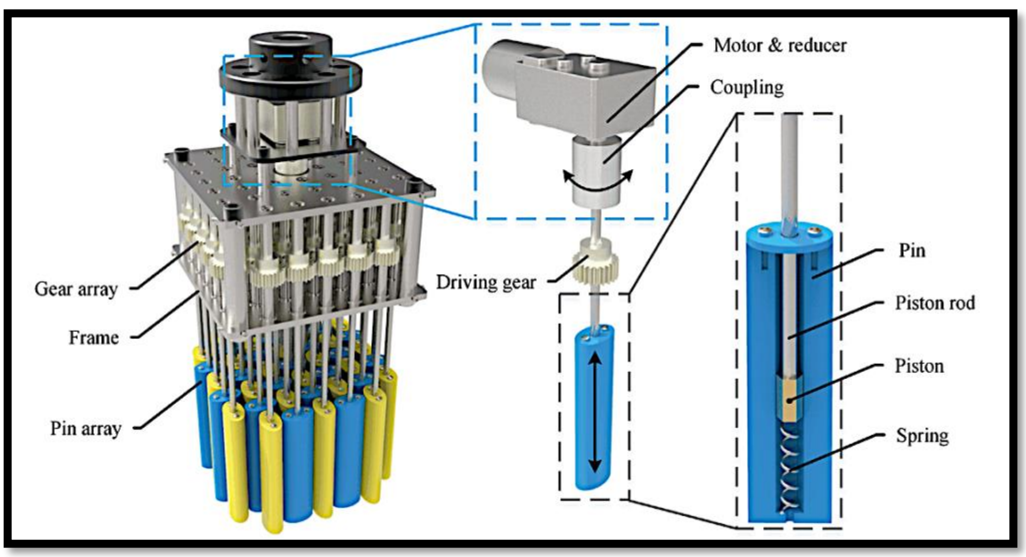

Figure 4: Meshed pin array gripper mechanism [15]

The working principle of the gripper [15] consists of 4 stages: approaching, adaptation, grasping, and lift. The first step is to hover over the object to make sure it is at its best grasping position. The second is the most important one where the pin array adapts to the shape of the object by pushing the pins up. Then, the driving mechanism equipped with springs is actuated to push the pins closer to each other horizontally to grasp the object. Finally, disengaging the actuation system and pushing the pins down releases the target object.

Figure 5: Grasp experiment on different objects [15]

While lots of designs are focused on grasping and mechanical techniques, the proposed design in [1] just left the grasping techniques to ancient climbers. Tavakoli, Marques, and Almeida in [1] proposed a design that is inspired by the ancient pole/tree climbing technique. The design combines the caging, and the forced closure approaches to grasp the object.

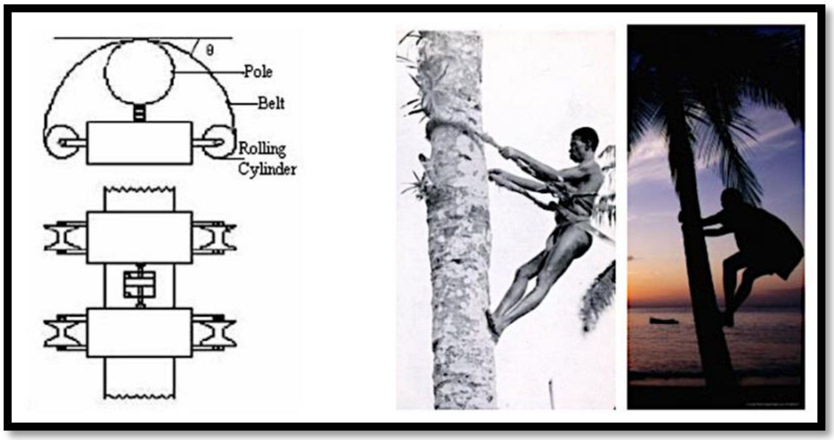

Figure 6: Gripper design (left), and inspiration from pole climbing technique (right) [1]

The gripper design in [1] also has three stages of grasping, not including the object release. They are caging, transition stage and flexibility adjustment, force closure, and releasing objects. The caging is the stage where the gripper belts try to wrap around the object. Then the belt contracts to adjust the flexibility according to the softness of the object by clipping the magnetic ends of the belts. Finally, the next step is to grasp/ force closure and release.

Apart from the conventional grippers comprised of different mechanical and pneumatic components, Okatani and Nishida of Kyusu Institute of Technology in [16] developed a smart magnetic fluid called Magnetorheological alpha (MRα) fluid. MR fluid can be controlled instantly between fluidization and solidification states at any shape by applying a magnetic force under the prevailing constraints [16]. MRα is the developed form of the MR fluid with the addition of non-magnetic material to increase the hardness of solidification.

Similarly, researchers in [17] presented their design focused on developing a robotic end effector that can help to climb walls and grasp many other objects. They came up with a novel vacuum pad that can climb uneven surfaces without damaging the surface, named "Universal Vacuum Gripper" (UVG).

2.3 Review on Smart Shopping

With the increase in the Internet of Things (IoT) and advanced artificial intelligence systems, the demand for e-commerce, and digital buying has risen by four folds [18]. Not only the technology industries but others, in general, are getting attracted to the stratification. It is not far that everything around you knows you [19]. The ease of use and interconnectivity is an obvious reason to attract every other sector towards smartification.

Through the interconnection of commonplace items, the Internet of Things (IoT) is transforming how people live. For instance, all the items in a grocery store may be linked to one another to create a smart shopping system [20]. Each product in such an IoT system might be given a low-cost radio frequency identification (RFID) tag that, when placed in a smart shopping cart, could be automatically scanned by a cart fitted with an RFID reader. Because of this, billing may be completed from the shopping cart, saving clients from standing in line at the register [20]. In addition to that, smart shelving can be added to the system that is equipped with RFID readers and can monitor the stock which will make inventory management much easier. As a result, the manual workload can be reduced to a low [20]. Researchers in [20] proposed the use of ultrahigh-frequency (UHF) technology in the system as UHF passive tags have a longer range.

Recently, another alternative, the smart cart is gaining popularity in smart shopping relieving customers with checkout work. There has been an increasing demand for easy and quick checkout at the grocery and other convenient stores. In [21], researchers proposed the concept of a smart cart that is capable of generating bills by itself on the cart's monitor. It is also equipped with a payment system that a customer can pay out more conveniently. With the growing interest, lots of outlets are already experimenting with the technology. The smart cart uses RFID technology with AVR controllers for peripheral interfacing and inventory management [21].

In [22], researchers presented a hypothetical but realistic case study of a single product that reduced food waste and rejected customers, and maximized profit by increasing inventory turnover which is one of the biggest problems in groceries business model. The paper [22] explained how groceries market has been affected during and by a global pandemic like COVID-19 when supply chain management, inventory management, and hygiene maintenance faced the biggest challenges. The research paper proposed a data-driven decision support system that uses the smart product-service system to manage the sustainable grocery store supply chain during outbreaks to prevent food waste as well as frantic buying.

Chapter 3: Robot Kinematics and Grasping

The importance of industrial robots and their application in different industries are undeniable. Some of them are discussed in Chapters 1 and 2, but it is important to understand how these machines are developed. Various technologies are implemented into a machine. Hence, acquiring knowledge of how robots work is essential because formulating suitable kinematics models for a robot mechanism is very crucial for analyzing the behavior of industrial manipulators [23]. In this chapter, we will discuss the basic understanding of kinematics, grasping technology, and other applied science to build a complete robot.

3.1 Introduction to Kinematics

In general, Kinematics is the study of motion [23]. It deals with the geometric range and capabilities of a machine disregarding any forces involved. While dynamics deals with the study of kinetic forces, static studies of machines are also important to ensure the strength of the machines. Kinematics defines a machine as a set of links and joints to transmit motion or forces via relative motion. To formulate the kinematic models for the robots/machines, there are two study processes for any machine. Analysis method and the synthesis method.

Kinematic analysis is basically a way to evaluate the behavior of a machine using the information about the machine. In this process, information about the physical components of the robot is known. While kinematic synthesis is the way most of the industry setup uses as robots have been widely used for handling materials, parts, and tools in the facilities [24]. It deals with the defined task and studies a way to complete the task using the robot.

While there are lots of external factors to consider during these studies, kinematics usually ignores all of those factors and deals with rigid bodies, and assumes conservation of energy for the force studies. Rigid bodies are not deformable during the motion or the whole study process. The conservation principle is the well-known one. It is also considered the highest and most general theorem of natural science that geniuses of different centuries led to [25]. The conservation of energy suggests that it is impossible to create work or energy out of nothing. It is commonly denoted as

$$U_1 + V_1 = U_2 + V_2 \tag{1}$$

where U represents the kinetic energy, and V represents the potential energy of any kind. There could be any mechanism involved such as spring, friction, viscous, etc. that can affect the potential energy values. Similarly, subscripts 1 and 2 represent the initial and the final states respectively.

Another important topic for any kinematic study is the degree of freedom (D.O.F). It is the go-to information to understand any mechanism right away. It is the number of independent parameters that are required to uniquely define the position of a rigid body at a given instant relative to the reference frame. For example, in Figure 7, there is an object in the X and Y reference frame. In order to determine the complete position of the body, it requires 3 parameters: P_x, P_y, and θ. P_x is the horizontal distance and P_y is the vertical distance from the frame, whereas θ is the angle between the X-axis of the reference frame and the X-axis of the rigid body. These three pieces of information will define the position as well as the orientation of the rigid but planar case. Similarly, for the spatial case, it requires six parameters in total. Hence, D.O.F becomes six.

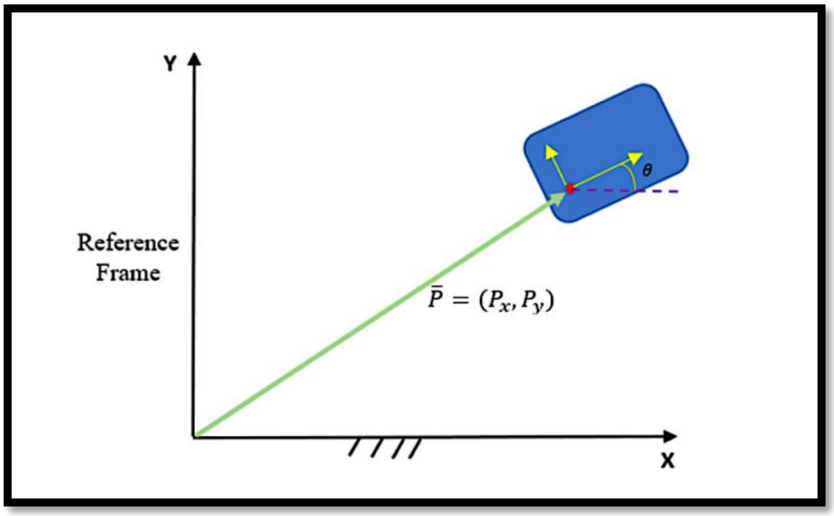

Figure 7: Rigid body in the reference frame

Little different from rigid bodies, robotics deals with the hierarchical forms of a similar study. It involves mechanisms. A mechanism, in general, is the combination of links and joints that are assembled to create a desired motion [26]. Degrees of freedom for mechanisms are also called mobility. Mechanically, it is also perceived as the number of actuators required to create a motion. Hence, mobility can also be assumed as the number of information required to specify the position of all the links and the joints.

For the planar and spatial cases, the degrees of freedom (D.O.F)/ mobility of the mechanism can be calculated using the Chebychev–Grübler–Kutzbach (K.G.C) equations as listed below.

$$M = 3(n-1) - \sum_{i=1}^{j} (3 - f_i)\,, for\ planar \tag{2}$$

$$M = 6(n-1) - \sum_{i=1}^{j} (6 - f_i) \text{ , } for\ spatial \qquad (3)$$

In both Equation 2 and Equation 3, M is the mobility, n is the number of links, j is the number of joints, and f_i is the degrees of freedom of the particular joint. Some examples of the types of joints and their f_i can be referred from the.

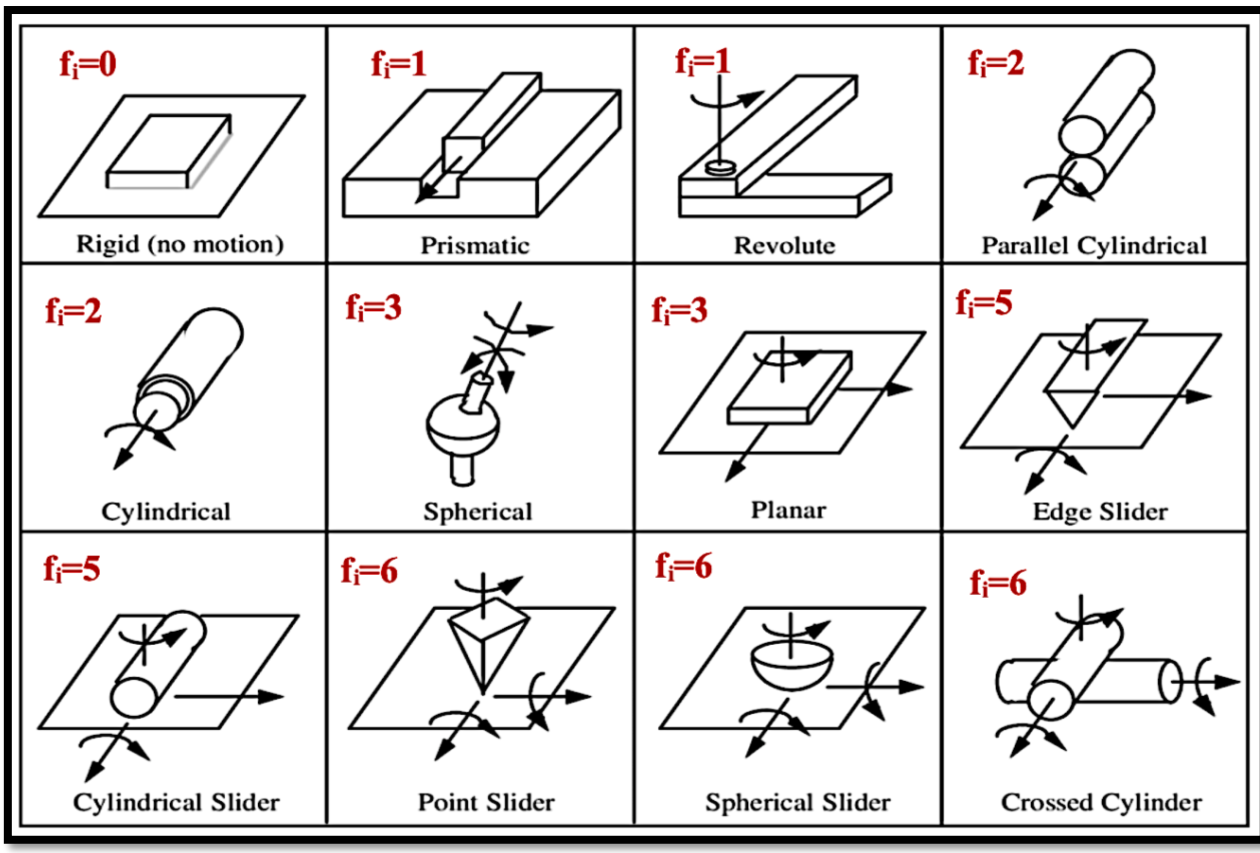

Figure 8: Joints and their Degrees of freedoms

Needless to say, not everything is perfect. There exist some mechanisms that in reality have mobility but the Chebychev–Grübler–Kutzbach equation specifies them as immobile. Mathematically, they have a non-positive integer value as their degrees of freedom but can create motion. They are widely known as over-constrained mechanisms. Most of the time, their mobility comes through the existence of special geometric conditions between the joints and the axes [26]. One of the examples of the over-constrained mechanism is depicted in Figure 9.

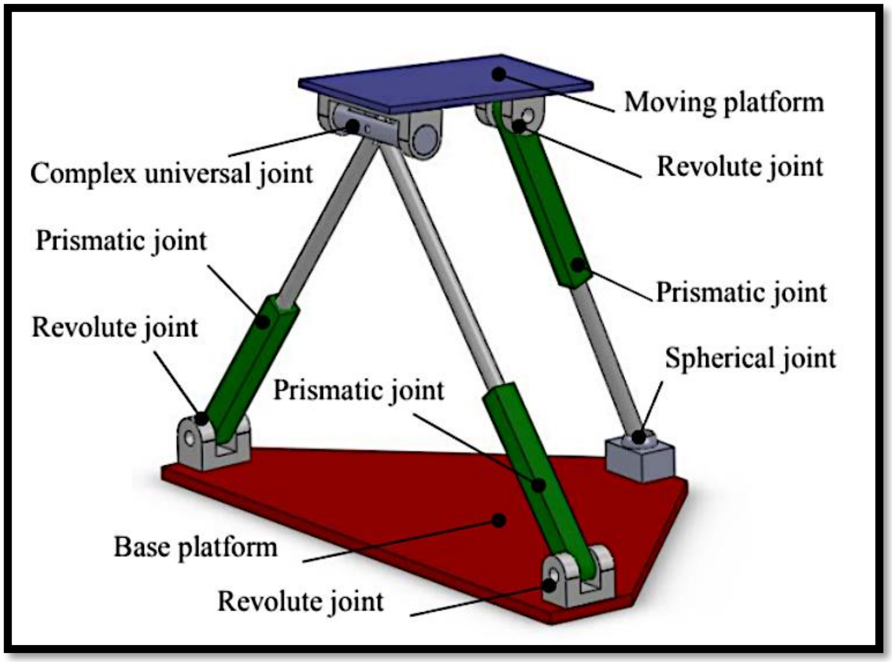

Figure 9: 3-DOF SPM 2-RPU&SPR over-constrained mechanism [27]

3.1.1 Linkage Analysis

Linkage analysis is the process to determine the position, velocity, and acceleration of any point in the linkage. The process begins with the kinematic sketch formation. It is the act of creating a sketch of the mechanisms with respect to their links and joints. The kinematic sketch is shown in Figure 10. The process is then followed by the mobility calculation using desired Chebychev–Grübler–Kutzbach equations. Finally, the position, velocity, and acceleration analyses are performed.

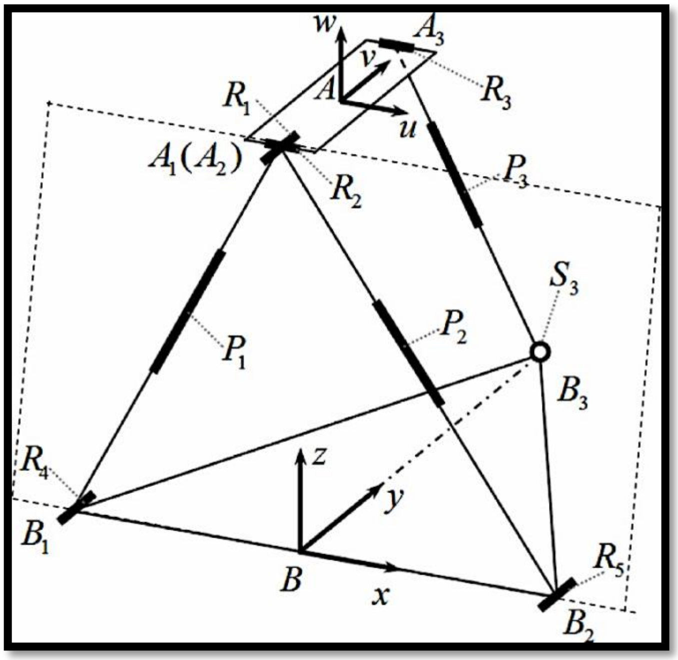

Figure 10: Kinematic sketch of 3-DOF SPM 2-RPU&SPR over-constrained mechanism [27]

The position analysis requires reference frames, defining variables, parameters, and vector coordinate points. For a 4-bar linkage mechanism depicted in Figure 11, parameter values can be determined in two ways: distance constraints method, and the loop equation method. With known input angle (θ), the output angle (ψ) can be calculated as,

$$\Psi = \arctan\left(\frac{(-2ab\ \sin\theta)}{(2b(g\ -\ a\cos\theta))}\right) \pm \arccos\left(\frac{2ag\cos\theta\ +\ h^2 - g^2 - b^2 - a^2}{\sqrt{((2b(g\ -\ a\cos\theta))^2 + (-2ab\ \sin\theta)^2\ )}}\right) \tag{4}$$

Finally, the coupler angle can be calculated as,

$$\emptyset = \arctan\left(\frac{b\sin\Psi - a\sin\theta}{g + b\cos\Psi - a\cos\theta}\right) - \theta \tag{5}$$

With this information, we can determine the position of any points in the 4-bar linkage.

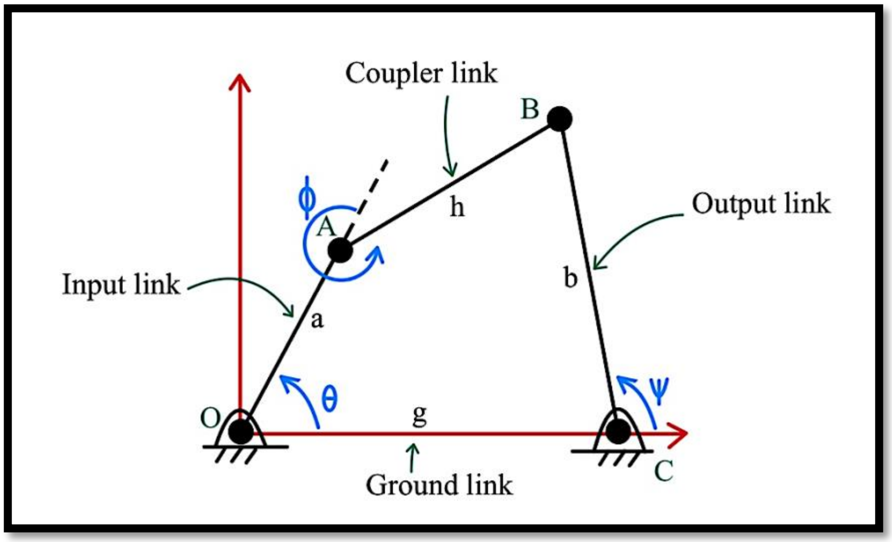

Figure 11: Conventional 4-bar linkage

Similarly, the process is followed by the velocity analysis and the acceleration analysis. The velocities of the points are obtained by taking derivatives in the loop equations and again the derivative is taken to obtain the acceleration of different points.

$$\dot{\emptyset} = \left(\frac{-a\sin(\Psi - \theta)}{h\sin(\Psi - \theta - \emptyset)} - 1\right)\dot{\theta}, \qquad \& \qquad \dot{\Psi} = \left(\frac{a\sin\emptyset}{b\sin(\theta + \emptyset - \Psi)}\right)\dot{\theta} \tag{6}$$

With a similar approach, the linkage analysis for the mechanisms like slider-crank mechanism, cam-follower mechanism, etc. can be done.

3.1.2 Linkage Synthesis

Linkage synthesis is the approach to design the linkage based on the required position/task. With the help of linkage selection and synthesis, a conventional linkage like 4-bar can easily be constructed. Graphical synthesis and algebraic synthesis are two different methods. As it sounds, graphical synthesis is the method in which perpendicular bisectors are drawn between the two desired positions and linkages are formed. It can be done for two or more desired positions by limiting the freedom of linkage joints. Graphical synthesis is one of the practical ways of creating 4-bar linkages. Whereas algebraic synthesis is performed by creating the design equations for the desired positions. It can be done by applying the distance constraints, and the loop equations.

Chapter 4: Novel Rotary Grasping Mechanism

This section introduces a new gripper mechanism capable of grasping objects of various sizes without the need for feedback control. Industries such as food and beverage are seeking grippers that are innovative, soft, and have a simplified control system. The proposed design utilizes a rotary mechanism with springs to achieve gentle grasping of objects. The gripper, designed in a cylindrical shape, is actuated by a stepper motor with a gearbox to enhance torque. Three stacked curvilinear and linear rails convert the motor's rotational motion into linear motion. The grasping component consists of three curved parts, each incorporating numerous compression springs. Currently, the gripper can effectively grasp objects ranging from five to nine centimeters in diameter, with a maximum height of ten centimeters. Importantly, the design is scalable based on specific application requirements. A comprehensive CAD model of the mechanism was developed, and multiple analyses, including motion, topology, and stress analysis, were conducted. Finally, a functional prototype of the gripper was constructed and successfully tested for grasping objects within the gripper's size range.

4.1 Parts and Specification of the Mechanism

Traditional end-of-arm designs have historically drawn inspiration from the intricate structure and functionality of the human hand and fingers. The human hand comprises interconnected bones and muscles, which are coordinated through neuron signals. In the realm of kinematics, bones serve as linkages, muscles act as actuators, and nerves establish connections to transmit voltage signals to control the motion. However, comprehending and creating a robotic hand with comparable capabilities is challenging. Designing such a robotic hand is more intricate than it may initially appear. As a result, soft and innovative grippers have emerged as viable alternatives, garnering significant interest for their potential to revolutionize hardware automation in recent years [28].

In this project, the proposed gripper comprises multiple components, as illustrated in Figure 12 and listed in TABLE I. At the core of the mechanism are three shutter components (#5), which are three equal pieces of a cylindrical extrusion. The shutters contain small holes (cylinders) intended for the insertion of small pistons (#12) and springs (#13), which together function as flexible grippers. Also, each shutter contains a small column on the top and bottom faces. Half of the column on top is rectangular extrude, the other half is a cylindrical extrude, and the bottom column only has a rectangular extrude (Figure 13). These columns enable the shutter to slide inside the circular plates above and below.

Two types of circular plates are in the design: a) linear guide circular plates located at the bottom (#3) and top (#6), featuring rectangular-shaped slots. These plates serve as guides for the shutters, ensuring they move in a straight path. b) curvilinear guide circular plate (#7) situated on top of the linear guide circular plate at the top (#6). The curvilinear slot in this plate spans 120 degrees of arc, starting from the bottom of one linear cut and ending at the top of another linear cut in the linear guide plate (#6). The curvilinear slots transfer torque from the motor to the shutters. To minimize friction between the plates, grease lubricant is applied, and steel bearing balls (#4) are incorporated within the designed rails between the circular plates to ensure smoother motion. Similar rails, with bearing balls, are implemented between the shutter and linear guide plates (#3 & #6) to facilitate smooth motion. All the components are enclosed within the outer shells (#1 & #2), which are fastened together to form a box-like structure or outer cover, allowing space at the bottom for the entry of the target object. The gripper's internal components (#3, #5, #6, & #7) are secured together by screws from the top part (#8), which also houses the motor.

The motion from the motor's rotation, transmit to the curvilinear guide circular plate (#7) through a shaft hole and key. This rotational motion is then transferred to the shutters, which can only follow the linear path defined by the linear guide circular plates, converting the motor's rotational motion into linear motion. The grasping state is achieved when the shutters come into contact and form a circular shape.

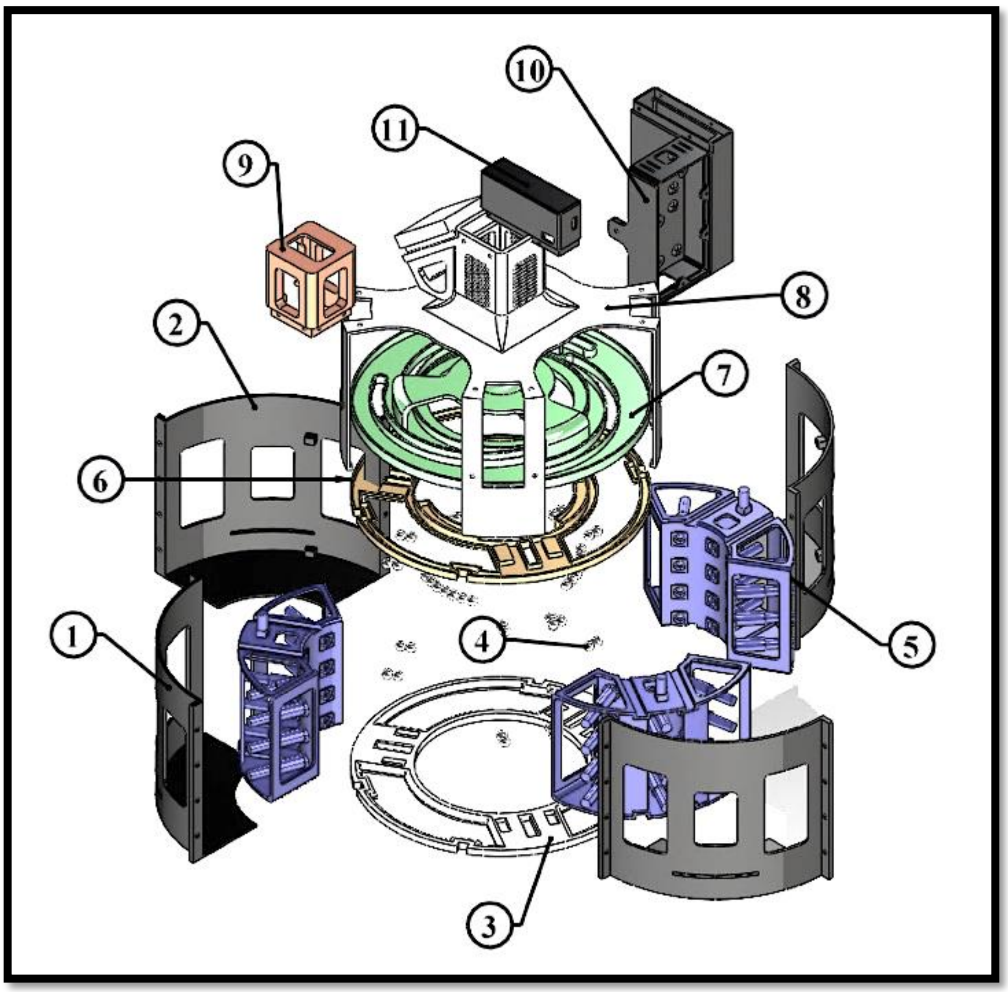

Figure 12: Exploded view of the assembly with part number

TABLE I: Designed Parts with Dimensions and Part Numbers (O = outer, R = radius, T = Thickness, H = Heigh; In detail in Appendix D

Part	Dimension (cm)	Part No.
Outer Shell A	H = 14.7, OR = 14.3, T = 0.3	1
Outer Shell B	H = 14.7, R = 14.3 T = 0.3	2
Rectangular Slot Plate (Bottom)	OR= 13.9, IR = 8, T = 0.75	3
Bearing Ball	D = 1	4
Shutter	OR = 11, IR= 5, H = 15.25	5
Rectangular Slot Plate (Top)	OR= 13.9, IR = 6.8, T = 0.75	6
Curvilinear Slot Plate	OR= 13.9, IR = 6.8, H = 5.4	7
Top	OR = 14.8, H = 24.6	8
Top cover	6.3 x 6.3 x 7.8	9
Electronics Box	10.2 x 10.275 x 14.7	10
Wire Cap	10.2 x 3.075 x 5.19	11
Piston	R = 0.15, H = 6	12
Spring	R = 0.5, T = 0.05, H = 2.5	13
Piston Blocker	OR = 0.6, IR = 0.25, H = 0.4	14

During the design-to-assembly (DFM) process, meticulous attention is given to each part to ensure precise assembly and optimal performance. Carefully determined dimensions facilitate easy assembly and enable the gripper to effectively grasp objects with diameters of 5 cm to 9 cm, encompassing typical vegetables and fruits in grocery stores. However, this design is fully scalable to manipulate objects of different sizes based on user requirements and specific applications. The gripper's diameter can be adjusted for varying object sizes, while the springs having different spring constants can be used to accommodate changes in material texture (e.g., squeezable, or fragile objects) or maximum weight.

In the current prototype, the overall assembly has a radius of approximately 14.3 cm, which corresponds to the radius of the outer shells (#1 & 2). The design's total height measures around 34.15 cm (excluding the wire cap), with the top part (#8) housing the motor and gearbox, adding to its height. The top part is rigidly connected to the outer shells. The motor, housed within the top part, imparts rotational motion, generating circular movement of the curvilinear-guide plate (#7), which features a 120-degree slot mechanism that drives the top column of the shutter (#5). All circular plates have an outer diameter of 27.8 cm and a thickness of 0.75 cm. The shutters have outer and inner diameters of 22 cm and 10 cm respectively along with the height of 15.25cm.

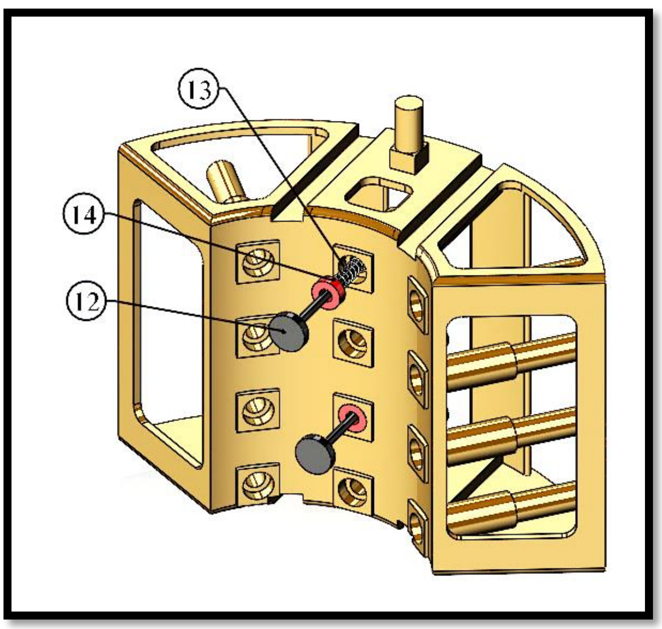

Figure 13: Shutter CAD model referencing TABLE I.

Figure 13 depicts an image of the shutter, showcasing a cylindrical column extending from its top face. This column maintains contact with two distinct plates: the linear guide circular plate (#6) and the curvilinear guide circular plate (#7). The linear guide plate incorporates a slider connection with 1 degree of freedom (D.O.F.), while the curvilinear guide plate features a roller connection with 2 D.O.F. A hidden rectangular extrusion is present on the bottom face, serving a similar function as the one on the top face. The motion is initiated when the motor rotates the curvilinear guide plate (#7), causing the circular column to follow the path defined by the slot. The linear guide plate (#6) constrains the motion, resulting in the linear movement of the shutter. The outer face of the shutter contains 12 precisely designed holes, intended for the integration of springs and pistons to provide grasping force. The springs are allowed to deflect fully, with a length of 2.5 cm. The pistons are equipped with sticky material at the contact tip to enhance grasping performance and are made of M3 screws, with a height of 6 cm from top to bottom. As depicted in the figure above, the piston blocker (#14) blocks the piston from coming out of the shutter holes. Figure 13 shows the exploded view (numbered in Figure 13) of the piston, spring, and piston blocker showcasing the state to see how it's assembled and the assembled state (bottom). All holes are equipped with parts #12, #13, & #14s, to finally look like the bottom state (non-numbered in Figure 13).

4.1.1 Mechanical Advantage

This mechanism is based on a kinematic concept that incorporates compression springs and a piston arrangement within moving shutters for object manipulation. What sets this design apart from other spring-based grippers is its ability to achieve both force-closure grasping and form-closure grasping simultaneously, ensuring enhanced safety during grasping operations. The design offers scalability through the flexibility to interchange compression springs with varying spring constants. The application of Hooke's Law allows for the calculation of the force exerted on the grasped object's surface by each piston, considering the respective spring constant. Additionally, the implementation of rough material on the grasping tip of the piston head enhances the friction between the object and the pistons, resulting in more efficient grasping performance. Initially, a NEMA17 Stepper motor with a torque rating of 59 N-cm was deemed sufficient based on calculations and motion analysis conducted in CAD software. However, further evaluation of the prototype revealed the presence of additional frictional and bending factors, necessitating the use of a motor with higher torque. To address this requirement, a planetary gearbox with a torque transmission ratio of 40:1 [29] was integrated into the design. Throughout the design process, stress analysis, motion analysis, and topology optimization were employed to refine the mechanism, resulting in a final design that prioritizes lightweight construction, reliability, and optimal grasping performance.

4.1.2 Material Selection

The grasping mechanism however is very vulnerable to external factors such as friction, and imbalanced moments. As it is more of a functional design and is currently in its initial phase of prototyping, phenomena such as bending, friction, and uneven force distribution make the material selection a crucial decision. Hence, the material used in this stage is ABS plastic. ABS plastic filament is mostly used in 3D printing, and it is one of the strongest among other materials that are light in weight. The material is more feasible for this design in terms of the geometric structure that the machine must print. It has sufficient tensile strength and can print with more precision. It can be sanded to desired smoothness without deformation, unlike some

PLA plastics that tend to melt down on machine sanding. While the whole design is printed with ABS plastic, the pistons are of steel. They are off-the-market screws [30] that are stiff and perfect for the size requirement.

The total weight of the gripper with its actuation system is crucial with regard to the maximum payload of the robotic arm it is attached to. As the prototype of the design is made of ABS plastic, the weight-to-strength ratio remains decent for the design. However, plastic parts bring frictional factors to their peak compared to fine-surface machined parts. Also, the use of plastic restricts the possibility of making it compact leaving the prototype big and less appealing. The only advantage is that it provides quick prototyping abilities with decent remodeling and 3D printing. The total weight of the system without the control/electronics system is 3.1 kg.

For the industrial version of this product, among all alternative materials with higher stress tolerance and lower friction coefficient, aluminum alloy 6061 can be the most appropriate option based on similar research and material data in [31]. Though, the final choice of material is made to be aluminum alloy 6061 but only for high friction-prone parts so that the overall weight of the system remains pretty much unchanged. Some of the specifications for these three materials are shown in TABLE II.

TABLE II: Material Properties Comparison

Properties	**Aluminum Alloy 6061**	**ABS**
Yield Strength	276 MPa	29.6 MPa
Ultimate Tensile Strength	310 MPa	40 MPa
Elastic Modulus	69000 MPa	2000 MPa

Poisson's Ratio	0.33	0.394
Mass Density	2700 kg/m3	1020 kg/m3
Shear Modulus	26000 MPa	318.9 MPa

4.1.3 Electrical Components

The design presented in the paper consists of some general mechatronic components. These components are listed in TABLE III.

TABLE III: Electrical Components

Electrical components	**Quantity**	**Component No.**
Arduino Uno R3	1	1
L298N Motor Driver Module	1	2
PKP Series 2-Phase Stepper Motor	1	3
Remote Control Module	1	4
HX1838 VS1838 NEC IR Receiver	1	5
6mm x 6mm x 5mm Tactile Push Button	3	6
10 kΩ Resistor	3	7

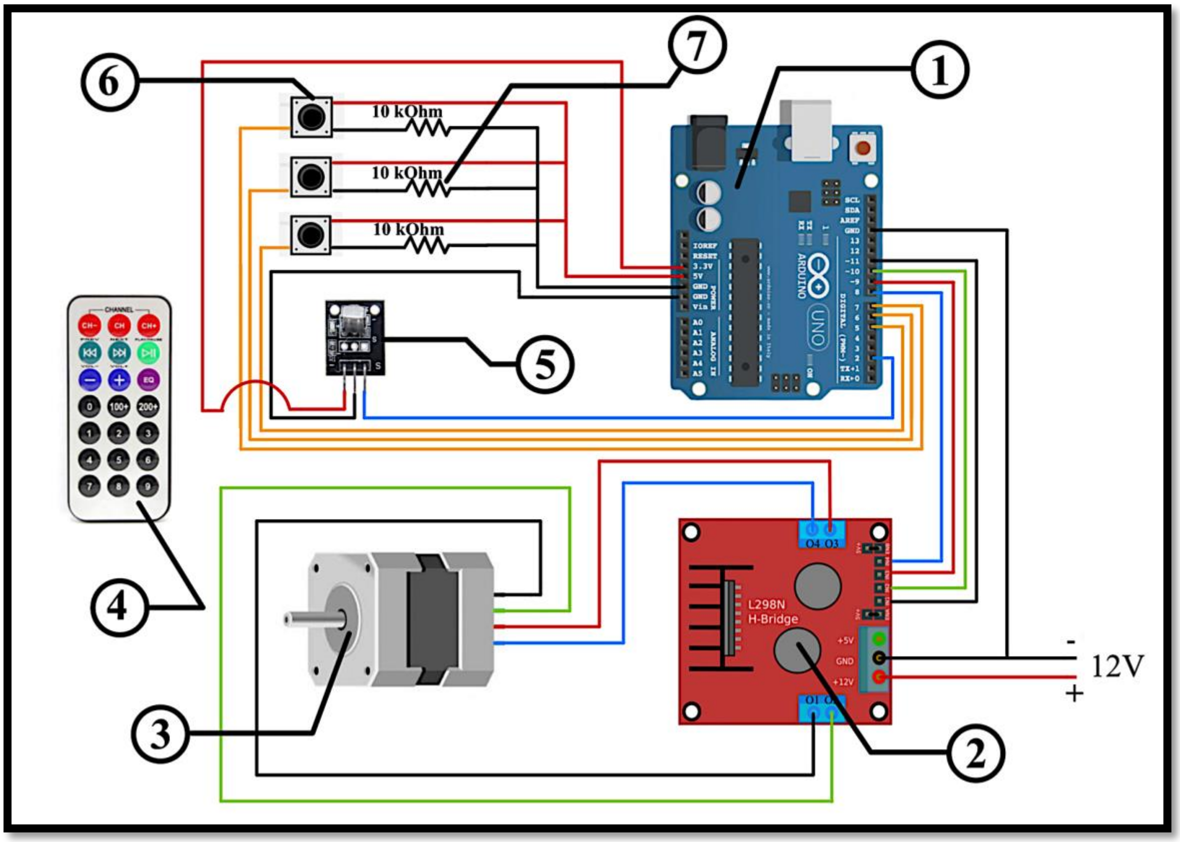

Figure 14: Electric circuit diagram [32][33][34][35]

The main electrical component used in most mechatronic projects is microcontrollers. An Arduino Uno R3 (#1) because of its proper size and enough pins for all electrical components has been selected for this system. This microcontroller has 14 digital and 6 analog pins with multiple grounds. It also consists of the voltage-out pin that can be used for powering different components such as sensors, buttons, motors, and so on. As depicted in Figure 14, Arduino Uno R3 is connected to all components. It is programmed to incorporate the remote control that communicates via the HX1838 remote (#4) and VS1838 NEC Infrared Wireless sensor module (#5). The sensor module is connected to Arduino to its digital pin 2, 3.3V pin, and the ground. It is programmed to control the clockwise and anticlockwise rotation of the PKP Series 2-phase stepper motor (#3).

The motor is connected to the Arduino Uno R3 via L298N Motor Driver Module (#2). The four wires coming out of the motor are identified with their colors using the description of the motor in [29]. They are connected as shown in Figure 3. Pin1, Pin2, Pin3, and Pin4 are connected to the Out1, Out2, Out3, and Out4 of the L298N module respectively. Further, the four wires from L298N Driver, IN1, IN2, IN3, and IN4 are connected to four digital pins, 8, 9, 10, & 11 respectively of the Arduino board for control purposes. The motor and the controller are powered using an external power source as shown. For safety and error minimization, 3 push buttons (#6) are used to bring the program to a stop. These buttons are placed to stop motion at its extreme positions. This helps the system to eliminate the step motion error in the motor over the long run and motor and parts damage. These push buttons are connected to each digital pin, 5V pin, and GND of Arduino with 10kΩ resistors (#7) in grounding.

The entire circuit has been tested and programmed to enable the system to achieve a 120-degree rotation, which is equivalent to one-third of a complete rotation. The programming was carried out using the Arduino IDE platform, with the Arduino code provided in Appendix A: Motor control code for Arduino. The motor's speed is set at 60 rpm, resulting in 1.5 rpm when combined with the 40:1 gear box. The motor can be programmed to operate at speeds of up to 400 rpm, while still maintaining a higher output torque range.

4.2 Kinematic Analysis

The side view of the moving parts in the proposed mechanism is shown in Figure 15. The motion begins with the curvilinear slot plate (Part A), which is rotated by the motor. The curvilinear slot plate drags the shutter (Part C) which is guided toward the direction of the motion by the rectangular slot plate (Part B). Because the force from the motor only applies to the top part of the mechanism, the friction and forces creating torques within the parts cause problems in the smooth motion of shutters. This problem has been almost solved by minimizing the friction between parts using the motion slots with bearing balls greased with NLGI Grade 2 Lithium Grease.

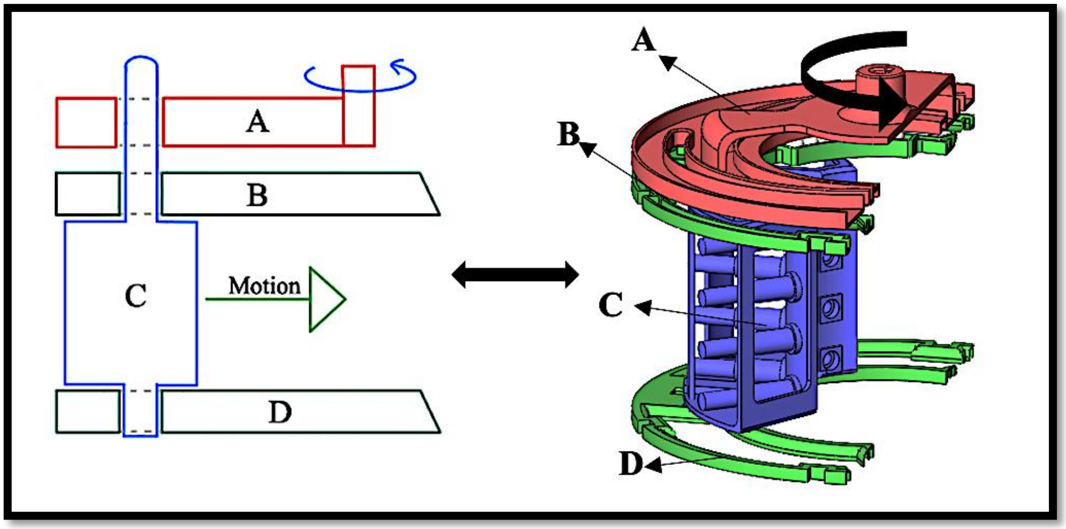

Figure 15: General study of motion (side views)

The mobility of a mechanism refers to the number of independent degrees of freedom of it, which determine the number of required actuators. The mobility of a mechanism can be determined using Equation (7) (Chebychev–Grübler–Kutzbach equation) for a planar motion. Over-constrained mechanisms, with zero or negative mobility, are considered structures and they cannot create any motion. However, some exceptional cases with negative mobility are still movable based on their particular geometry (e.g., Bennett linkage [36]). In the current mechanism, based on the geometry of its axes of motion, the mobility can be considered in the subgroup of motion and analyzed as a planar motion.

$$M = 3(n-1) - \sum_{i=1}^{j}(3 - f_i), \tag{7}$$

where n is the number of links, j is the number of joints, f_i is the degree of freedom for each type of joint.

Figure 16 illustrates the kinematic sketch of the mechanism, providing a clearer understanding of the motion. Although the kinematic sketch is not drawn to scale, it accurately demonstrates the intended motion of the proposed mechanism. Within this sketch, the ground link is denoted as L1, the curvilinear slot plate (#7) as L2, the extruded column of the shutter (#5) as L3, and the slider is grounded. The mechanism comprises three joints: J1, which is revolute; J2, a roller; and J3, a slider. J1 and J3 each possess one degree of freedom, while J2 possesses two degrees of freedom. By considering the number of joints, links, and degrees of freedom for each joint and applying them in Equation (7), the mobility of the machine can be determined as one, as indicated by Equation (8). Consequently, this mechanism requires only one actuator to generate motion, which is ideal in terms of minimizing the weight of the mechanism.

$$M = 3(3-1) - 2(3-1) - 1(3-2) = 1 \quad (8)$$

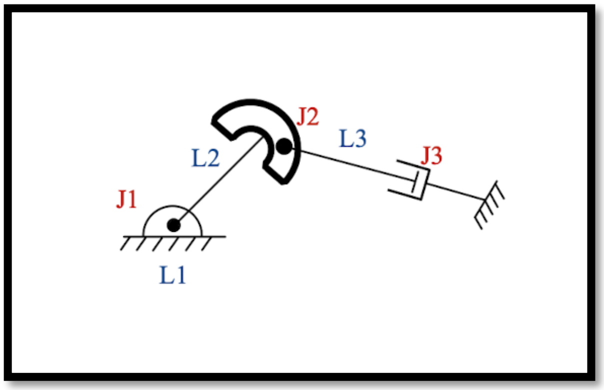

Figure 16: Kinematic sketch of the mechanism.

4.3 Force Analysis

The design is based on computer analysis and the forces involved are divided into two main forces: the force from the actuator and the springs force. The force from the actuator makes the motion of the shutter mechanisms. The applied torque is calculated using the motor torque curve in Figure 17.

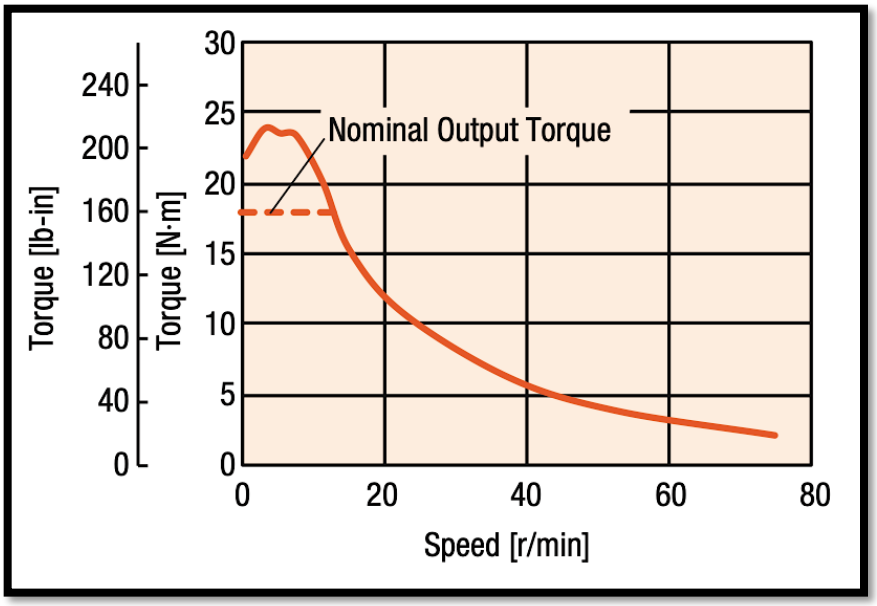

Figure 17: Speed (rpm) vs Torque (N-mm) chart for the motor [29].

Based on the relation between torque and speed of the motor in Figure 17 and to have the maximum torque, this motor is programmed to rotate at a speed of 0-20 rpm. With the maximum deviation angle of θ = 38.05 degrees from the tangential torque at a 9.5cm radius, the normal force being applied is calculated using the free body diagram in planar condition as depicted in Figure 18.

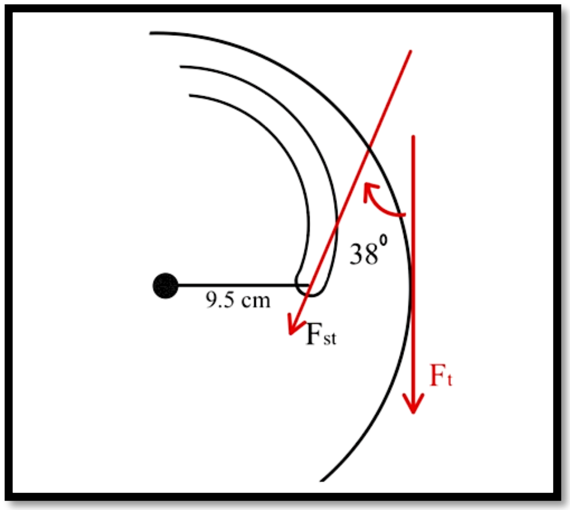

Figure 18: Tangential angle between curve path and motor rotation path.

The tangential force (F_t) is calculated using Equation (9) where force is the only unknown term.

$$Torque\ (\tau) = F_t\ \cdot radius\ (r), \tag{9}$$

Using Equation (9) and referring to the free body diagram presented in Figure 18, the tangential forces acting on the slot curve denoted as (F_{St}), will be computed according to Equation (10). These tangential forces serve as the driving force for the actuation of the mechanism. It is important to emphasize that the centers of rotation and the curve path are different from each other.

$$F_t\ = F_{St}\ \cdot \cos(\theta), \tag{10}$$

Another significant force in this mechanism is the grasping force, generated through the compression of the springs. From Equation (11), the force exerted by a spring is influenced by two factors: displacement (x) and the spring constant (k). The spring constant is determined by the spring's dimensions (length, thickness) and its material properties. Moreover, the size of the object being grasped affects the displacement of the spring, with larger-diameter objects experiencing greater forces.

$$F_{spring} = -k \cdot x, \tag{11}$$

This spring-based grasping mechanism proves highly effective for grasping objects with varying diameters and shapes, if all objects possess a similar texture (i.e., soft or hard) and proper springs are selected. Furthermore, the interaction between the target object and the contact fingers (in this case, the pistons) significantly influences the grasping force.

Like other mechanical designs, the components within this mechanism possess a specific lifetime and require replacement after a certain period to maintain a reliable grasping system. The incorporation of springs in this mechanism provides the gripper with the unique capability of grasping diverse objects. However, the properties of springs gradually diminish over time, necessitating their replacement.

Grasping analysis is necessary for any robotic gripper. This study has been done on this mechanism to ensure whether the object is being grasped properly and whether it is stable and safe inside of the gripper when the robotic manipulator has moved around. The mechanism presented in this paper includes force-closed grasping with soft fingers. However, because of using several fingers all around the object, it can be considered as a form closure gripper too. A complete grasping of the object depends upon three main factors: numbers & positions of the fingers, types of fingers, and geometry of the object and it can be expressed by Equation (12).

$$\left\{ \sum_{i=1}^{k} n_i N_i,\ \ n_i \in \ \mathbb{R} \right\} = s\ e^* \tag{12}$$

where ‘n’ is the normal force with respect to different axes, ‘N’ is the wrench space, and ‘i’ is the number of fingers.

The soft fingers provide optimum grasping with a force normal to the surface (F_{spring} in this case), frictional forces in the tangent plane, and the frictional moment in the normal direction resulting in a 4-dimensional wrench subspace, as presented in Figure 19 and Equation (13).

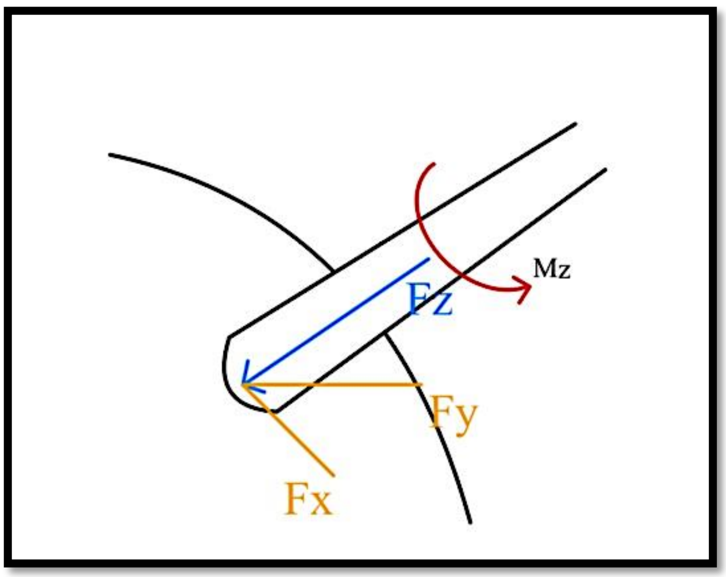

Figure 19: Soft finger & forces related.

(13)

In the equation above, F_x, F_y, and F_z represent the normal forces caused by friction between contact surfaces in the x, y, and z directions. Additionally, M_z is the constraining moment in the z-axis. Normal forces restrain movement in specific directions, while the moment prevents undesired rotation around the contact point. This ensures that the object being grasped will not slip or change orientation, allowing for a secure grip.

4.4 Stress Analysis

The design process of the proposed mechanism has involved iterative simulations within a CAD software environment to obtain an optimized design. Most components underwent validation through finite element analysis (FEA) to ensure they met the criteria for maximum allowable deformation. Due to the intended attachment of the gripper to a high-speed industrial robotic arm (with speeds of up to 8000 mm/s), a high factor of safety was selected to prevent failures and ensure safety in the working environment. However, certain parts, such as the boxes for electrical components and the actuation system, were designed without stress analysis, as they were not subjected to significant forces. Also, during the stress analysis of various components, it was observed that the top part (#8) experienced the highest stress compared to others, attributable to factors such as bearing the weight of the entire mechanism and employing minimal thickness for this part.

Furthermore, to minimize the total weight of the mechanism, a topology study was conducted to identify areas of each part where material could be removed while maintaining the same stress and load capacities. The studies were performed considering a maximum load of 45N, which is 1.5 times the maximum payload of the robotic arm. The results of the topology study were then used to refine and validate the design through FEA.

The design process involved creating, analyzing, and improving the design using FEA and topology studies. The outcomes of these studies for the top part (#8) are presented in Figure 20, Figure 21 and Figure 22.

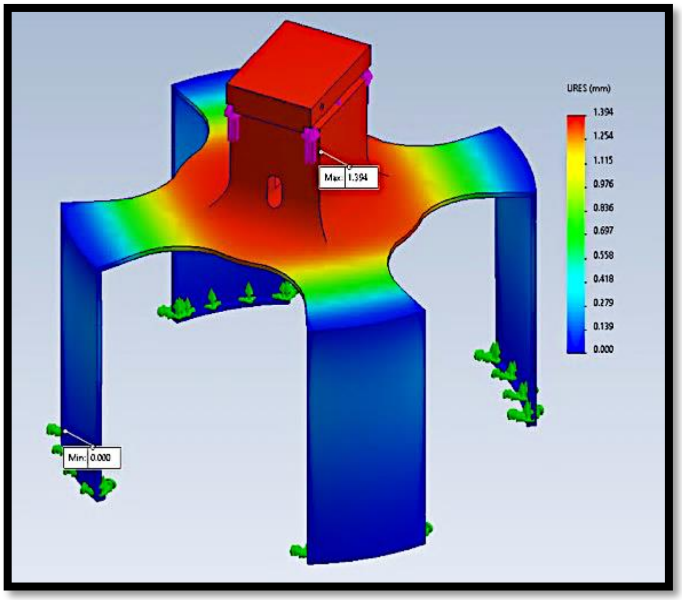

Figure 20: FEA static analysis of the part TOP.

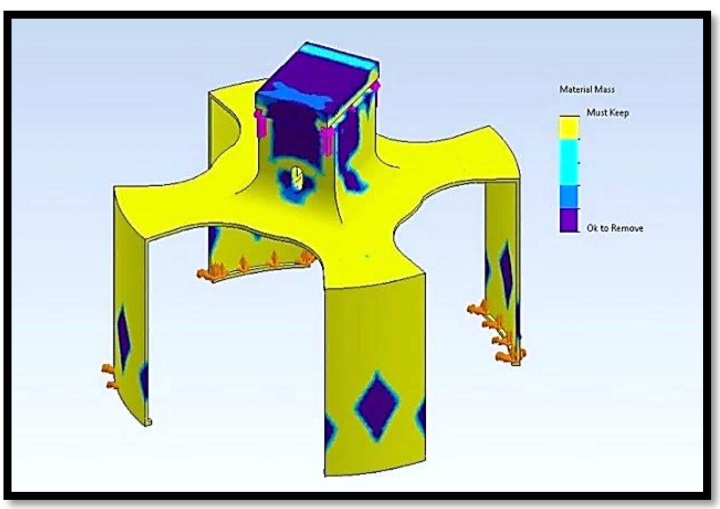

Figure 21: Topology study of the part TOP.

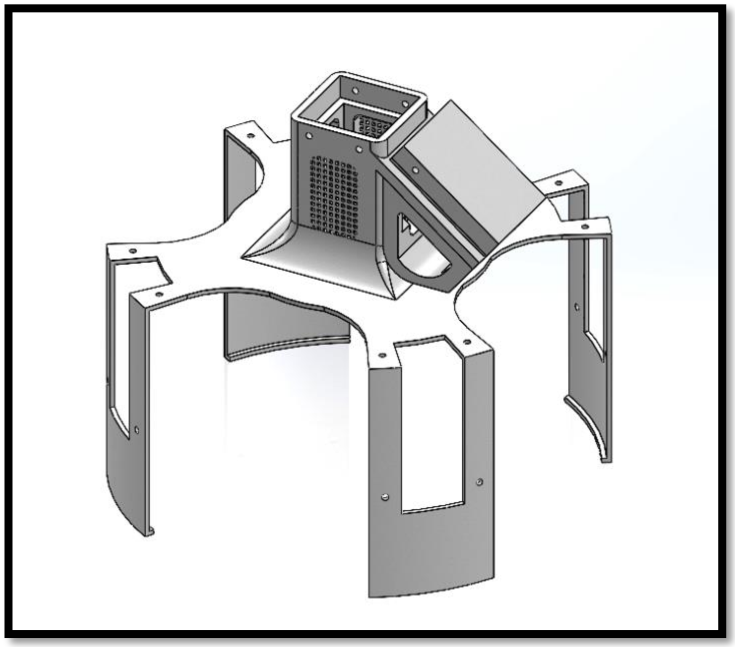

Figure 22: Improved TOP considering analytical studies.

4.5 Motion Analysis

This section of the paper discusses the motion analysis part after the initial design process is complete. The motion analysis is performed to determine if the design can achieve the desired range of motion or if there is something that needs to be changed. It is performed also to calculate the torque required to achieve the motion. With limited ability to facilitate an actual condition, the simulation for motion study is done using available aluminum contact settings. The chart below shows the torque required to rotate the mechanism for the desired action.

Motion analysis is performed under two different conditions, the one where the top rotating plate is not constrained for its vertical motion and vice-versa. The first condition resulted in undesired vertical motion of the top plates due to imbalanced moments seen on the shutter parts as depicted in the figure below. The problem occurred due to the actuation force being applied only to the top part which created a moment about a point somewhere in the lower portion of the part.

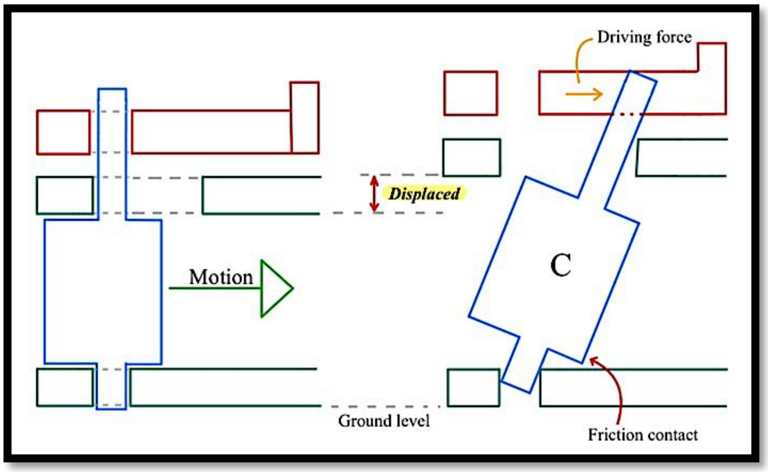

Figure 23: Visual representation of the motion study for non-constrained vertical motion of the curved plate.

It is concluded that the top plate is needed to be constrained for vertical displacement to maintain the smooth planar motion of the shutter. Hence, the top plate is constrained to its position for the second study to replicate more realistic conditions for better results.

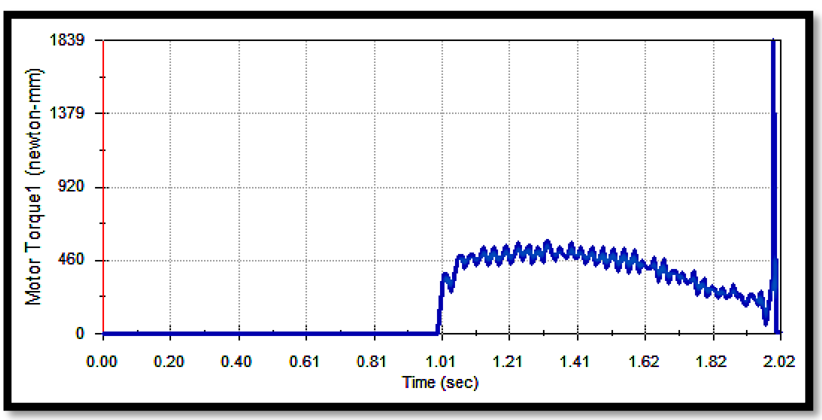

Figure 24: Motion study results for the torque required to actuate the system.

The chart for the torque applied (Figure 24) showed that the maximum torque required to create the desired motion is about 575 N-mm. Needless to say, all the existing frictional factors contribute to high resistance to motion resulting in a high torque requirement. The rise in the torque at the end shown in the chart above is just because it hit the point where there is no room for motion. In this paper, the prototyping is done using 3-D printed ABS plastics that don't have smooth textured surfaces. Even with sanding, it is very hard to achieve the required smoothness also at the cost of precision. Hence, a little sanding and NGLI grade 2 grease are used to minimize friction as much as possible. Also, the motor with a 40:1 gearbox is used to generate enough torque for achieving the required motion.

Chapter 5: Smart Shelf with Load Cells and Touchscreen Interface

The smart shelf envisioned in this project is the platform that works as the on-site component of the system which will incorporate multi-interface with sensor and image processing data. It should be able to generate and communicate the load cell information and LED light information for the image processing camera. Users, after completion of this project, would be able to use VR (Virtual Reality) headsets and communication platforms such as mobile application software to see, choose, and pick the objects virtually. On implementation of haptic sensors in gripper pins on-site, and haptic feedback gloves off-site can facilitate users to have an exact feel of grasping objects in real-time. Not only in grocery object handling, but this technology can also be useful in space sample collection. With the completed system, users will have three ways to choose the object,

- Collecting the objects based on the total weight (using an optimization method)
- Collecting the objects based on the number of object (randomly)
- Collecting the specific items (using camera and image processing system)

In this stage of the project, the focus was only on designing the smart shelf with the ability of displaying the weight of objects placed on it in real-time using load cells allowing the ability to feed data to the optimization algorithm. The weight is shown on a Thin Film Transistor (TFT) touch screen, which can also receive touch input for controlling the light-guiding system for image processing technology. The technology resonates with RFID-based shelves in terms of some applications, but it can provide more real-time information without any pre-shelf work. The chapter will cover the part's dimensions, working process, electrical components, and other related topics.

5.1 Parts and Specification of the Mechanism

As this part of the system works as the shelf for the object, it is a platform box as it sounds. The box is designed using CAD software. It consists of the 9 sub-platforms, designed to accommodate up to 8 different items as well as load cells for the prototype version. Every sub-platform is equipped with a 1kg load cell intended for any general grocery store items. The shelf is 36 cm x 36 cm x 6.7cm in dimension. It is a hollow box with a room inside to accommodate load cells and wiring connections. Each sub-platform has a circular pattern cut on the top for the load cell to reach out to its object platform. The circular cut is 7.128 cm in diameter.

Other important parts are the base stand for the load cell and the cup as the object platform. The load cell stand is around 1.85 cm x 4.65 cm x 3.26 cm in dimension whereas the cup is 6.68 cm x 6.68 cm x 2.7 cm. It is carefully considered that the cup on the load cell does not touch the top face of the respective sub-platform to avoid a false weight reading. The shelf also consists of the connection brackets and the support columns for the top lid.

TABLE IV: Parts, Dimensions, Part Numbers, and Quantities; In detail in Appendix E

Parts	Dimensions (cm)	Part Number	Quantity
Middle Top	12 x 12 x 2.9	1	3
Center Top	12 x 12 x 2.9	2	1
Corner Top	12 x 12 x 2.9	3	4
Base	18 x 18 x 2.9	4	4
Load Cell Stand	1.85 x 4.65 x 3.26	5	8
Load Cells	8 x 1.27 x 1.27	6	8

Object Platform	6.68 x 6.68 x 2.72	7	8
Closed Top	12 x 12 x 2.9	8	1
Screen Base	20.4 x 13.9 x 8	9	1
Screen Cover	20.4 x 11.78 x 1	10	1

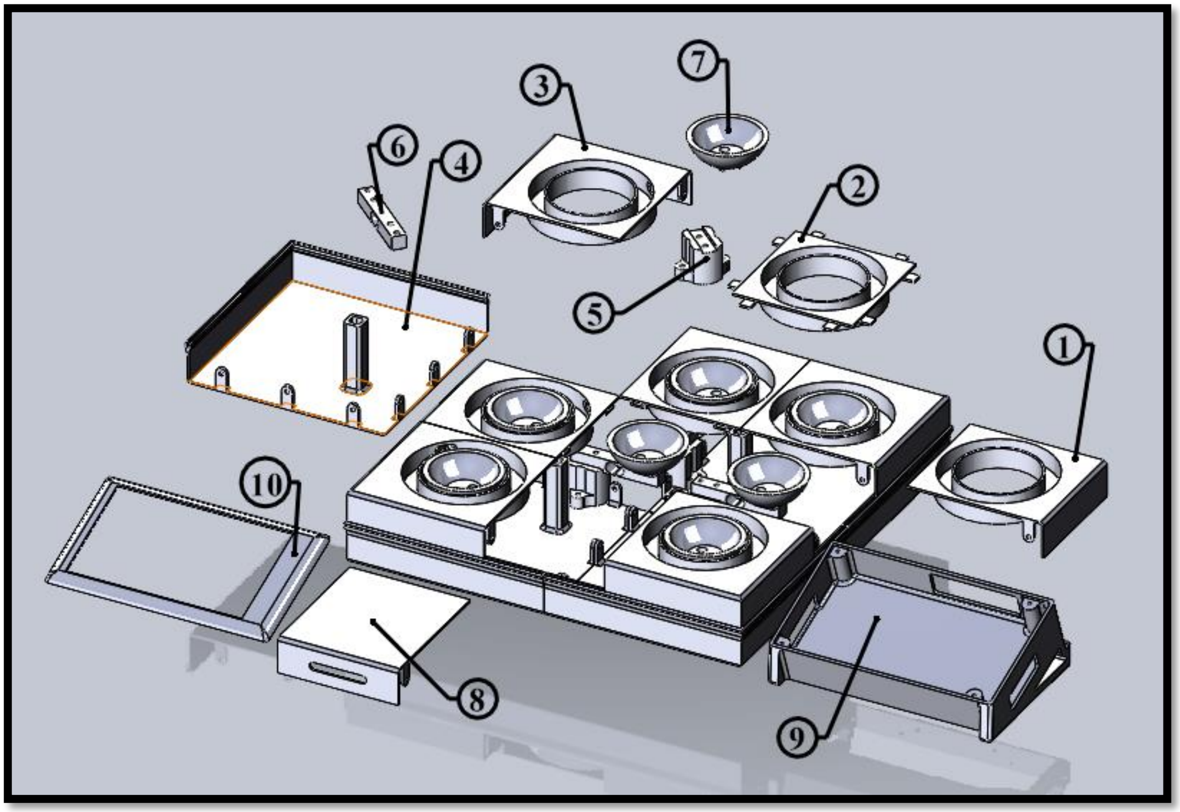

Figure 25: Parts assembly (Exploded view)

5.1.1 Mechanical Component – Load Cell

This system is designed to be smart and has only one mechanical component, unlike the grasping mechanism which has various parts such as springs, bearing balls, and kinematic designs. This system only utilizes a 1 kg load cell.

Load cells have long been used to sense and measure force and torque. When properly designed and used, they are very accurate and reliable sensors [37].

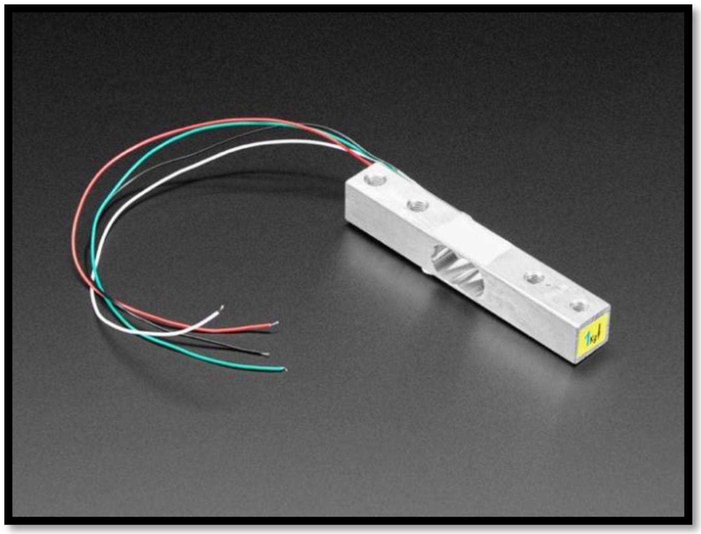

Figure 26: Load cell [38]

A load cell, basically, is a transducer that can translate pressure or force into an electrical signal [38]. Although there are three main types of load cells: hydraulic load cells, pneumatic load cells, and strain gauge load cells, the one that is used in this project is the strain gauge one. The strain gauge load cell senses the force by measuring the deformation of the strain gauge. Strain gauge load cells are available for different sensing ranges, out of which a 1 Kg load cell is used following the thumb rule of rated weight to be double of maximum measuring weight as most of the fruits, vegetables, and other grocery store items are less than or around 500 grams.

In strain gauge load cells, the cell is arranged in a "Z" arrangement so that torque can be applied to the bar while the cell's four strain gauges: two monitoring compression and two tension, measure the bending distortion. It is easy to precisely measure the tiny variations in resistance from the strain gauges when these four strain gauges are arranged in a Wheatstone bridge arrangement [38].

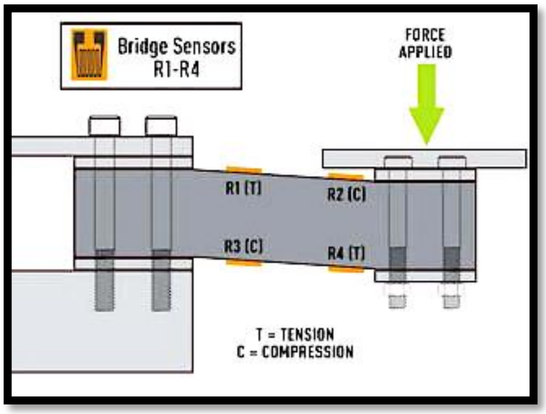

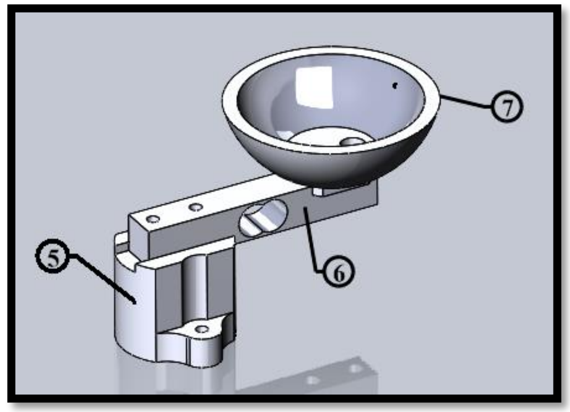

Figure 27: Strain gauge load cell setup [39]

Figure 28: Actual load cell setup

A stain gauge is a device that measures the electrical resistance values that vary with changes in strain values. It has a varying sensitivity to strain that can be expressed by gauge factor (GF). As accurate as it can be for different applications, its measurement values are hardly a whole number. For instance, very small changes like 0.12 Ω are not even detectable by most devices. This is where an amplifier such as HX711 comes to use. The HX711 Amplifier is a mechatronic component that amplifies the electrical values to the level where they can be detected and easily read in numerical values.

Figure 29: HX711 Amplifier [40]

5.1.2 Material Selection

Examining and scrutinizing this facet of the project proves to be relatively straightforward. As the various components only experience minimal exposure to external forces, there exists a plethora of options to select from. Notably, the components within this category are fabricated using PLA plastic, a material known for its durability and lightness. Nevertheless, the load cell typically consists of either aluminum, alloy steel or stainless steel [39].

5.1.3 Electrical Components

This section also utilizes a microcontroller, like the grasping mechanism. As this section of the project is heavier on electronic components, there are other mechatronic components used for human-machine interface development. Please refer to the table below for a list of electrical components used in this section.

TABLE V: Electronics, their Quantities, and Sources

Component	Quantity	Component No.
1 Kg Strain Gauge Load Cell	8	1
HX711 Amplifier	8	2
Arduino Mega 2560 Rev3	1	3
TFT LCD Mega Shield V2.2	1	4
7” TFT LCD Screen 800x480	1	5

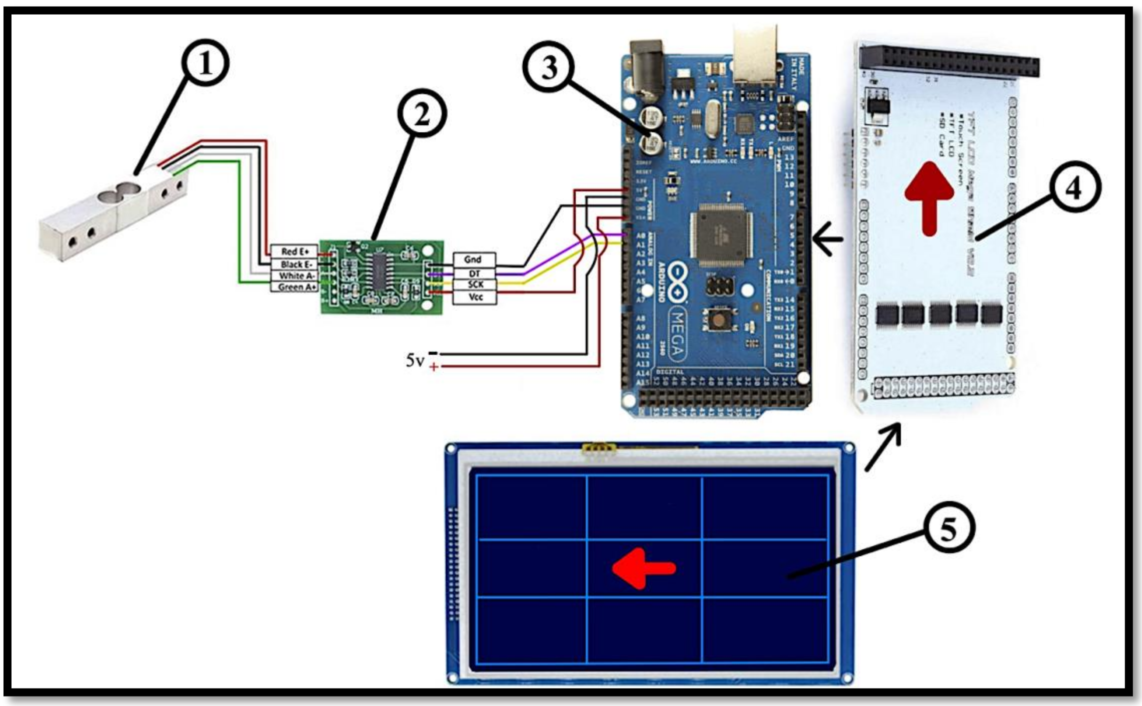

Figure 30: Electrical circuit diagram (only one of the load cells (#1) is shown instead of eight in total) [41][42]

The figure above visually represents the electrical/wiring schematic for this section. Load cells (#1) are connected to the Arduino Mega (#3) via HX711 Amplifiers (#2). It is important to understand that each load cell is connected to different HX711 Amplifiers. As depicted in Figure 29, HX711 has pins on one end to be connected to the load cell and pins on the other end to the Arduino.

Before connecting load cells to the amplifiers, they are tested for any defect that might generate false data/reading. It is done by measuring the input and output impedance. Impedance values measured should be equal or near to the value mentioned in the datasheet of the load cell. In this case, it is 1130 Ohm and 1000 Ohm respectively where input impedance is measured between black and red, while the output impedance is measured between green and white wires coming out of the load cells.

Finally, load cells are connected to the HX711 Amplifiers as depicted in the figure above. Red, Black, White, and green wires are connected to E+, E-, A+, and A- respectively. From the other end, GND and the VCC are connected to the GND and 5V, while DT and SCK are connected to the A0 and A1 (analog pins) of the Arduino respectively. Similarly, the remaining seven load cells are connected using common GND and 5V of the Arduino while their DTs and SCKs are connected to A2 through A15 pins on Arduino. With this, the load cell is ready to generate data by running the program provided in Appendix B: Arduino code for smart shelf.

On the other hand, the TFT LCD Mega Shield V2.2 (#4) is attached to the top of the Arduino Mega that creates a platform for a 7” TFT LCD Screen 800x480 (#5) physically and electrically. The screen is connected to the Arduino shield by aligning the bold arrows in Figure 30 in the same orientation. After completing the electric circuit, a program is created and implemented to extract and display load cell data.

5.2 Touchscreen Interface

In this project, the touchscreen interface plays a crucial role as it determines the system's efficiency and smartness. The electronic components are set up to use the Arduino controller for programming the screen interface. The process involves iterative program coding to establish the interface layers. Interface layers refer to the order of display and events that follow a touch action. The controller board will be used with a touchscreen to send instructions to light up the LED lights, indicating the user's selection which also will facilitate the image processing system. The home screen of the touch screen is displayed in Figure 31, which presents eight options to choose from. The weights of each object are shown in their respective boxes, enabling customers to make informed decisions. The program allows the customer to submit a touch command, which the system promptly acts upon. Similarly, the working prototype is displayed in Figure 32.

Figure 31: Home screen of the touchscreen interface

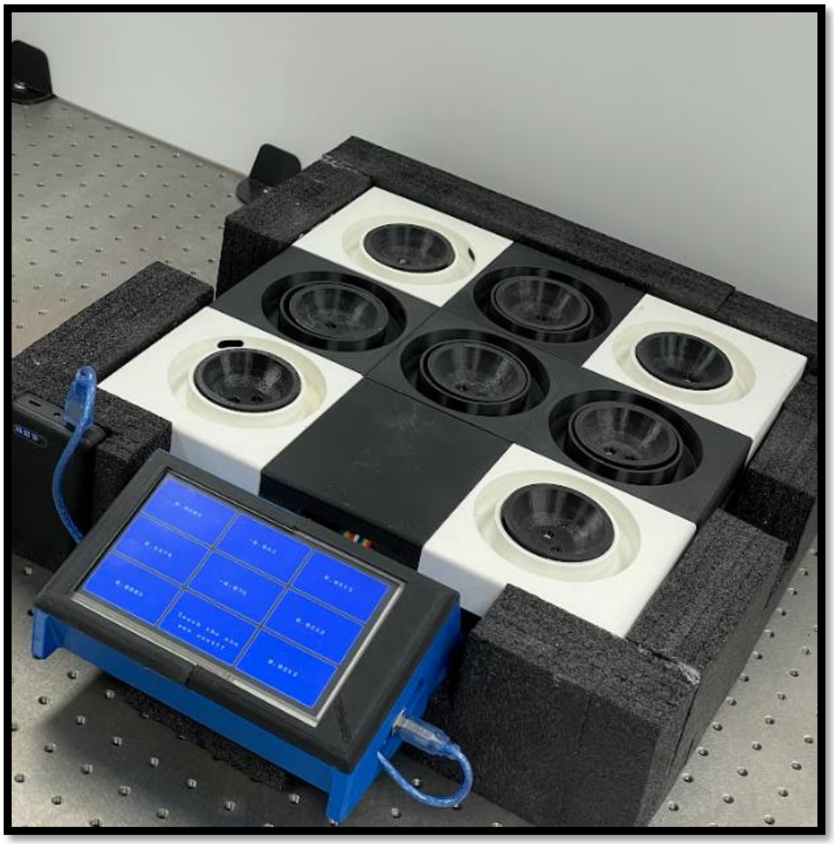

Figure 32: Prototype of the smart shelf

Chapter 6: Results, Discussions, and Conclusions

This project uses a novel grasping mechanism with minimum actuation and a smart shelf with a touchscreen interface. The design is created considering every possible factor that can be improved. It is completely scalable as per the application which showcases another aspect of novelty in design. Two sub-sections of the project combined in a system can form an advanced packaging system that can uplift the back-end business-to-business packaging or front-end business-to-customer packaging experience. While a cohesive system sounds interesting, both sub-designs have their essence in separate applications too. The grasping mechanism can further be used in different sectors such as beverage bottling facilities, autonomous navigation robots [43], space exploration and sampling robots [44], and so on. Similarly, a smart shelf with a touchscreen interface can be used in large fruit-shipping facilities, fish markets, and so on.

The grasping mechanism inspired by the camera shutter brought transformed the motion using slot and slider mechanisms. It transformed circular motion into a linear slide to press against the target object. Besides, the smart interface system used IoT devices along with the load cell to allow customers to make informed purchase decisions.

Thus, the prototype of the presented design was created using 3D-printed parts out of ABS plastic. Besides, all the parts that are engineered to work, some parts are designed to accommodate the controller, motor driver, and battery for powering the actuation system. The actuation system is designed and enclosed to hide all messy wire networks & electronics and to allow the user to use the whole gripper like a sophisticated product off the shelves.

The grasping test is performed by grasping various-sized and shaped objects to validate the design. The gripper has two major working stages: closing to grasp & opening to release.

As the motor receives command via IR receiver, the motor rotates to close the shutters so that the pistons with springs are pressed in by the target object in the closing to grasp stage.

Opening to release is just the stage where motion occurs that is exactly the reverse of the previous stage.

The final version of the model is depicted in Figure 33 (without electronics), while the real-life prototype is shown in Figure 34.

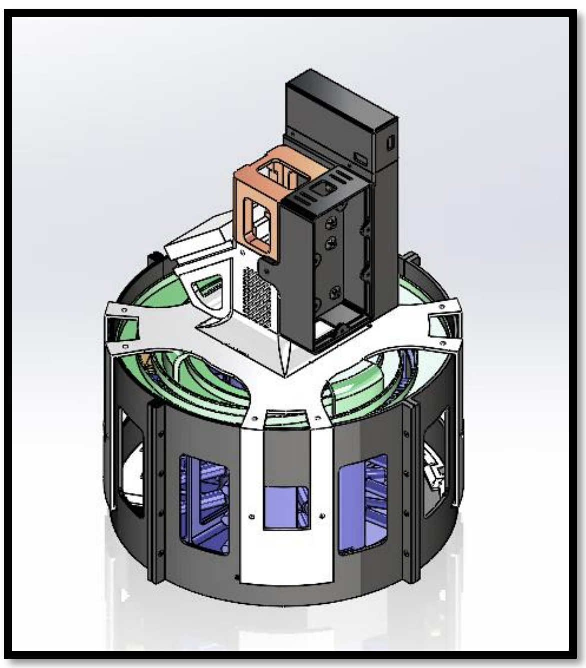

Figure 33: Whole design assembly (Excluding electronics and actuation system).

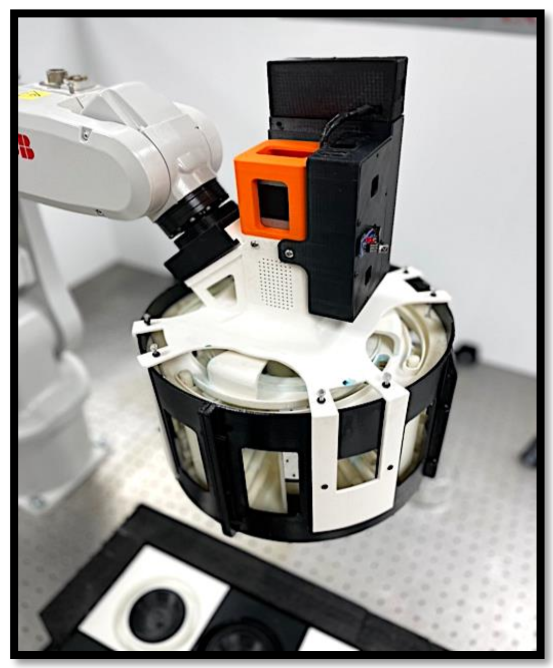

Figure 34: Actual prototype attached to the robotic arm.

6.1 Robotic Arm Path Planning for Efficient Task Execution

The initial stage of achieving successful grasping involves ensuring that the gripper possesses the capability to reach the intended target object. Consequently, a manipulation system becomes essential for executing the grasping action and subsequently transporting the object across diverse locations. Additionally, to facilitate the gripper's movement between task points, it becomes imperative to analyze the robot's kinematics and devise an appropriate path plan for the end-effector. For this specific project, a small-scale industrial robot, ABB IRB120 has been selected as the manipulation system based on the project's requirements.

In many cases, grasping operations are performed as part of a series of pick-and-place actions. To accomplish this, the robotic arm needs to be programmed to move and reach various target points. However, the robots can have limitations to reach the target points due to the loss of one or more degrees of freedom, which are referred to as singularities in robotics.

Singularity occurs when the robot's tip is unable to move or generate velocities in specific directions. This condition is determined by evaluating the Jacobian Matrix, represented as $J_{(\theta)}$. In the case of a serial 6-DOF (Degree of Freedom) robot, singularity arises when the determinant of the Jacobian matrix becomes zero, as indicated by the condition in Equation (14). It is important to know that the expression of the Jacobian matrix can be in either the world frame or the body frame, while the singularity configuration remains independent of the chosen reference frame.

For a serial 6-DOF robotic arm, there exist several cases or conditions of singularity, and this study focuses on the five most common ones.

$$\det\left(J_{s(\theta)}\right) = 0 \;\rightarrow\; rank\left(J_{s(\theta)}\right) < 6 \tag{14}$$

Case I: Two collinear joints. In this case, when there are two joints with their z-axis in the same direction, the robotic end-effector cannot move at least in certain directions.

Case II: Three coplanar and parallel revolute joints.

Case III: Four revolute joints intersecting at a common point.

Case IV: Four coplanar revolute joints.

Case V: Six revolute joints intersecting the common line.

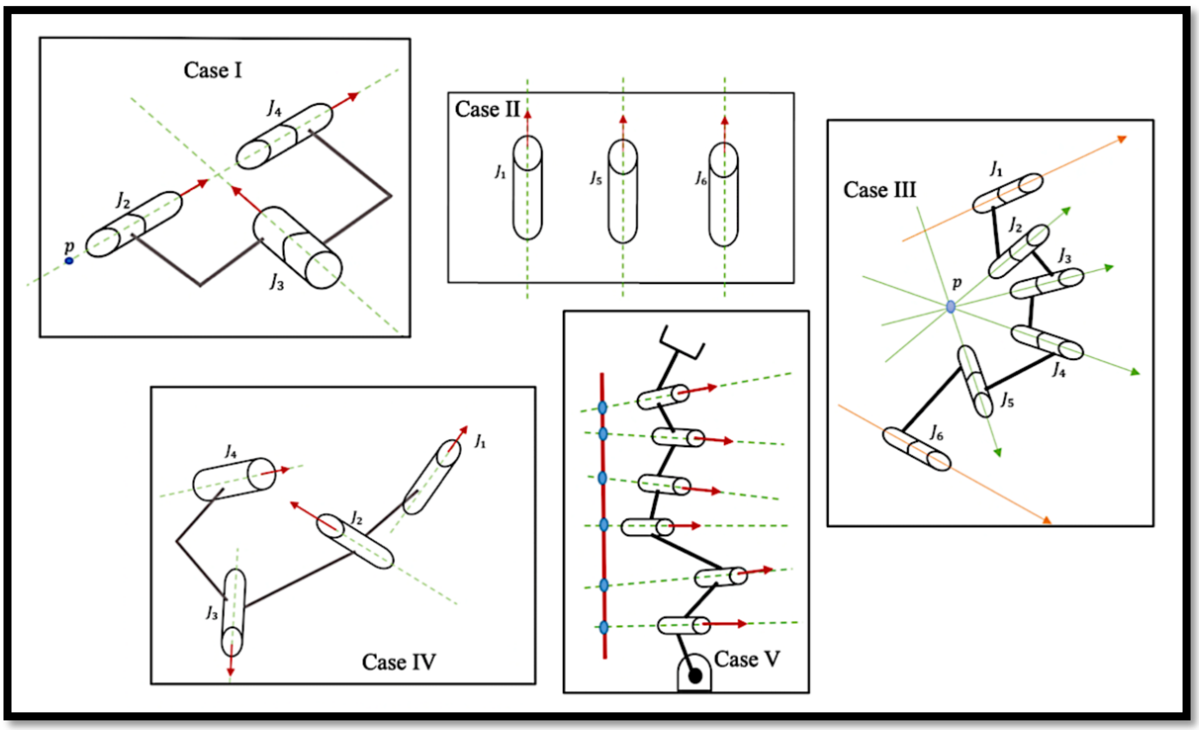

Figure 35: Five cases of singularity for a serial 6-DOF robotic manipulator

During the task definition process for testing the gripper with the robotic manipulator, careful consideration is given to ensure that none of the tasks fall into the singularity configuration of the robotic arm. Additionally, to avoid encountering any singularity positions between consecutive tasks, an interpolation technique is employed where 10 points are defined. The singularity of these points is assessed by calculating the determinant of the Jacobian Matrix to verify that none of them equals zero. This analysis is conducted to identify any potential singular or near-singular conditions before the final testing phase.

The Jacobian matrices for all the joints and transformations of the ABB IRB120 robot are already defined in [45]. Furthermore, a D-H parameter table is constructed based on the ABB IRB 120, as depicted in Figure 36. This information generates rotational Jacobian matrices using Equation (15).

$$J_R = \frac{\partial \omega_n}{\partial \dot{q}} \tag{15}$$

Where J_R is the rotational Jacobian, ω_n is the joint angular velocity and q is the joint angle. Similarly, the translational Jacobian matrix is created using a similar method as the rotational Jacobian matrices. However, it focuses on the transformation of the joint frames. Using the set of codes provided in Appendix C: MATLAB code for calculating determinant of Jacobian, the determinant and rank of the matrices associated with the robot joints are computed for ten interpolated points configurations along the defined path for grasping. The results are shown in TABLE VI.

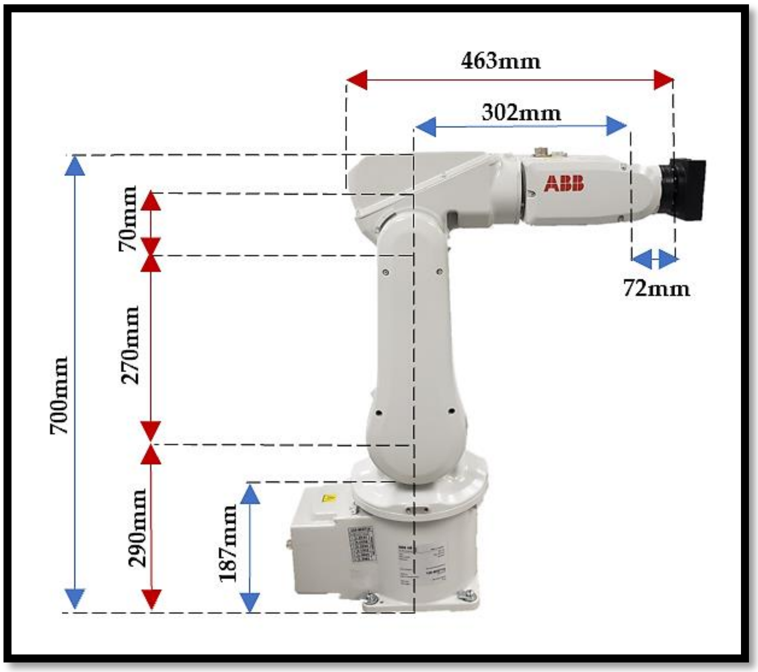

Figure 36: Robotic-arm joint and links breakdown for D-H parameter.

TABLE VI: Determinant (Det.) & Rank of the Jacobian from MATLAB®

Joint Angle Orientation: q1, q2, q3, q4, q5, q6 in degrees	**Det.**	**Rank**
1.98, 3.10, -9.94, -3.12, 56.79, 6.58	-0.0196	6
-26.19, 20.20, -27.12, 17.75, 59.85, -26.26	-0.0198	6
-26.19, 18.38, 6.15, 30.32, 31.47, -43.63	-0.0152	6
-26.19, 22.05, 12.92, 42.40, 43.01, -57.16	-0.0186	6
-26.19, 19.09, 8.08, 32.67, 29.24, -46.35	-0.0143	6
-26.19, 18.49, -17.33, 19.31, 52.86, -29.06	-0.0118	6
15.60, 12.09, -8.52, 15.09, 48.65, 25.56	-0.0199	6
39.66, 35.63, -39.88, -28.25, 64.97, 48.83	-0.0144	6

39.66, 34.93, -6.41, -44.15, 38.01, 73.47	-0.0172	6
39.66, 38.77, -2.22, -52.66, 32.66, 83.87	-0.0159	6

The analysis presented in TABLE VI confirms that the selected path for the manipulator is devoid of singularities. The robotic arm has been programmed based on this path to autonomously execute pick-and-place tasks for a diverse range of objects. Several distinct objects were employed during the grasping test, all of which were successfully grasped by the robot. The successful outcome of the test for grasping various objects with different shapes, sizes, and textures is visually demonstrated in Figure 37 below.

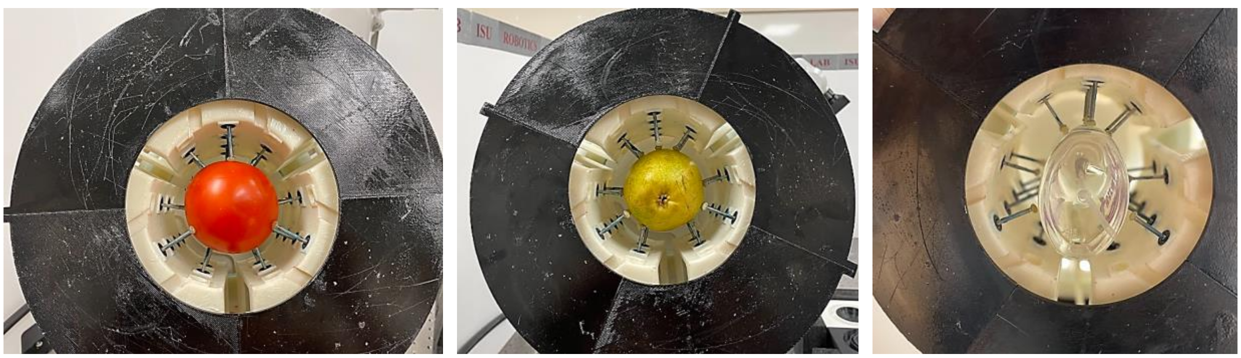

(a) **(b)** **(c)**

Figure 37: Grasping (a) a tomato, (b) a guava, and (c) a hand-sanitizer bottle (all bottom view of the gripper)

6.2 Weight Data Extraction and Display

This section of the paper discusses the ability of the smart shelf to display the weight data on the touchscreen display using load sensors. As depicted in the figure below, the object is placed on the cup-like section of the shelf to display the weight of that object. Load cells are calibrated using the tare and load technique. The process also helps to determine the calibration factor that will help to measure and display the weight values. The values displayed are either zero or close to zero when no object is placed due to minor measurement errors. As shown in the figure 38, the hand sanitizer bottle's weight is 109.68 grams in the screen’s bottom left-hand corner.

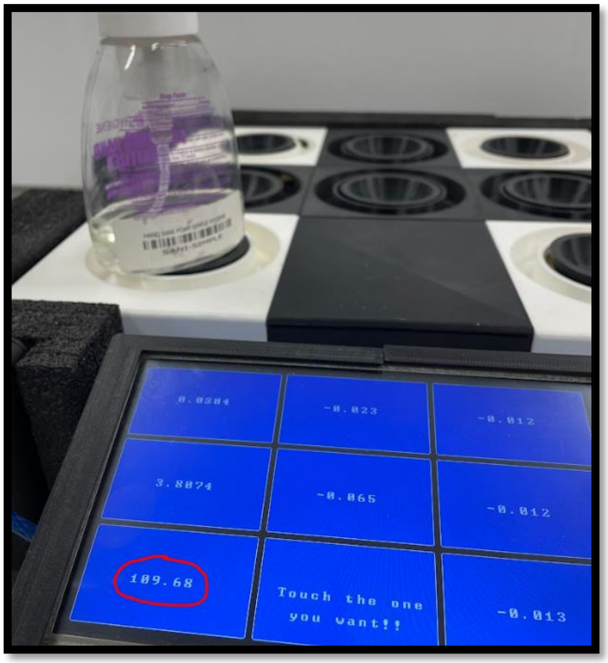

Figure 38: Smart shelf displaying the weight of the hand sanitizer bottle.

The screen can be re-programmed to desired display and interface layers. As mentioned, the application of the ring lights around each object holder will allow the system to employ image processing and machine learning abilities. Finally, the customers will be able to choose in two different manners. One with the weight information, and the second being the specific object on the shelf. Furthermore, the vision of embedding virtual reality with tactile sensors in gripper and tactile feedback gloves off-site will empower the user with virtual shopping experience.

References

[1] M. Tavakoli, L. Marques, and A. T. de Almeida, "Flexirigid, a novel two phase flexible gripper," in *2013 IEEE/RSJ International Conference on Intelligent Robots and Systems*, IEEE, 2013, pp. 5046–5051.

[2] F. Saito, T. Fukuda, and F. Arai, "Swing and locomotion control for a two-link brachiation robot," *IEEE Control Syst. Mag.*, vol. 14, no. 1, pp. 5–12, 1994.

[3] S. Anagnoste, "Robotic Automation Process-The next major revolution in terms of back office operations improvement," in *Proceedings of the International Conference on Business Excellence*, 2017, pp. 676–686.

[4] J. Dixon, B. Hong, and L. Wu, "The robot revolution: Managerial and employment consequences for firms," *Manag. Sci.*, vol. 67, no. 9, pp. 5586–5605, 2021.

[5] B. Kastan, "Autonomous Weapons Systems: A Coming Legal" Singularity"?," *U Ill JL Tech Pol*, p. 45, 2013.

[6] Z. Samadikhoshkho, K. Zareinia, and F. Janabi-Sharifi, "A brief review on robotic grippers classifications," in *2019 IEEE Canadian Conference of Electrical and Computer Engineering (CCECE)*, IEEE, 2019, pp. 1–4.

[7] H. Lasi, P. Fettke, H.-G. Kemper, T. Feld, and M. Hoffmann, "Industry 4.0," *Bus. Inf. Syst. Eng.*, vol. 6, pp. 239–242, 2014.

[8] "IBISWorld - Industry Market Research, Reports, and Statistics." https://www.ibisworld.com/default.aspx (accessed Mar. 20, 2023).

[9] P. V. P. Reddy and V. Suresh, "A review on importance of universal gripper in industrial robot applications," *Int J Mech Eng Robot Res*, vol. 2, no. 2, pp. 255–264, 2013.

[10] F. Sherwani, M. M. Asad, and B. S. K. K. Ibrahim, “Collaborative robots and industrial revolution 4.0 (ir 4.0),” in *2020 International Conference on Emerging Trends in Smart Technologies (ICETST)*, IEEE, 2020, pp. 1–5.

[11] P. Dario, E. Guglielmelli, B. Allotta, and M. C. Carrozza, “Robotics for medical applications,” *IEEE Robot. Autom. Mag.*, vol. 3, no. 3, pp. 44–56, 1996.

[12] Y. Hao *et al.*, “Universal soft pneumatic robotic gripper with variable effective length,” in *2016 35th Chinese control conference (CCC)*, IEEE, 2016, pp. 6109–6114.

[13] Y. Zheng, G. Lei, M. Zhang, and Q. Che, “Mechanical design and analysis of a gripper for non-cooperative target capture in space,” *Adv. Mech. Eng.*, vol. 10, no. 11, p. 1687814018810649, 2018.

[14] D. Zhang, B. Cheng, and Z. Yue, “Design and analysis of cable-driven mechanical gripper for complex manipulation,” in *Journal of Physics: Conference Series*, IOP Publishing, 2020, p. 022048.

[15] A. Mo and W. Zhang, “A novel universal gripper based on meshed pin array,” *Int. J. Adv. Robot. Syst.*, vol. 16, no. 2, p. 1729881419834781, 2019.

[16] Y. Okatani, T. Nishida, and K. Tadakuma, “Development of universal robot gripper using MRα fluid,” in *2014 Joint 7th International Conference on Soft Computing and Intelligent Systems (SCIS) and 15th International Symposium on Advanced Intelligent Systems (ISIS)*, IEEE, 2014, pp. 231–235.

[17] M. Fujita, S. Ikeda, T. Fujimoto, T. Shimizu, S. Ikemoto, and T. Miyamoto, “Development of universal vacuum gripper for wall-climbing robot,” *Adv. Robot.*, vol. 32, no. 6, pp. 283–296, 2018.

[18] E. Ramirez-Asis *et al.*, “Smart logistic system for enhancing the farmer-customer corridor in smart agriculture sector using artificial intelligence,” *J. Food Qual.*, vol. 2022, 2022.

[19] C. Technology, “THE ‘SMARTIFICATION’ OF EVERYTHING,” *Medium*, Nov. 08, 2017. https://medium.com/@CodeBlueTechnology/the-smartification-of-everything-224042e275e1 (accessed Mar. 21, 2023).

[20] R. Li, T. Song, N. Capurso, J. Yu, J. Couture, and X. Cheng, “IoT applications on secure smart shopping system,” *IEEE Internet Things J.*, vol. 4, no. 6, pp. 1945–1954, 2017.

[21] S. Gupta, A. Kaur, A. Garg, A. Verma, A. Bansal, and A. Singh, “Arduino based smart cart,” *Int. J. Adv. Res. Comput. Eng. Technol.*, vol. 2, no. 12, 2013.

[22] O. Kabadurmus, Y. Kayikci, S. Demir, and B. Koc, “A data-driven decision support system with smart packaging in grocery store supply chains during outbreaks,” *Socioecon. Plann. Sci.*, vol. 85, p. 101417, 2023.

[23] S. Kucuk and Z. Bingul, *Robot kinematics: Forward and inverse kinematics*. INTECH Open Access Publisher London, UK, 2006.

[24] E. Appleton and D. J. Williams, *Industrial robot applications*. Springer Science & Business Media, 2012.

[25] E. Mach, *History and Root of the Principle of the Conservation of Energy*. Cambridge University Press, 2014.

[26] C. Mavroidis and M. Beddows, “A spatial overconstrained mechanism that can be used in practical applications,” in *Proceedings of the 5th Applied Mechanisms and Robotics Conference, Cincinnati, OH*, 1997.

[27] B. Li, Y. Li, W. Ge, X. Zhao, and Y. Yang, "Dynamics analysis of a novel over-constrained three-DOF parallel manipulator," in *2014 IEEE International Conference on Mechatronics and Automation*, IEEE, 2014, pp. 828–833.

[28] K. Scott and A. Perez-Gracia, "Design of a prosthetic hand with remote actuation," in *2012 Annual International Conference of the IEEE Engineering in Medicine and Biology Society*, IEEE, 2012, pp. 3056–3060.

[29] "PKP245D23A2-R2E / PLE40-40B / P00027, Stepper Motor with Planetary Gearhead (40:1)," *Oriental Motor USA*. https://catalog.orientalmotor.com/item/42mm-frame-stepper-motors/42mm-pkp-series-2-phase-bipolar-stepper-motors/pkp245d23a2-r2e-ple40-40b-p00027 (accessed May 19, 2023).

[30] "Passivated 18-8 Stainless Steel Phillips Flat Head Screw, M3 x 0.5 mm Thread, 60 mm Long | McMaster-Carr." https://www.mcmaster.com/92010A817/ (accessed Jun. 27, 2023).

[31] P. Wegrowski, W. Thomas, J. Lemrick, and T. Deemyad, "Advanced Folding Robotic Arm for Quadcopters," in *2022 Intermountain Engineering, Technology and Computing (IETC)*, IEEE, 2022, pp. 1–6.

[32] "H-Bridge with L298N motor driver - parts submit," *fritzing forum*, Nov. 13, 2019. https://forum.fritzing.org/t/h-bridge-with-l298n-motor-driver/7711 (accessed Jun. 29, 2023).

[33] "Download HD Big Image - Push Button Switch Png Transparent PNG Image," *NicePNG.com*. https://www.nicepng.com/maxp/u2q8u2i1i1u2y3w7/ (accessed Jun. 29, 2023).

[34] V. Badami, "A tour of the Arduino UNO board," *HackerEarth Blog*, Oct. 21, 2016. https://www.hackerearth.com/blog/developers/a-tour-of-the-arduino-uno-board/ (accessed Jun. 29, 2023).

[35] B. on Tech, "Tutorial 9 - Control Arduino with remote (HX1838 VS1838)," *IYYOoyjQS-8*. https://arduino-tutorials.net/tutorial/control-arduino-with-ir-receiver-and-remote (accessed Jun. 29, 2023).

[36] T. Deemyad, N. Hassanzadeh, and A. Perez-Gracia, "Coupling mechanisms for multi-fingered robotic hands with skew axes," in *Mechanism Design for Robotics: Proceedings of the 4th IFToMM Symposium on Mechanism Design for Robotics*, Springer, 2019, pp. 344–352.

[37] I. Muller, R. M. de Brito, C. E. Pereira, and V. Brusamarello, "Load cells in force sensing analysis--theory and a novel application," *IEEE Instrum. Meas. Mag.*, vol. 13, no. 1, pp. 15–19, 2010.

[38] S. Al-Mutlaq, "Getting started with load cells," *Conteúdo Online*, 2016.

[39] "How Does a Strain Gauge Load Cell Work? | Load Cell Central | Load Cell Central." https://www.800loadcel.com/load-cell-and-strain-gauge-basics.html (accessed Mar. 28, 2023).

[40] "AiTrip 6pcs Hx711 Weight Weighing Load Cell Conversion Module Sensors Ad Module for Arduino Microcontroller: Amazon.com: Industrial & Scientific." https://www.amazon.com/AiTrip-Weighing-Conversion-Sensors-Microcontroller/dp/B07SGPX7ZH/ref=sr_1_5?crid=32GZGH5IZSOEC&keywords=HX711&qid=1680040965&s=industrial&sprefix=hx711%2Cindustrial%2C159&sr=1-5 (accessed Mar. 28, 2023).

[41] "ShangHJ 4 Sets Digital Load Cell Weight Sensor + HX711 ADC Module Weighing Sensor for Arduino DIY Portable Electronic Kitchen Scale Kit (5kg): Amazon.com: Industrial & Scientific." https://www.amazon.com/ShangHJ-Digital-Weighing-Portable-

Electronic/dp/B09VYSHW16/ref=sr_1_4?crid=Y6ZS3K1X8NJZ&keywords=Load%2Bcell&qid=1688063557&sprefix=load%2Bcell%2B%2Caps%2C376&sr=8-4&th=1 (accessed Jun. 29, 2023).

[42] “Large 7" Inch TFT LCD Screen 800x480 SSD1963 Touch PWM AVR PC Controller Module for Arduino Max 36V High Quality Colorful Image: Amazon.com: Industrial & Scientific.” https://www.amazon.com/dp/B07KF9XXFC/ref=pe_386300_440135490_TE_item (accessed Jun. 29, 2023).

[43] R. Moeller, T. Deemyad, and A. Sebastian, “Autonomous navigation of an agricultural robot using RTK GPS and Pixhawk,” in *2020 Intermountain Engineering, Technology and Computing (IETC)*, IEEE, 2020, pp. 1–6.

[44] Y. Zhang *et al.*, “Mechanism design of an extraterrestrial regolith-boring robot,” in *2021 6th IEEE International Conference on Advanced Robotics and Mechatronics (ICARM)*, IEEE, 2021, pp. 370–375.

[45] T. L. NGOC and T. L. Nguyen, “Quasi-physical modeling of robot IRB 120 using Simscape Multibody for dynamicand control simulation,” *Turk. J. Electr. Eng. Comput. Sci.*, vol. 28, no. 4, pp. 1949–1964, 2020.

Appendices

Appendix A: Motor control code for Arduino

```
#include <IRremote.h> //it requires IRremote to be installed and included in the code
#include <Stepper.h> //Install and include the Stepper library to control the Stepper motor
const int IRpin = 2; // Pin for IR receiver
//const int stopButtonPin = 7; // Pin for stop button
const int stepsPerRevolution = 200; // Change this value to match your stepper motor

IRrecv irrecv(IRpin);
decode_results results;
Stepper myStepper(stepsPerRevolution,8,9,10,11); //define pins for the stepper motor (In actual
there is LN298 driver to control the motor)

void setup() {
  Serial.begin(9600);
  irrecv.enableIRIn();
  //pinMode(stopButtonPin, INPUT_PULLUP);
}
// voidloop below implements the switch cases for the different conditions,
//and contains the IR remote button instructions to rotate the motor in 4 different modes.
void loop() {
  if (irrecv.decode(&results)) { //decodes the IR remote instruction (i.e. button press)
    switch (results.value) {
      case 0xFFA25D: // Button "UP"
        myStepper.setSpeed(60); //sets the speed to 60 rpm
        myStepper.step(1200); //rotates the motor for 1200 steps
        break;
      case 0xFFE01F: // Button "UP"
        myStepper.setSpeed(60);
        myStepper.step(150);
        break;
      case 0xFFE21D: // Button "DOWN"
        myStepper.setSpeed(60);
        myStepper.step(-1200);
        break;
      case 0xFFA857: // Button "DOWN"
        myStepper.setSpeed(60);
        myStepper.step(-150);
        break;
    }
    irrecv.resume(); //resume to look for the IR instructions after
//implementing the previous instruction.
  }
}
```

Appendix B: Arduino code for smart shelf

```
//the code is written with the help of different insightful videos and implemented to adjust to the requirement of the project.
//the code below creates the HMI using the 7" TFT touchscreen to let the user choose the object based on the weight data transferred received from Load Cells (they are load sensors used to measure the weight of
//an object) and displayed on the screen. It draws 9 different boxes on the screen that accommodates 8 different load cells and displays data inside the corresponding boxes.
// This is C++ based code written for Arduino microcontroller

#include <UTFT.h> //install and include UTFT library
#include <HX711.h> //install and include HX711 library, it is the ampliphier for the load sensor data.
#include <URTouch.h> //install and include URTouch library
#include <URTouchCD.h> //install and include URTouchCD library
#include <UTFT_Buttons.h> //install and include UTFT_Buttons library

//Remember each and every library included may not be required, they are all included to make things work just in case. Please check if you require the library.

// Define the pins for the LCD screen and HX711 load cells
#define TOUCH_ORIENTATION LANDSCAPE
#define HX711_DOUT_1 A15
#define HX711_SCK_1 A14
#define HX711_DOUT_2 A13
#define HX711_SCK_2 A12
#define HX711_DOUT_3 A11
#define HX711_SCK_3 A10
#define HX711_DOUT_4 A9
#define HX711_SCK_4 A8
#define HX711_DOUT_5 A7
#define HX711_SCK_5 A6
#define HX711_DOUT_6 A5
#define HX711_SCK_6 A4
#define HX711_DOUT_7 A3
#define HX711_SCK_7 A2
#define HX711_DOUT_8 A1
#define HX711_SCK_8 A0

int led = 13;
int button1on = 0;
int x, y;

int interval = 1;
unsigned long previousMillis = 0;
```

```
int previoussecs = 0;
int currentsecs = 0;

int bg[] = {
  0, 0, 255
};

int fg[] = {
  255, 255, 255
};

UTFT myGLCD(CTE70, 38, 39, 40, 41);  //ITDB50
URTouch myTouch(6, 5, 4, 3, 2);

extern uint8_t BigFont[];
extern uint8_t SevenSegNumFont[];

// Initialize the HX711 library with the correct pins and calibration factor
HX711 Loadcell_1;
HX711 Loadcell_2;
HX711 Loadcell_3;
HX711 Loadcell_4;
HX711 Loadcell_5;
HX711 Loadcell_6;
HX711 Loadcell_7;
HX711 Loadcell_8;

float calibration_factor_1 = 1069.0;
float calibration_factor_2 = 1069.0;
float calibration_factor_3 = 1069.0;
float calibration_factor_4 = 1069.0;
float calibration_factor_5 = 1069.0;
float calibration_factor_6 = 1065.0;
float calibration_factor_7 = 1050.0;
float calibration_factor_8 = 1065.0;


void drawButtons() {
  // put your setup code here, to run once:
  myGLCD.setColor(bg[0], bg[1], bg[2]);

  myGLCD.fillRoundRect(10, 10, 260, 155);
  myGLCD.fillRoundRect(270, 10, 520, 155);
  myGLCD.fillRoundRect(530, 10, 780, 155);

  myGLCD.fillRoundRect(10, 165, 260, 310);
```

```
  myGLCD.fillRoundRect(270, 165, 520, 310);
  myGLCD.fillRoundRect(530, 165, 780, 310);

  myGLCD.fillRoundRect(10, 320, 260, 465);
  myGLCD.fillRoundRect(270, 320, 520, 465);
  myGLCD.fillRoundRect(530, 320, 780, 465);

  myGLCD.setColor(fg[0], fg[1], fg[2]);
  myGLCD.drawRoundRect(10, 10, 260, 155);
  myGLCD.drawRoundRect(270, 10, 520, 155);
  myGLCD.drawRoundRect(530, 10, 780, 155);

  myGLCD.drawRoundRect(10, 165, 260, 310);
  myGLCD.drawRoundRect(270, 165, 520, 310);
  myGLCD.drawRoundRect(530, 165, 780, 310);

  myGLCD.drawRoundRect(10, 320, 260, 465);
  myGLCD.drawRoundRect(270, 320, 520, 465);
  myGLCD.drawRoundRect(530, 320, 780, 465);

  //myGLCD.print(" Cell 1", 20, 70);
  //myGLCD.print(" Cell 3", 20, 235);
  //myGLCD.print(" Cell 4", 20, 390);

  //myGLCD.print(" Cell 5", 280, 70);
  //myGLCD.print(" Cell 2", 280, 235);
  myGLCD.print(" Touch the one", 280, 390);
  myGLCD.print(" you want!!", 300, 420);


  //myGLCD.print(" Cell 6", 540, 70);
  //myGLCD.print(" Cell 7", 540, 235);
  //myGLCD.print(" Cell 8", 540, 390);

  myGLCD.setBackColor(0, 0, 255);
  myTouch.InitTouch();
  myTouch.setPrecision(PREC_MEDIUM);
}

void setup() {
  // Initialize the LCD screen
  Serial.begin(9600);
  myGLCD.InitLCD();

//Initial Setup
  myGLCD.InitLCD();
```

```
  myGLCD.clrScr();

  myTouch.InitTouch();
  myTouch.setPrecision(PREC_MEDIUM);

  myGLCD.setFont(BigFont);

  myGLCD.setBackColor(0, 0, 255);
  drawButtons();

  // Initialize the HX711 load cells
  Loadcell_1.begin(HX711_DOUT_1, HX711_SCK_1);
  Loadcell_1.set_scale(calibration_factor_1);
  Loadcell_1.tare();

  Loadcell_2.begin(HX711_DOUT_2, HX711_SCK_2);
  Loadcell_2.set_scale(calibration_factor_2);
  Loadcell_2.tare();

  Loadcell_3.begin(HX711_DOUT_3, HX711_SCK_3);
  Loadcell_3.set_scale(calibration_factor_3);
  Loadcell_3.tare();

  Loadcell_4.begin(HX711_DOUT_4, HX711_SCK_4);
  Loadcell_4.set_scale(calibration_factor_4);
  Loadcell_4.tare();

  Loadcell_5.begin(HX711_DOUT_5, HX711_SCK_5);
  Loadcell_5.set_scale(calibration_factor_5);
  Loadcell_5.tare();

  Loadcell_6.begin(HX711_DOUT_6, HX711_SCK_6);
  Loadcell_6.set_scale(calibration_factor_6);
  Loadcell_6.tare();

  Loadcell_7.begin(HX711_DOUT_7, HX711_SCK_7);
  Loadcell_7.set_scale(calibration_factor_7);
  Loadcell_7.tare();

  Loadcell_8.begin(HX711_DOUT_8, HX711_SCK_8);
  Loadcell_8.set_scale(calibration_factor_8);
  Loadcell_8.tare();

}

void loop() {
```

```
  // Read the weight from the load cells
  float weight_1 = Loadcell_1.get_units(5);
  float weight_2 = Loadcell_2.get_units(5);
  float weight_3 = Loadcell_3.get_units(5);
  float weight_4 = Loadcell_4.get_units(5);
  float weight_5 = Loadcell_5.get_units(5);
  float weight_6 = Loadcell_6.get_units(5);
  float weight_7 = Loadcell_7.get_units(5);
  float weight_8 = Loadcell_8.get_units(5);

  // Clear the screen and print the weight on the screen
  myGLCD.printNumF(weight_1, 2, 80, 390, '.', 3);
  myGLCD.printNumF(weight_2, 2, 340, 235, '.', 3);
  myGLCD.printNumF(weight_3, 2, 80, 235, '.', 3);
  myGLCD.printNumF(weight_4, 2, 80, 70, '.', 3);
  myGLCD.printNumF(weight_5, 2, 340, 70, '.', 3);
  myGLCD.printNumF(weight_6, 2, 600, 70, '.', 3);
  myGLCD.printNumF(weight_7, 2, 600, 235, '.', 3);
  myGLCD.printNumF(weight_8, 2, 600, 390, '.', 3);

}

void waitForIt(int x1, int y1, int x2, int y2) {
  myGLCD.setColor(255, 0, 0);
  myGLCD.drawRoundRect(x1, y1, x2, y2);
  while (myTouch.dataAvailable()) {
  }
  delay(20);

  //list all files in the card with date and size

  myGLCD.setColor(fg[0], fg[1], fg[2]);
  myGLCD.drawRoundRect(x1, y1, x2, y2);
}
```

Appendix C: MATLAB code for calculating determinant of Jacobian

```
clear all;
clc;
close all;

syms q1 q2 q3 q4 q5 q6 d1 d2 d3 d4 d5 d6 a1 a2 a3 a4 a5 a6
% According to the DH parameter table, the a, d, and A are defined below.

% Defining link lengths, these are fixed numbers and are a design
% parameter of the robot
d1 = 0.290; % Link lengths as per respective axis
d2 = 0; % Link lengths as per respective axis
d3 = 0; % Link lengths as per respective axis
d4 = 0.302; % Link lengths as per respective axis
d5 = 0; % Link lengths as per respective axis
d6 = 0.072; % Link lengths as per respective axis
a1 = 0; % Link lengths as per respective axis
a2 = 0.27; % Link lengths as per respective axis
a3 = 0.07; % Link lengths as per respective axis
a4 = 0; % Link lengths as per respective axis
a5 = 0; % Link lengths as per respective axis
a6 = 0; % Link lengths as per respective axis
% A1 = -pi/2; Angles...
% A2 = 0; Angles...
% A3 = -pi/2; Angles...
% A4 = pi/4; Angles...
% A5 = -pi/2; Angles...
% A6 = 0; Angles...

% Assign q values as per the orientation of the robot.
q1 = 39.66 *pi/180
q2 = 34.93 *pi/180
q3 = -6.41 *pi/180
q4 = -44.15 *pi/180
q5 = 38.01 *pi/180
q6 = 73.47 *pi/180

% Defining Rotational Jacobian Matrix for the transformation from frame
% '0' to the frame '6'.

JR(1, 1) = ((cos(q6))*(cos(q4))*(cos(q5)) - (sin(q4))*(sin(q6)))*(cos(q2+q3)) -
(sin(q5))*(sin(q2+q3))*(cos(q6));
JR(2, 1) = -((sin(q6))*(cos(q4))*(cos(q5)) + (cos(q6))*(sin(q4)))*(cos(q2+q3)) +
(sin(q5))*(sin(q2+q3))*(sin(q6));
JR(3, 1) = -sin(q5)*cos(q4)*cos(q2+q3) - cos(q5)*sin(q2+q3);
```

```
JR(1, 2) = -cos(q6)*sin(q4)*cos(q5) - sin(q6)*cos(4);
JR(2, 2) = sin(q4)*sin(q6)*cos(q5) - cos(q6)*cos(q4);
JR(3, 2) = sin(q5)*sin(q4);

JR(1, 3) = -cos(q6)*sin(q4)*cos(q5) - sin(q6)*cos(q4);
JR(2, 3) = sin(q4)*sin(q6)*cos(q5) - cos(q6)*cos(q4);
JR(3, 3) = sin(q5)*sin(q4);

JR(1, 4) = sin(q5)*cos(q6);
JR(2, 4) = -sin(q5)*sin(q6);
JR(3, 4) = cos(q5);

JR(1, 5) = -sin(q6);
JR(2, 5) = -cos(q6);
JR(3, 5) = 0;

JR(1, 6) = 0;
JR(2, 6) = 0;
JR(3, 6) = 1;

% Similarly we need translational Jacobian.
% For that, we need to define the link centroid to the  corresponding
% attached frame so that, the centroid is later reduced to be w.r.t the
% base frame and use for more precise calculation.

syms x y z
x = 0;
y = 0;
z = -0.007;

% Now defining the JT translational Jacobian Matrix

JT(1, 1) = -sin(q1)*(((cos(q6)*x-sin(q6)*y)*cos(q5)-sin(q5)*(d6 + z))*cos(q4)-(cos(q6)*y +
sin(q6)*x)*sin(q4)+a3)*sin(q2+q3)-sin(q1)*((d6+z)*cos(q5)+(cos(q6)*x-
sin(q6)*y)*sin(q5)+d4)*cos(q2+q3)-sin(q1)*a2*sin(q2) + ((cos(q6)*y +
sin(q6)*x)*cos(q4)+sin(q4)*((cos(q6)*x-sin(q6)*y)*cos(q5)-sin(q5)*(d6+z)))*cos(q1);
JT(2, 1) = cos(q1)*(((cos(q6)*x-sin(q6)*y)*cos(q5)-sin(q5)*(d6+z))*cos(q4)-
(cos(q6)*y+sin(q6)*x)*sin(q4)+a3)*sin(q2+q3)+((d6+z)*cos(q5)+(cos(q6)*x-
sin(q6)*y)*sin(q5)+d4)*cos(q1)*cos(q2+q3)+cos(q1)*a2*sin(q2)+sin(q1)*((cos(q6)*y+sin(q6)*
x)*cos(q4)+sin(q4)*((cos(q6)*x-sin(q6)*y)*cos(q5)-sin(q5)*(d6+z)));
JT(3, 1) = 0;

JT(1, 2) = (((cos(q6)*x-sin(q6)*y)*cos(q5)-sin(q5)*(d6+z))*cos(q4)-cos(q6)*sin(q4)*y-
sin(q4)*sin(q6)*x+a3)*cos(q1)*cos(q2+q3)-((d6+z)*cos(q5)+(cos(q6)*x-
sin(q6)*y)*sin(q5)+d4)*cos(q1)*sin(q2+q3)+a2*cos(q1)*cos(q2);
```

JT(2, 2) = (((cos(q6)*x-sin(q6)*y)*cos(q5)-sin(q5)*(d6+z))*cos(q4)-cos(q6)*sin(q4)*y-sin(q4)*sin(q6)*x+a3)*sin(q1)*cos(q2+q3)-((d6+z)*cos(q5)+(cos(q6)*x-sin(q6)*y)*sin(q5)+d4)*sin(q1)*sin(q2+q3)+a2*sin(q1)*cos(q2);
JT(3, 2) = (((-cos(q6)*x-sin(q6)*y)*cos(q5)+sin(q5)*(d6+z))*cos(q4)+cos(q6)*sin(q4)*y+sin(q4)*sin(q6)*x-a3)*sin(q2+q3)-((d6+z)*cos(q5)+(cos(q6)*x-sin(q6)*y)*sin(q5)+d4)*cos(q2+q3)-a2*sin(q2);

JT(1, 3) = (((cos(q6)*x-sin(q6)*y)*cos(q5)-sin(q5)*(d6+z))*cos(q4)-cos(q6)*sin(q4)*y-sin(q4)*sin(q6)*x+a3)*cos(q1)*cos(q2+q3)-((d6+z)*cos(q5)+(cos(q6)*x-sin(q6)*y)*sin(q5)+d4)*cos(q1)*sin(q2+q3);
JT(2, 3) = (((cos(q6)*x-sin(q6)*y)*cos(q5)-sin(q5)*(d6+z))*cos(q4)-cos(q6)*sin(q4)*y-sin(q4)*sin(q6)*x+a3)*sin(q1)*cos(q2+q3)-((d6+z)*cos(q5)+(cos(q6)*x-sin(q6)*y)*sin(q5)+d4)*sin(q1)*sin(q2+q3);
JT(3, 3) = (((-cos(q6)*x+sin(q6)*y)*cos(q5)+sin(q5)*(d6+z))*cos(q4)+cos(q6)*sin(q4)*y+sin(q4)*sin(q6)*x-a3)*sin(q2+q3)-((d6+z)*cos(q5)+(cos(q6)*x-sin(q6)*y)*sin(q5)+d4)*cos(q2+q3);

JT(1, 4) = cos(q1)*((-cos(q6)*y-sin(q6)*x)*cos(q4)+((-cos(q6)*x+sin(q6)*y)*cos(q5)+sin(q5)*(d6+z))*sin(q4))*sin(q2+q3)-(((-cos(q6)*x+sin(q6)*y)*cos(q5)+sin(q5)*(d6+z))*cos(q4)+(cos(q6)*y + sin(q6)*x)*sin(q4))*sin(q1);
JT(2, 4) = sin(q1)*((-cos(q6)*y-sin(q6)*x)*cos(q4)+((-cos(q6)*x+sin(q6)*y)*cos(q5)+sin(q5)*(d6+z))*sin(q4))*sin(q2+q3)+(((-cos(q6)*x+sin(q6)*y)*cos(q5)+sin(q5)*(d6+z))*cos(q4)+(cos(q6)*y + sin(q6)*x)*sin(q4))*cos(q1);
JT(3, 4) = cos(q2+q3)*(((-cos(q6)*x+sin(q6)*y)*cos(q5)+sin(q5)*(d6+z))*sin(q4)-(cos(q6)*y+sin(q6)*x)*cos(q4));

JT(1, 5) = -cos(q1)*((-cos(q6)*x+sin(q6)*y)*cos(q5)+sin(q5)*(d6+z))*cos(q2+q3)-(cos(q1)*cos(q4)*sin(q2+q3)+sin(q1)*sin(q4))*((d6+z)*cos(q5)+(cos(q6)*x-sin(q6)*y)*sin(q5));
JT(2, 5) = -sin(q1)*((-cos(q6)*x+sin(q6)*y)*cos(q5)+sin(q5)*(d6+z))*cos(q2+q3)+((d6+z)*cos(q5)+(cos(q6)*x-sin(q6)*y)*sin(q5))*(-cos(q4)*sin(q1)*sin(q2+q3)+cos(q1)*sin(q4));
JT(3, 5) = -((d6+z)*cos(q5)+(cos(q6)*x-sin(q6)*y)*sin(q5))*cos(q4)*cos(q2+q3)+sin(q2+q3)*((-cos(q6)*x+sin(q6)*y)*cos(q5)+sin(q5)*(d6+z));

JT(1, 6) = -cos(q1)*((cos(q4)*cos(q5)*y+sin(q4)*x)*cos(q6)+sin(q6)*(cos(q4)*cos(q5)*x-sin(q4)*y))*sin(q2+q3)-sin(q5)*cos(q1)*(cos(q6)*y+sin(q6)*x)*cos(q2+q3)-(cos(q5)*sin(q4)*y-cos(q4)*x)*sin(q1)*cos(q6)-sin(q1)*sin(q6)*(cos(q5)*sin(q4)*x +cos(q4)*y);
JT(2, 6) = -sin(q1)*((cos(q4)*cos(q5)*y+sin(q4)*x)*cos(q6)+sin(q6)*(cos(q4)*cos(q5)*x-sin(q4)*y))*sin(q2+q3)-sin(q1)*sin(q5)*(cos(q6)*y+sin(q6)*x)*cos(q2+q3)+(cos(q5)*sin(q4)*y-cos(q4)*x)*cos(q1)*cos(q6)-cos(q1)*sin(q6)*(cos(q5)*sin(q4)*x +cos(q4)*y);

```
JT(3, 6) = ((-cos(q4)*cos(q5)*y-sin(q4)*x)*cos(q6)+sin(q6)*(-
cos(q4)*cos(q5)*x+sin(q4)*y))*cos(q2+q3)+(cos(q6)*y+sin(q6)*x)*sin(q5)*sin(q2+q3);

Jacobian = [JT;JR]
det(Jacobian)
rank(Jacobian)
```

Appendix D: Drawing for gripper parts

Part #1 [Table 1]

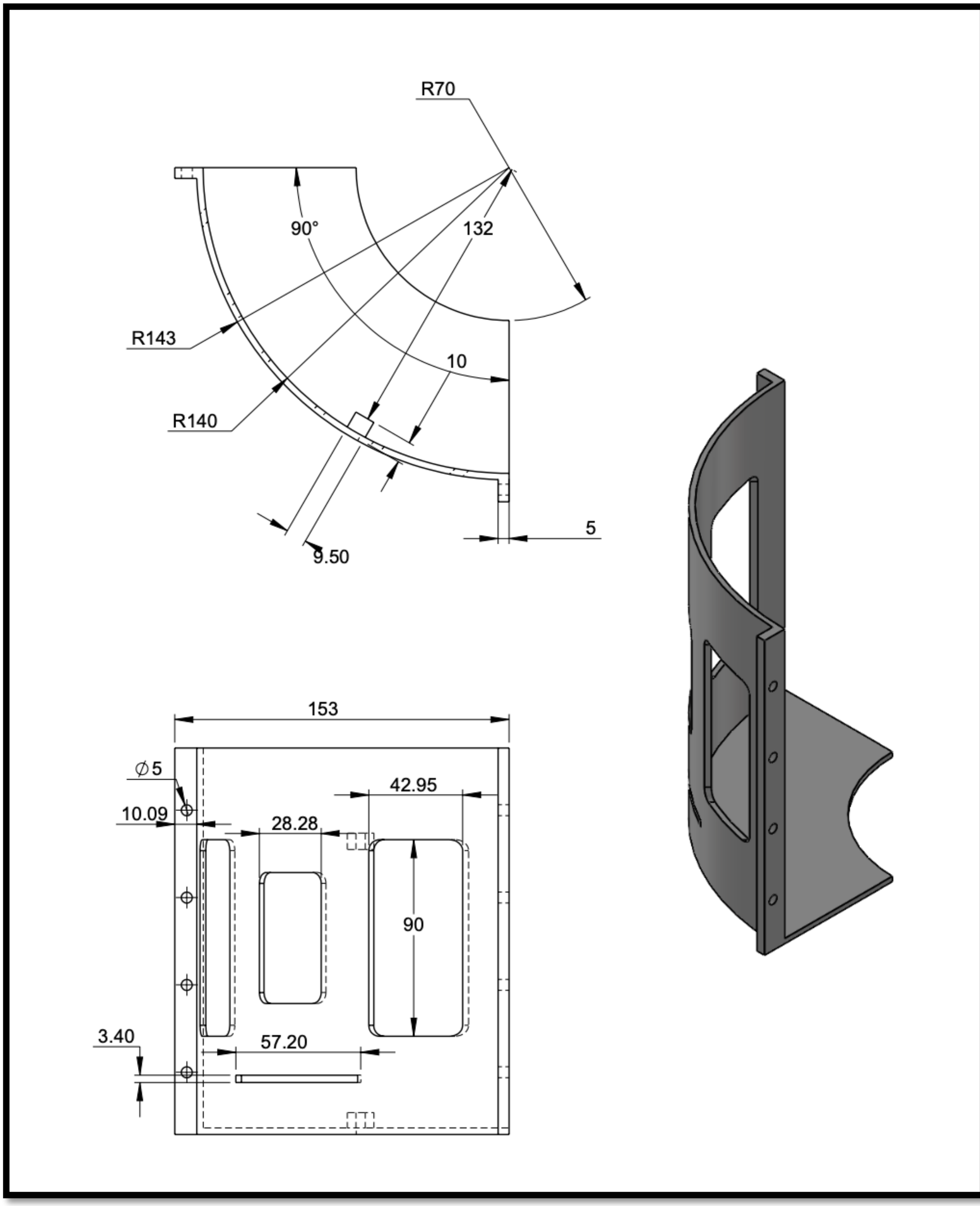

Part #2 [Table 1]

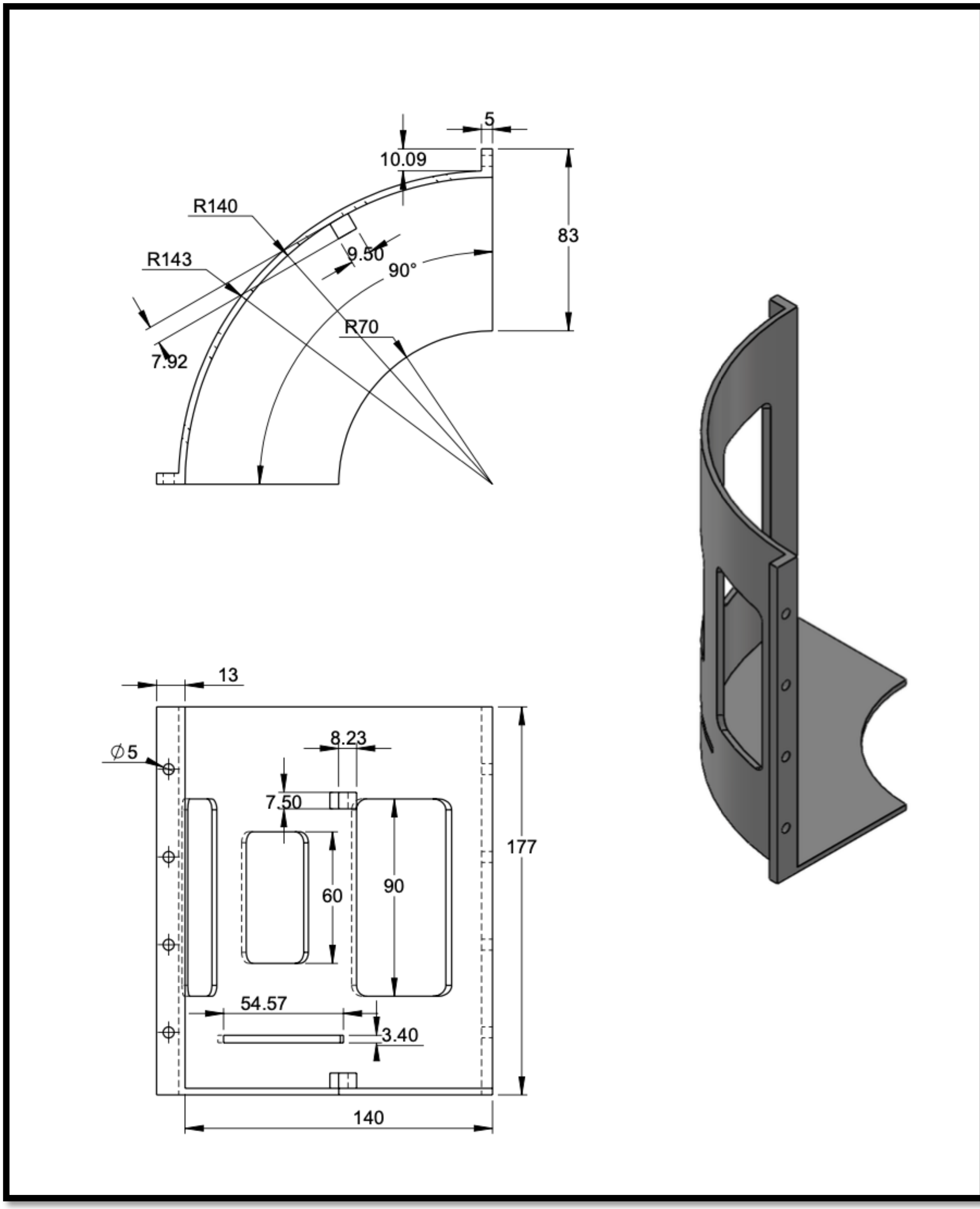

Part #3 [Table 1]

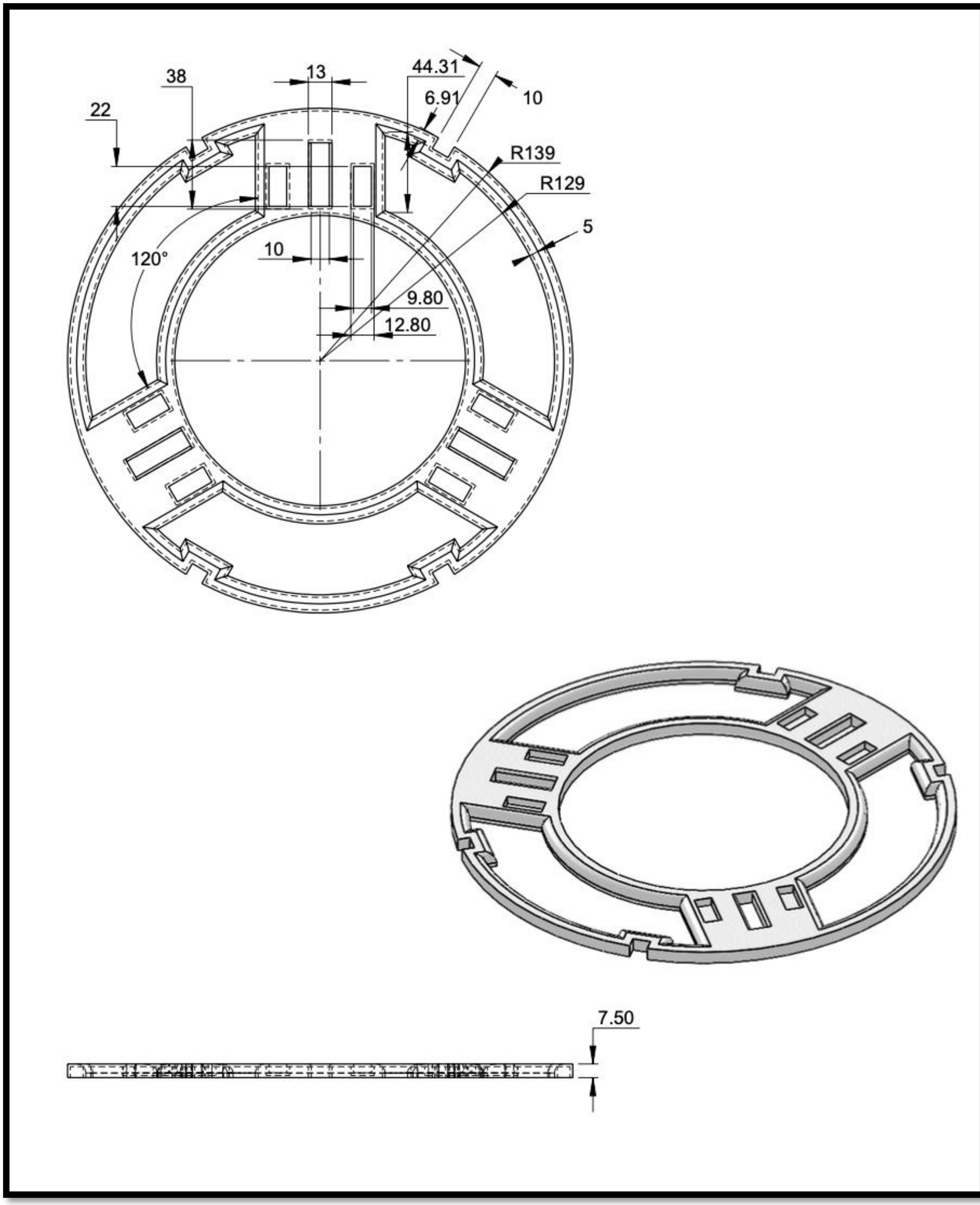

Part #4 [Table 1]: 10-millimeter steel bearing balls

Part #5 [Table 1]

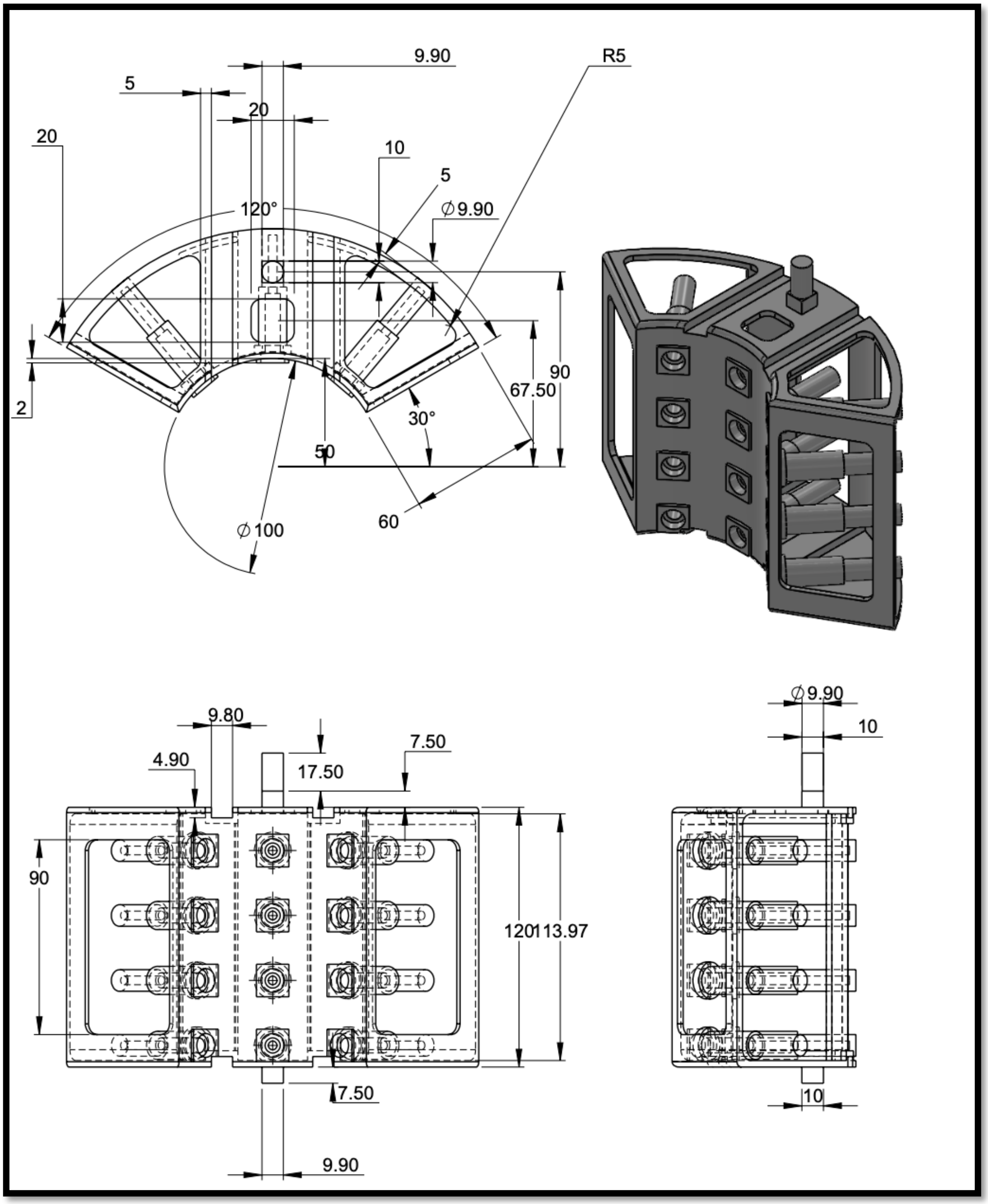

Part #6 [Table 1]

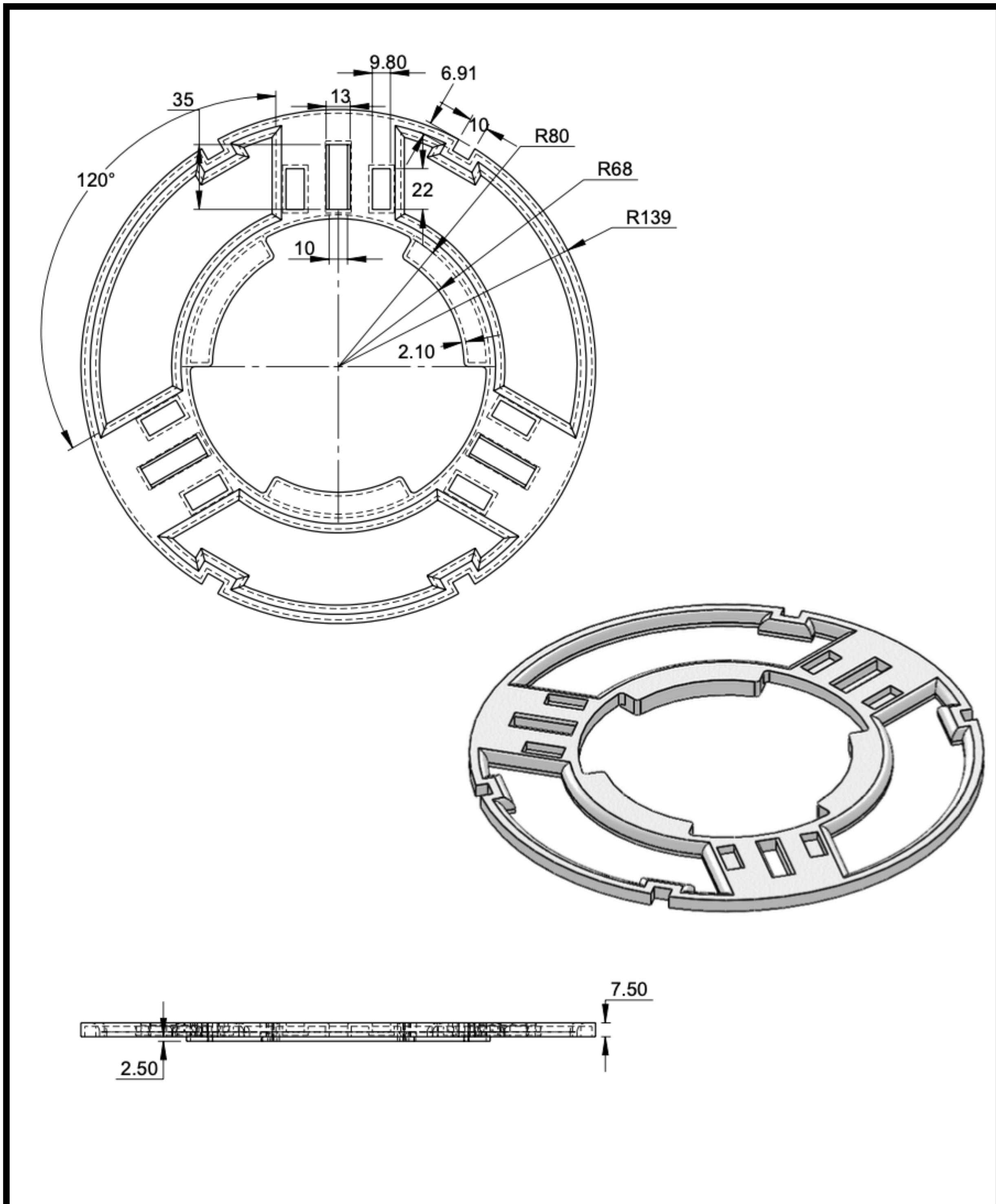

Part #7 [Table 1]

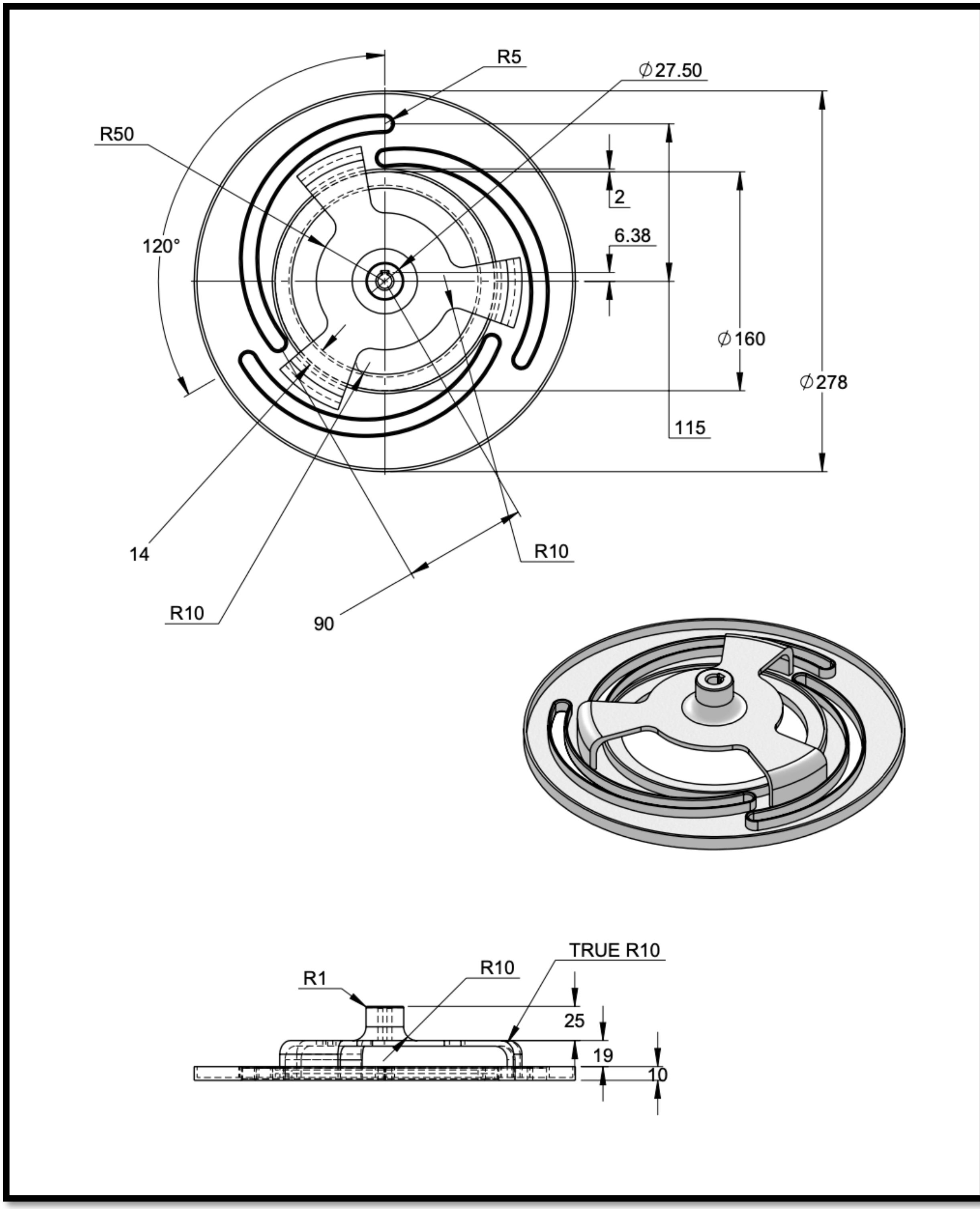

Part #8 [Table 1]

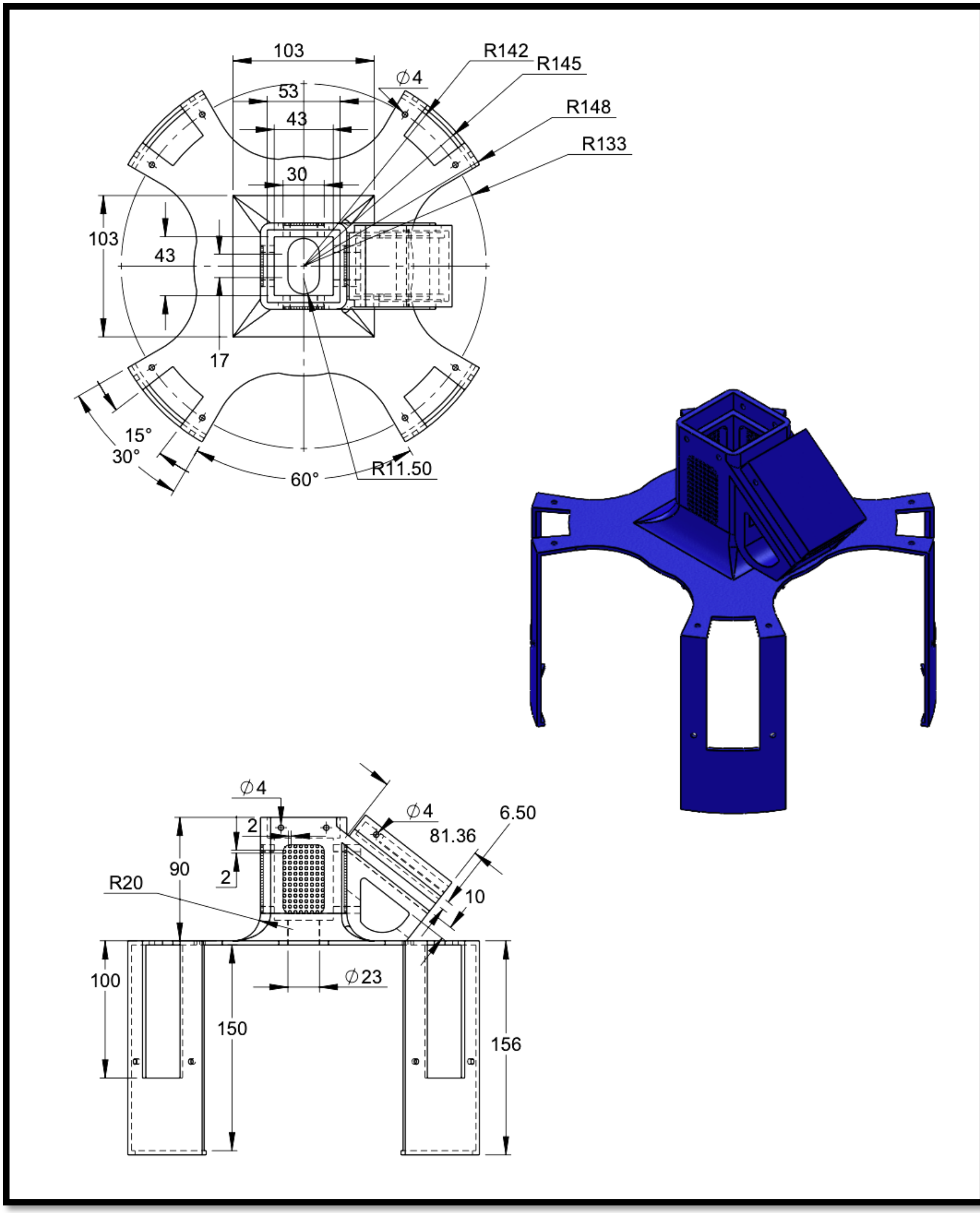

Part #9 [Table 1]

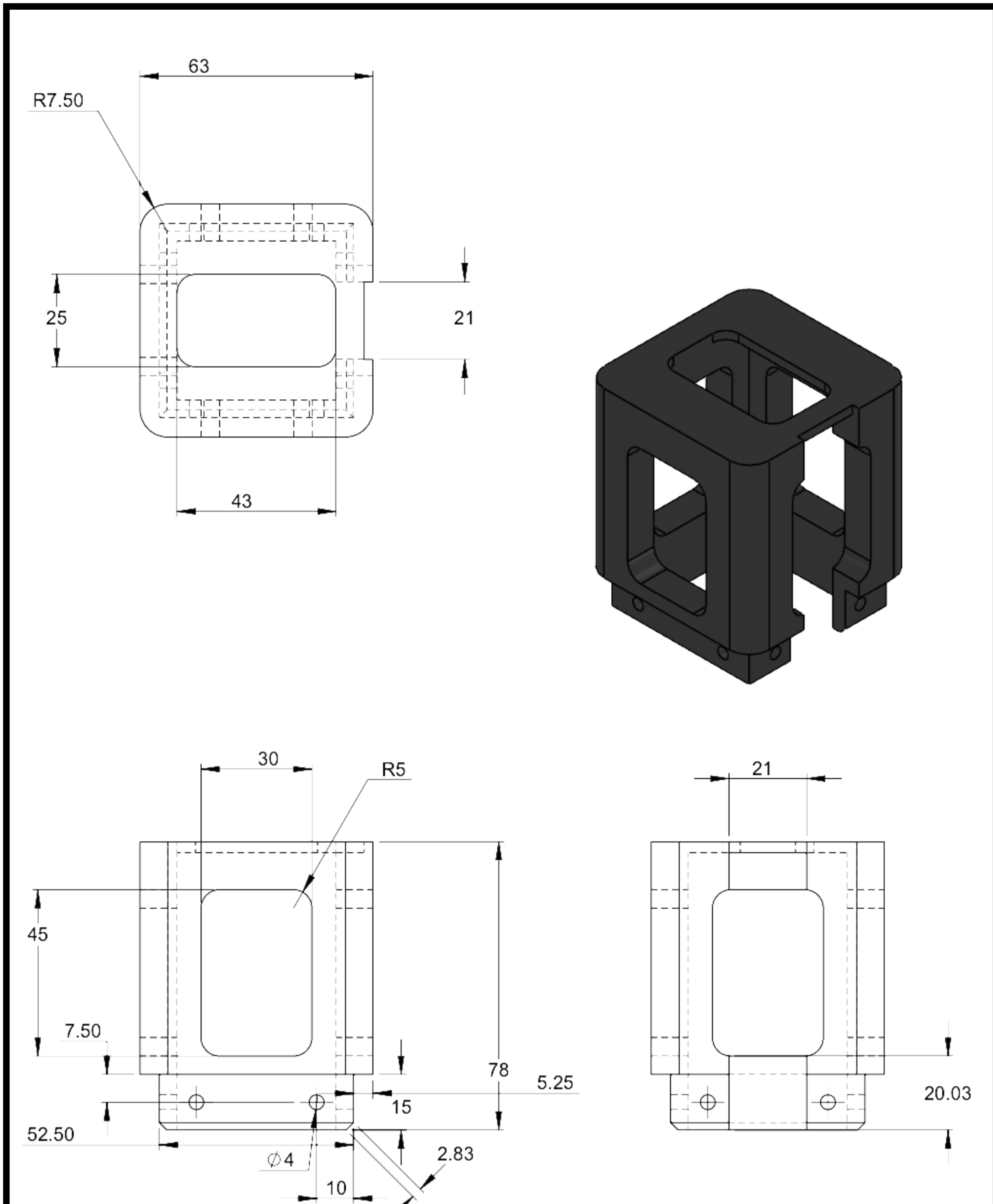

Part #10 [Table 1]

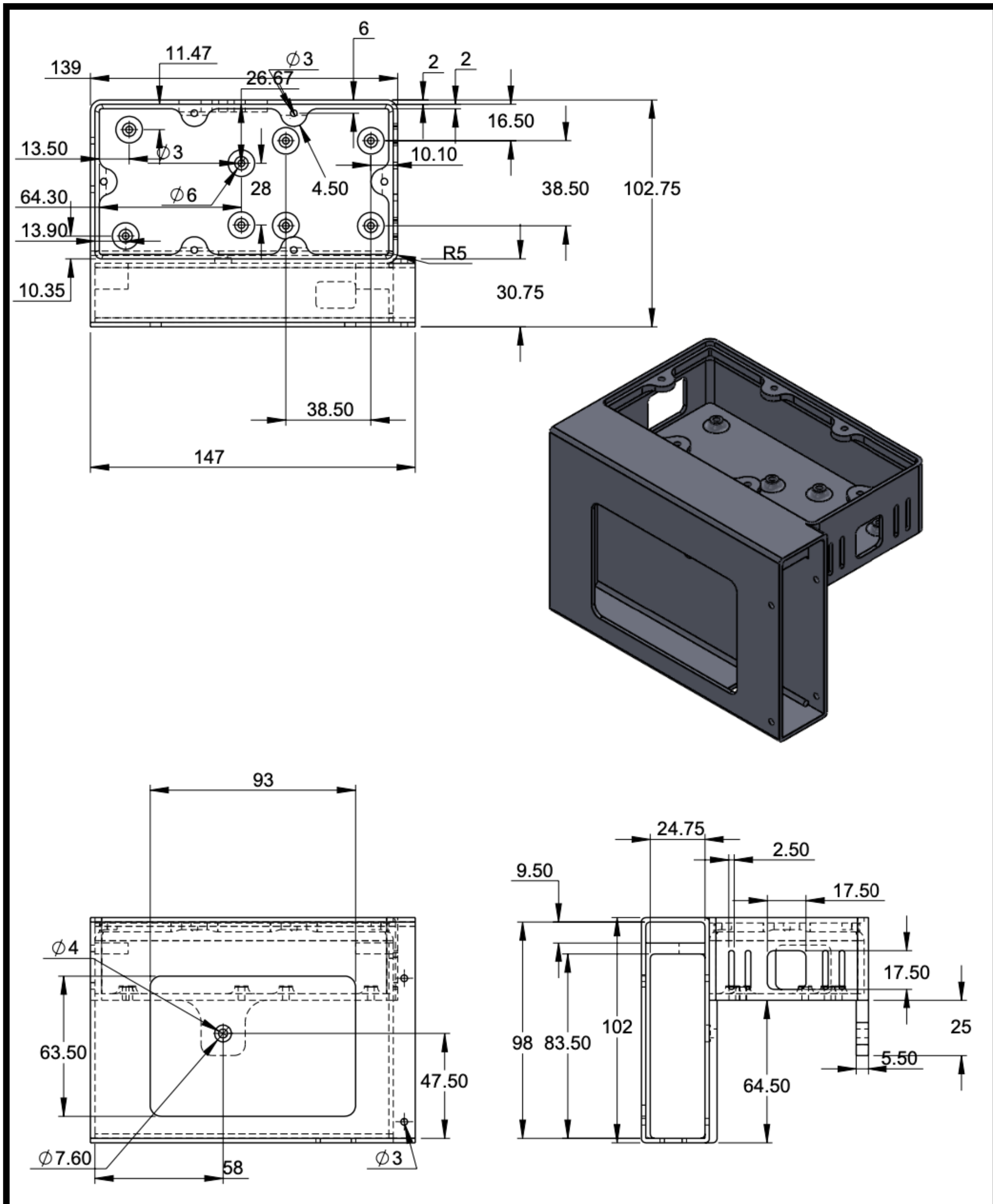

Part #11 [Table 1]

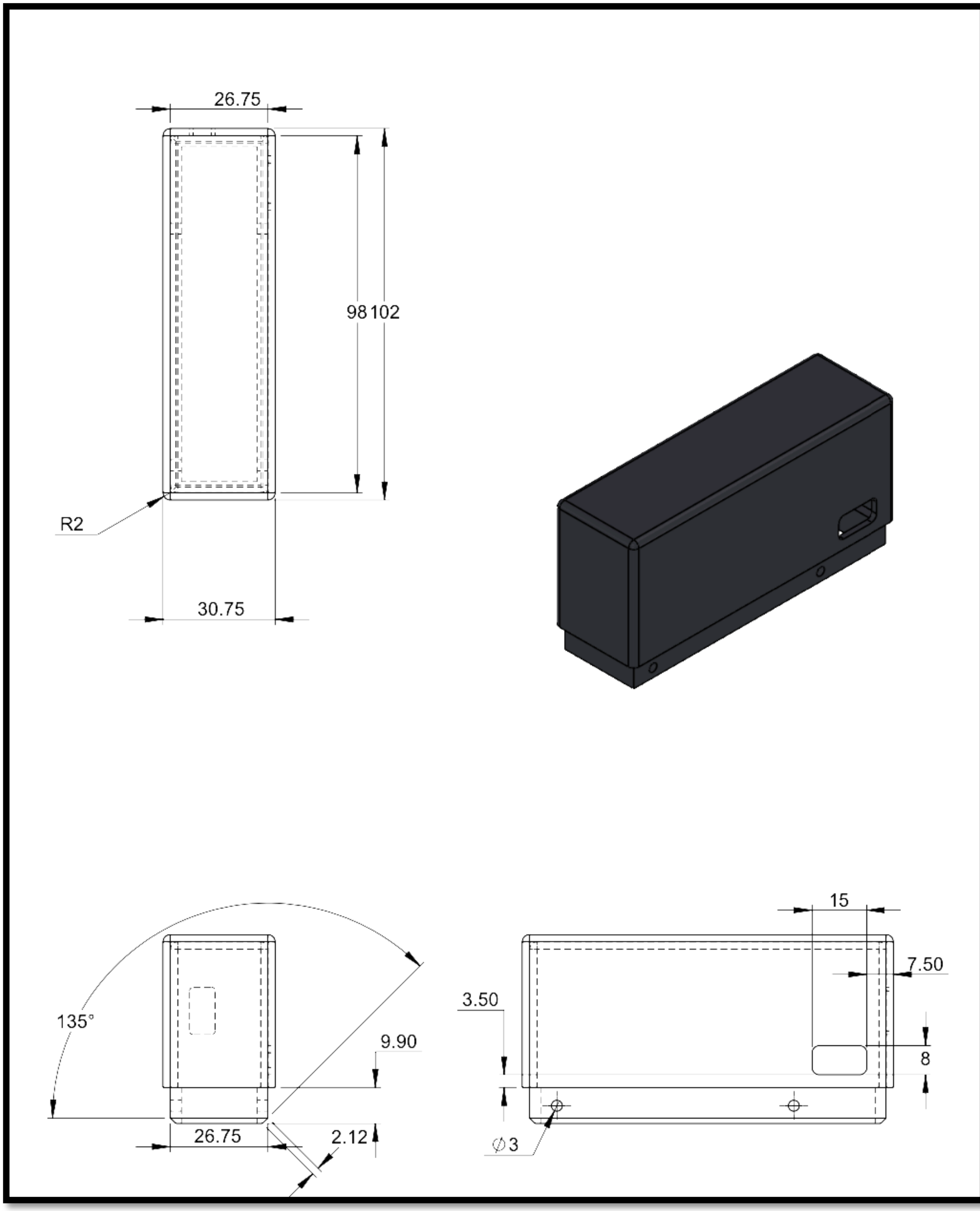

Part #12 [Table 1]: M3 Screw 6 cm

Part #13 [Table 1]: 5 mm x 0.6 mm x 25 mm spring

Part #14 [Table 1]

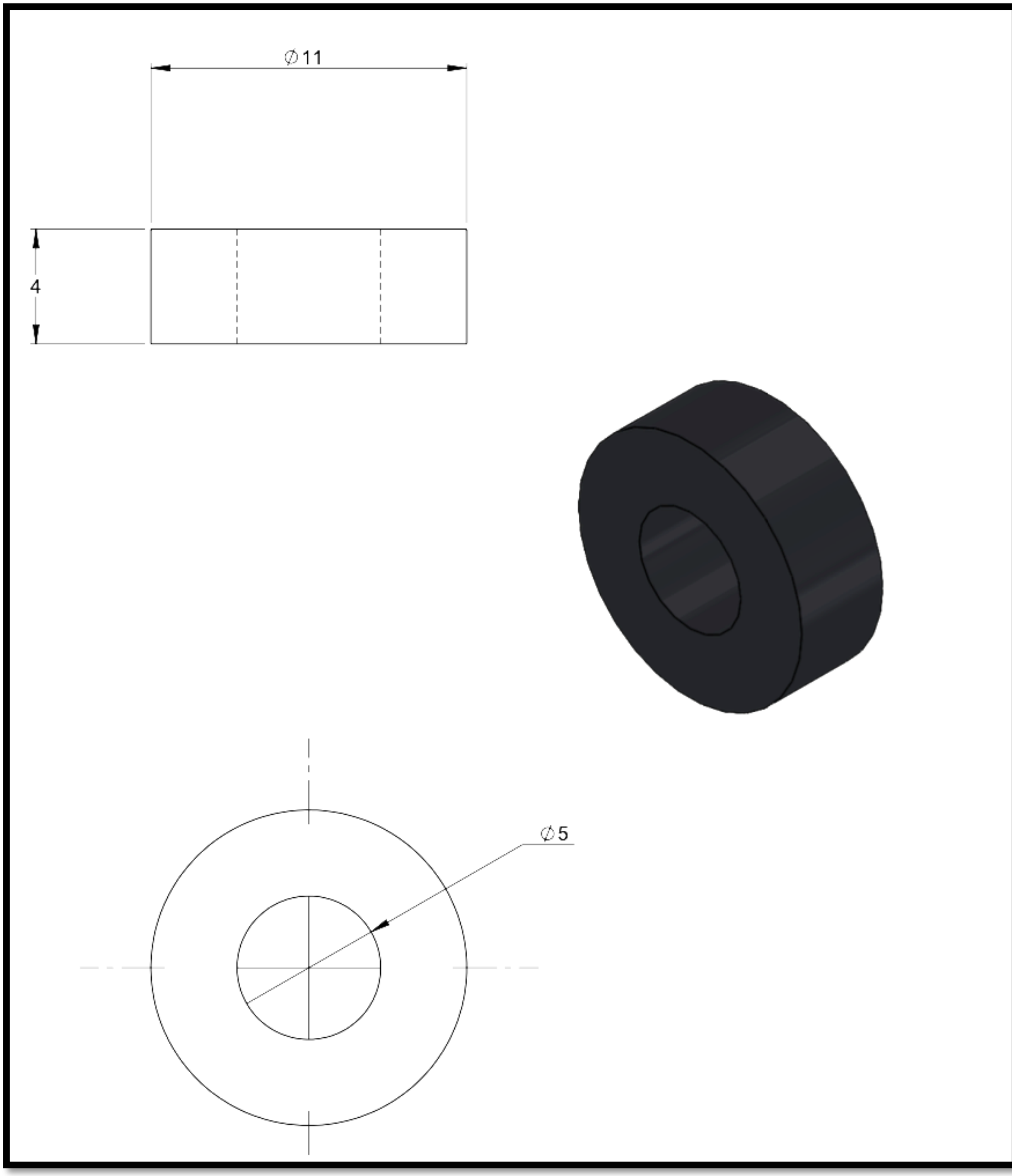

Appendix E: Drawing parts for Smart Shelf parts

Part #1 [Table 4]

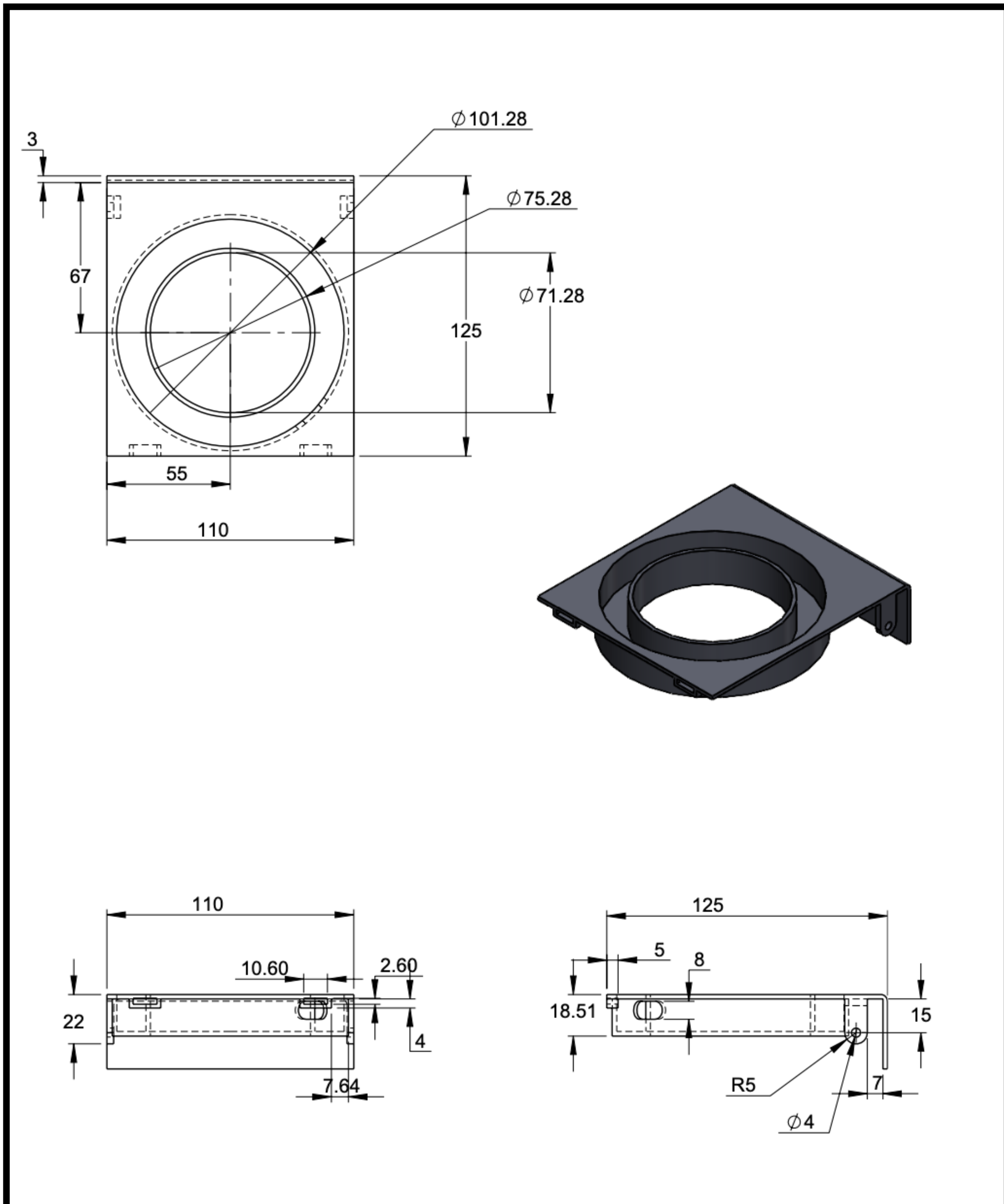

Part #2 [Table 4]

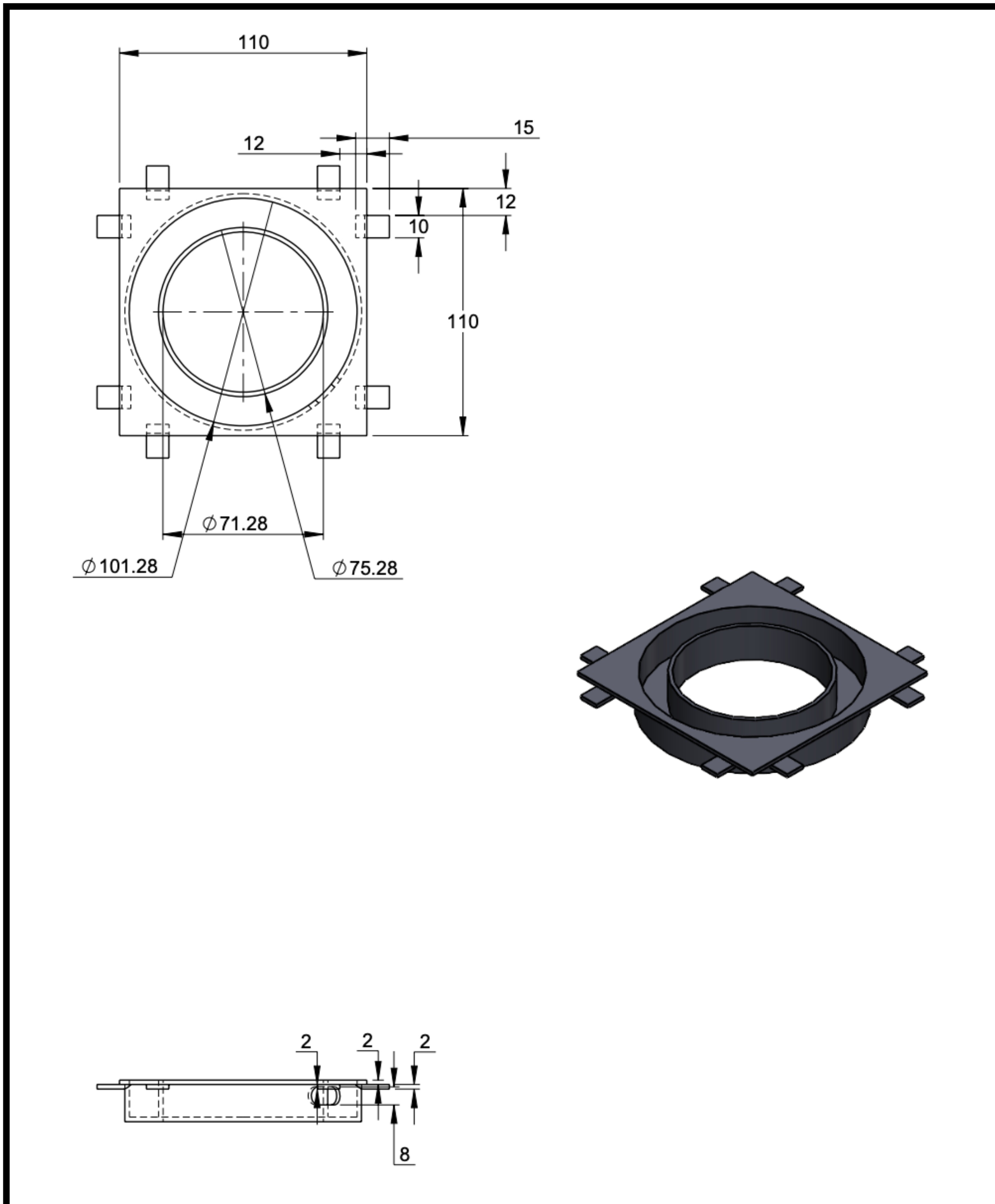

Part #3 [Table 4]

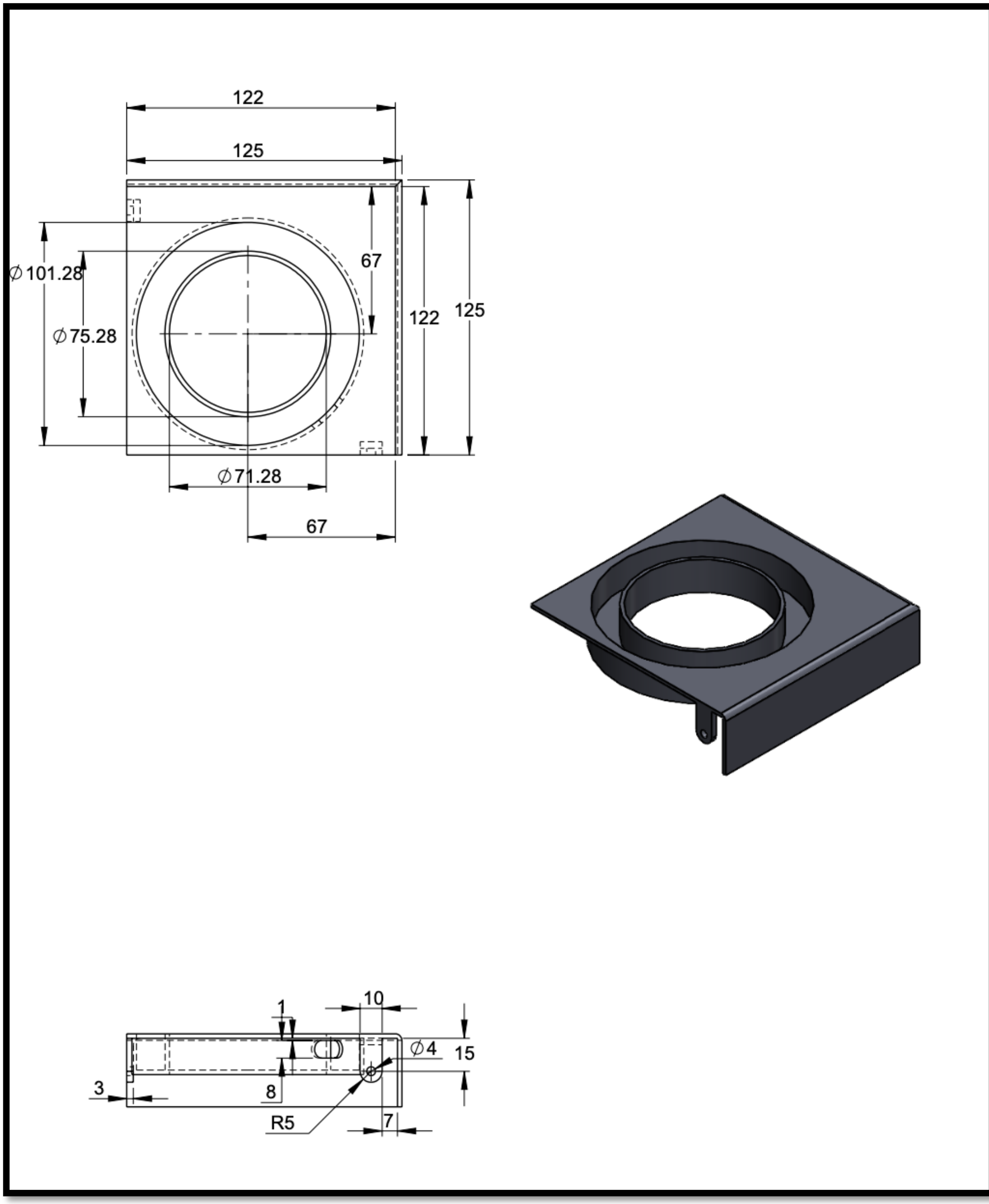

Part #4 [Table 4]

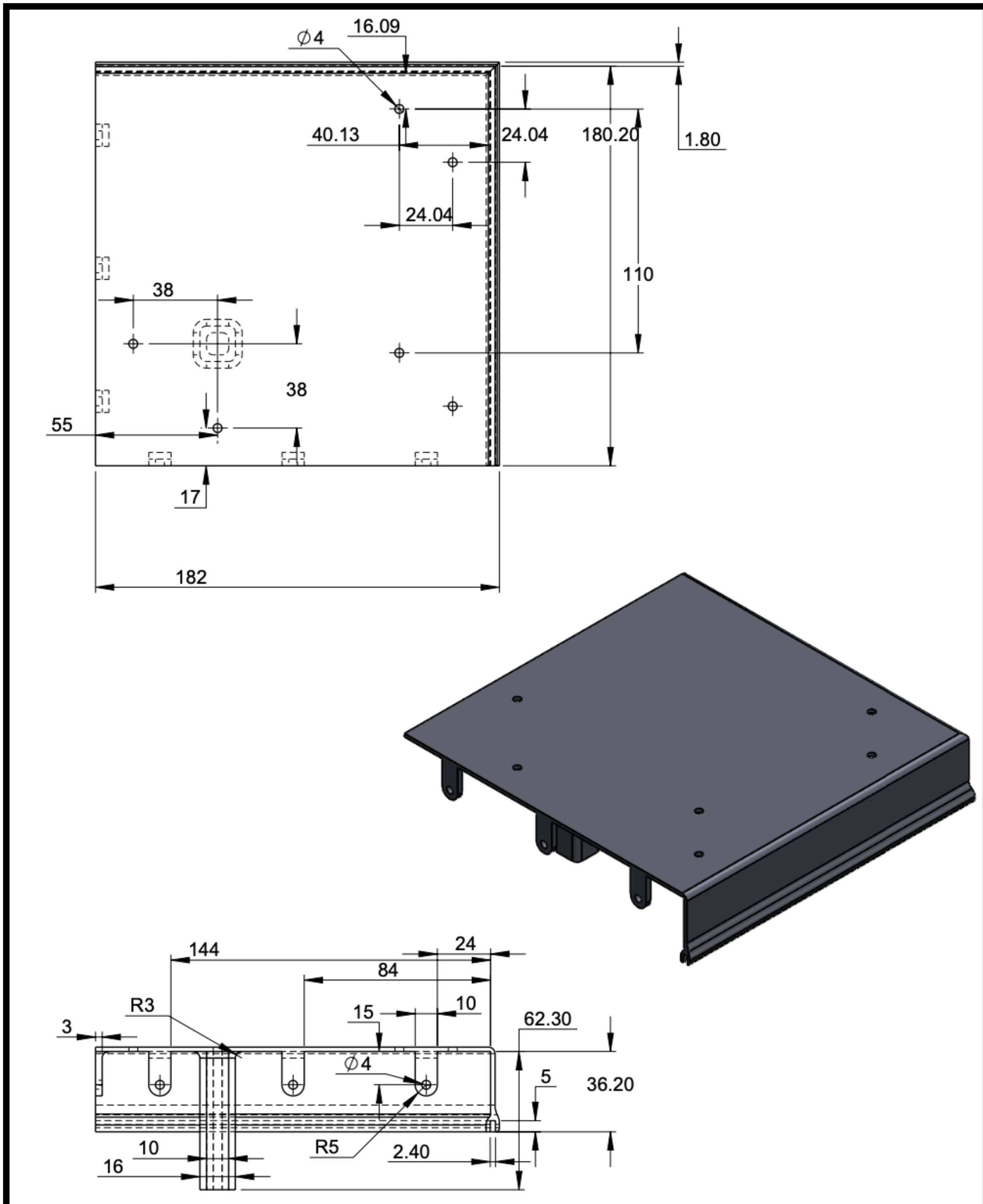

Part #5 [Table 4]

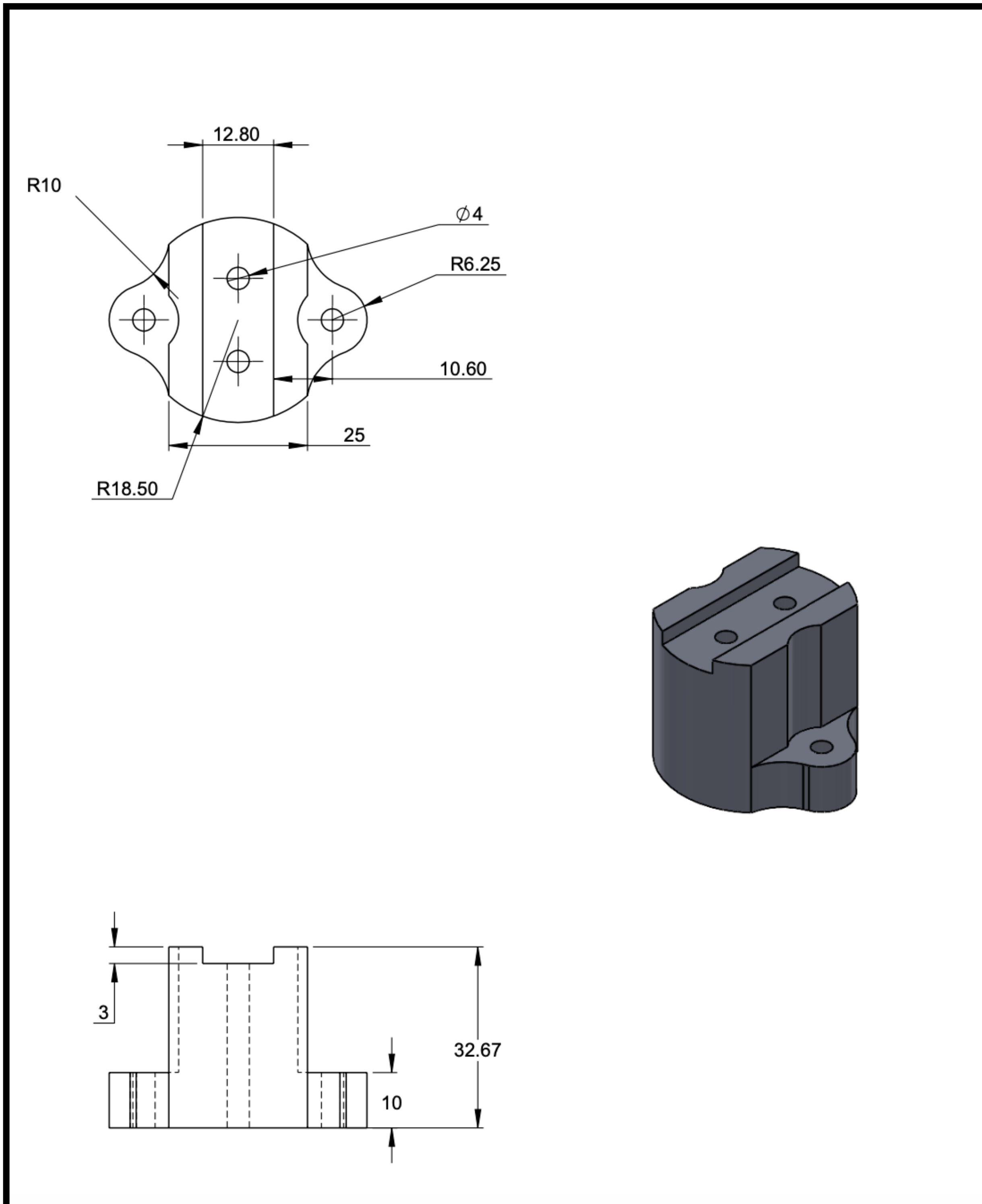

Part #6 [Table 4]: Load cell

Part #7 [Table 4]

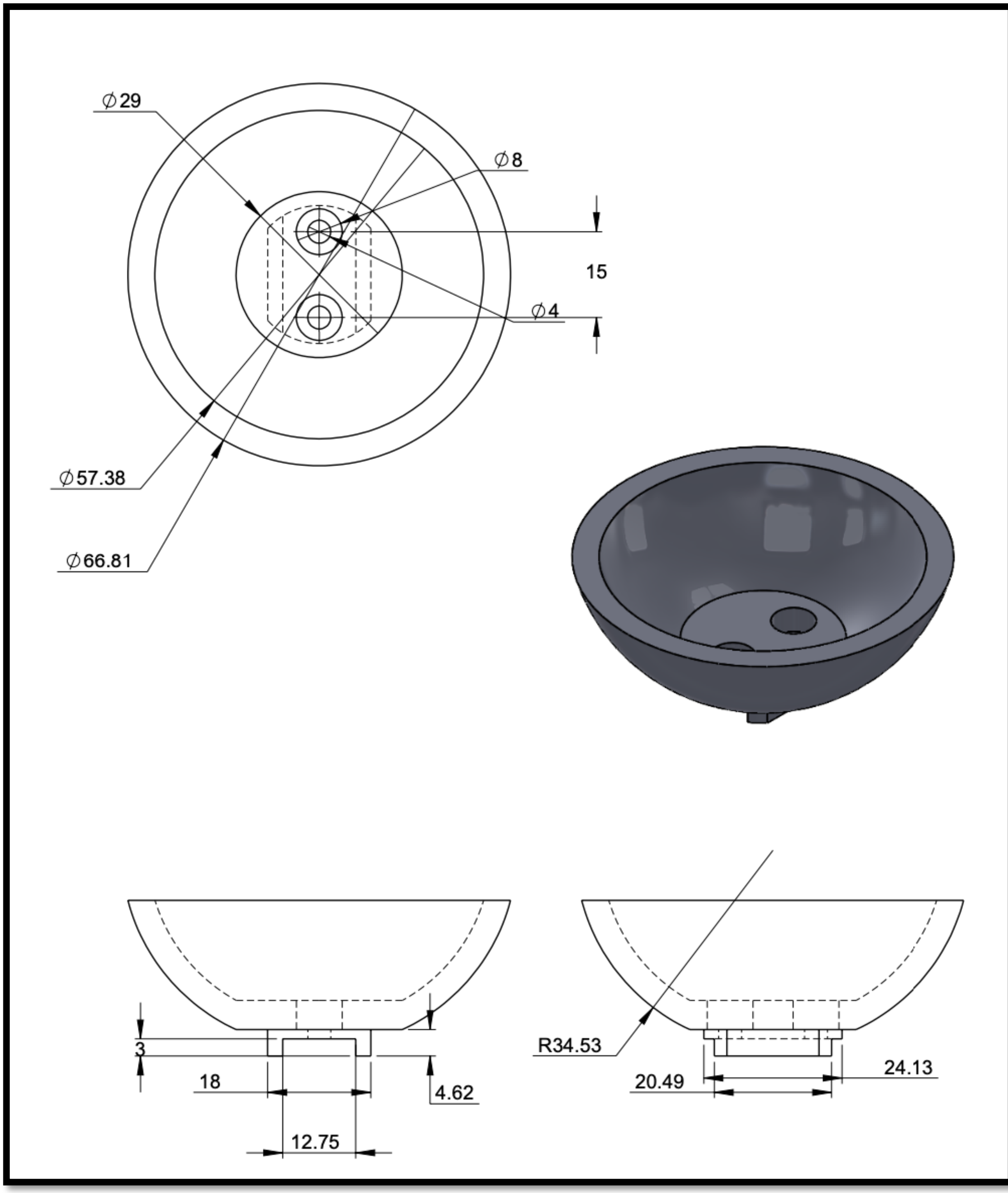

Part #8 [Table 4]

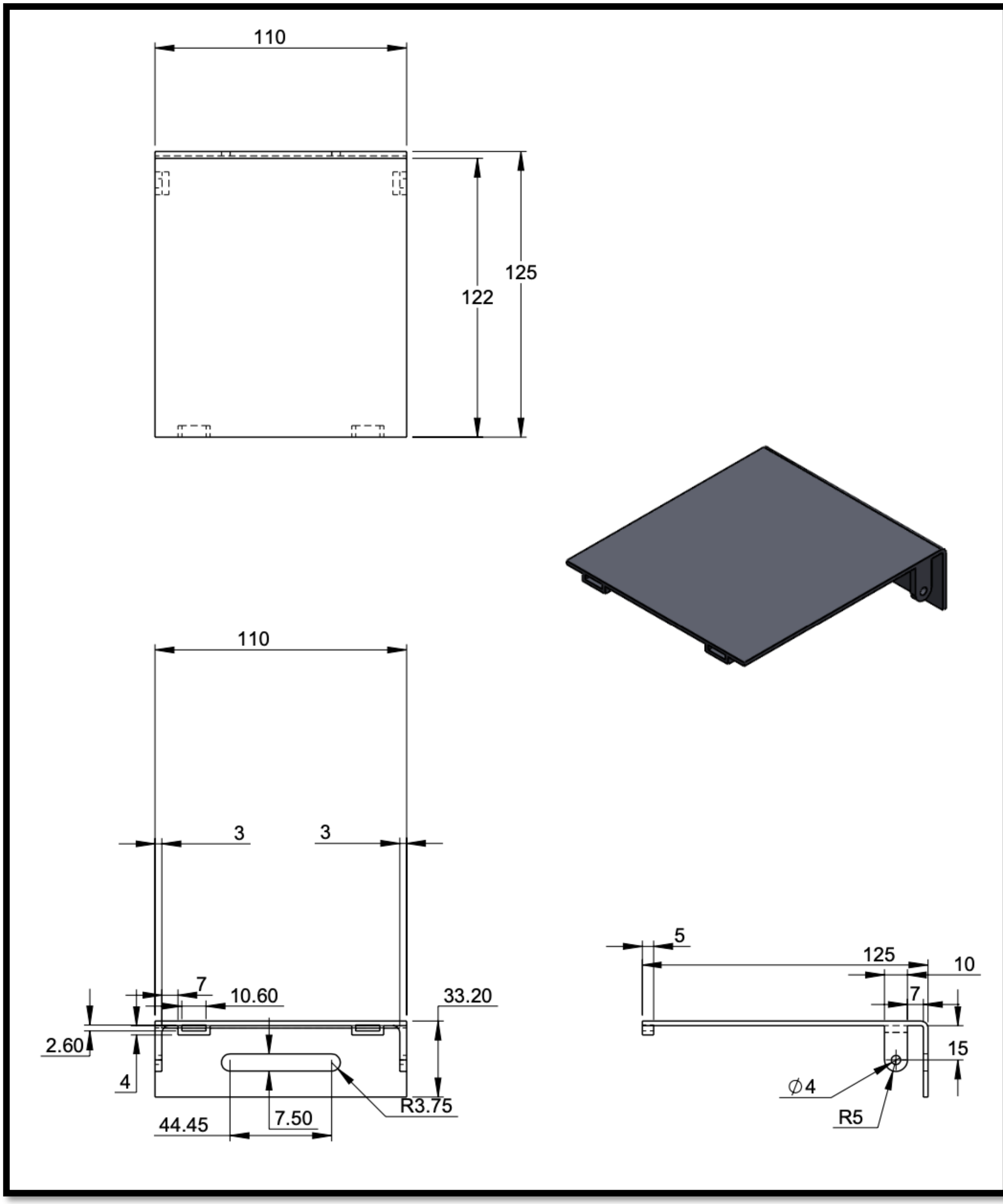

Part #9 [Table 4]

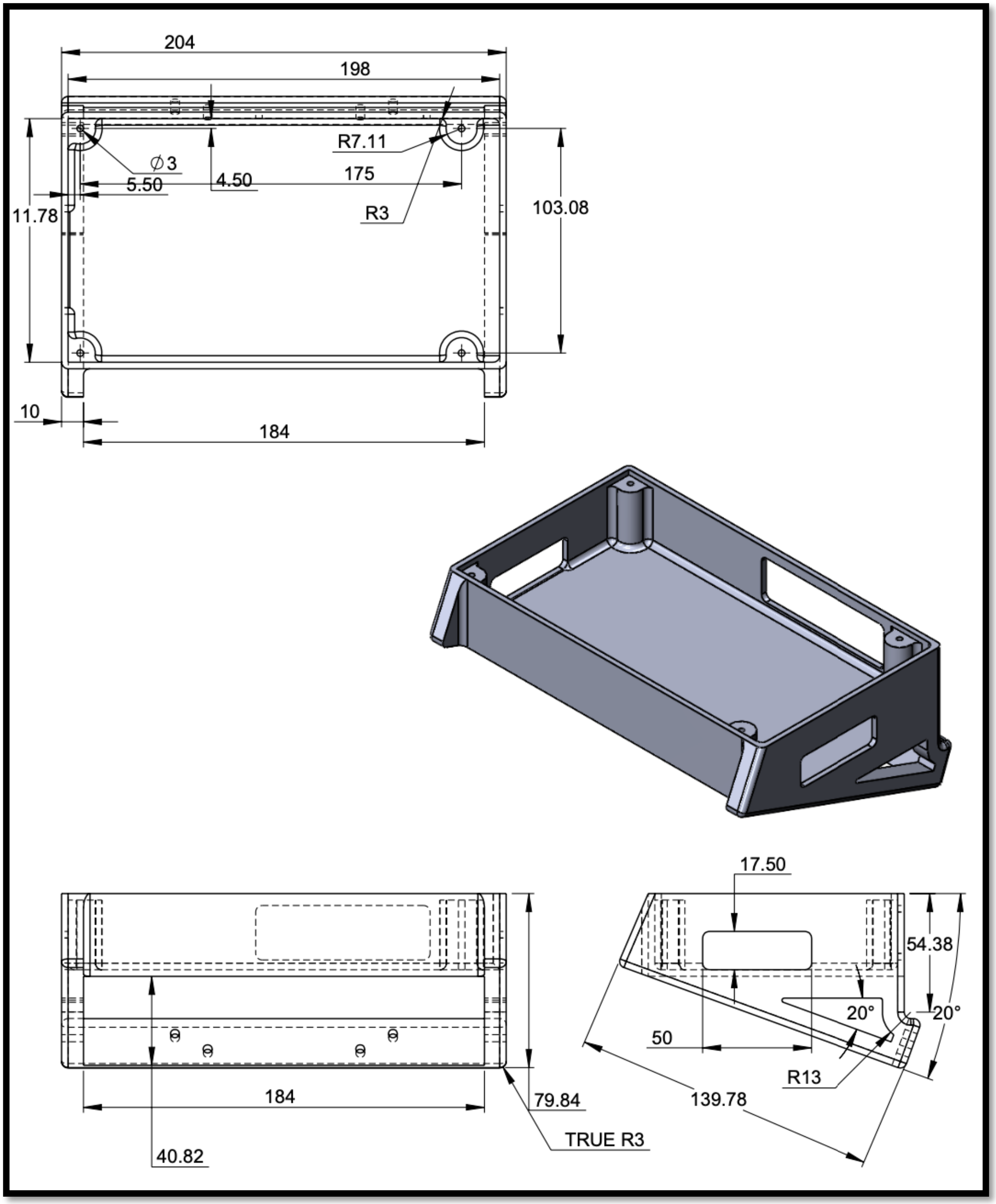

Part #10 [Table 4]

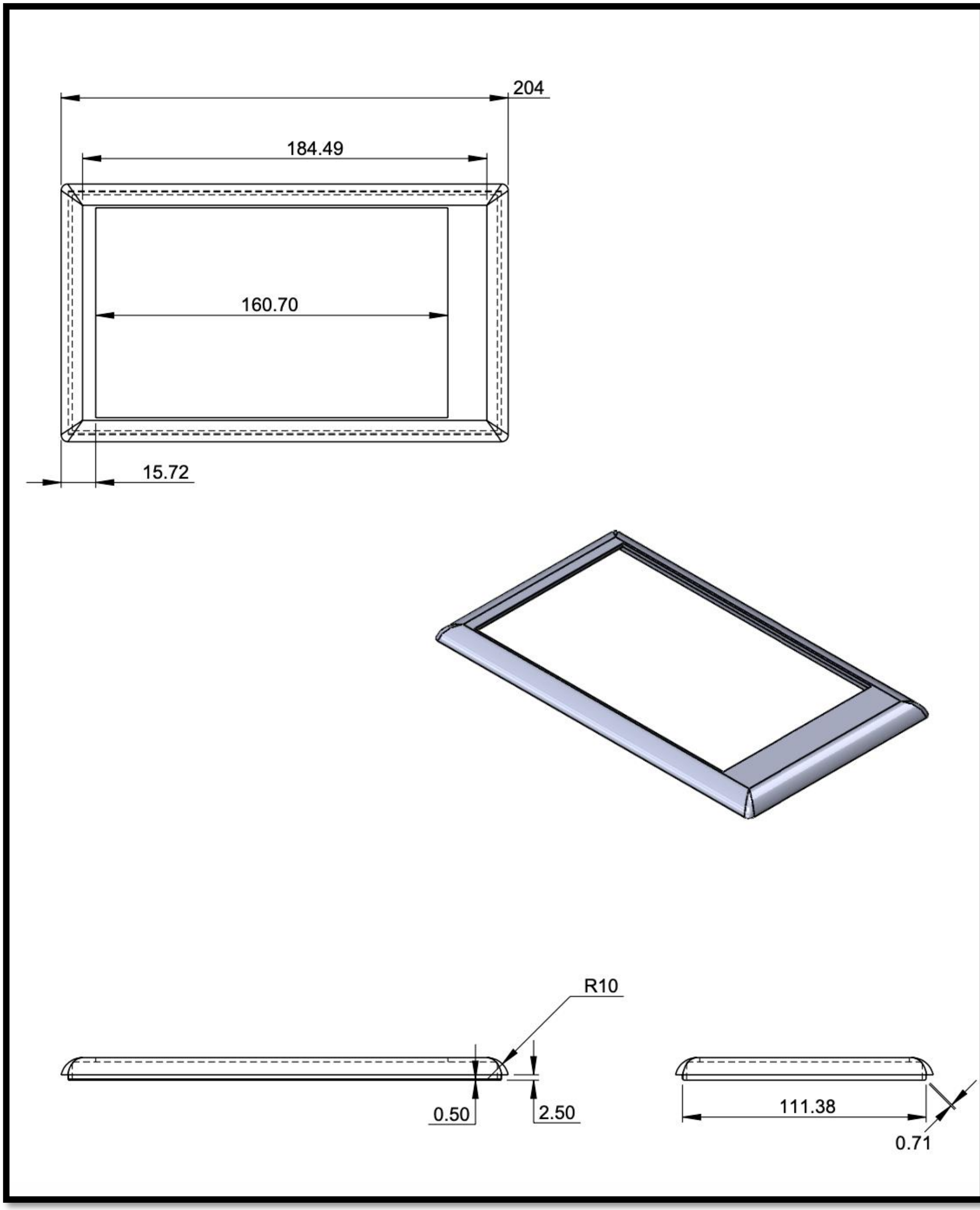

Appendix F: Load cell product specification used.

Product Specifications	
Mechanical	
Housing Material	Aluminum Alloy
Load Cell Type	Strain Gauge
Capacity	20kg
Dimensions	55.25x12.7x12.7mm
Mounting Holes	M5 (Screw Size)
Cable Length	550mm
Cable Size	30 AWG (0.2mm)
Cable - no. of leads	4
Electrical	
Precision	0.05%
Rated Output	1.0±0.15 mv/V
Non-Linearity	0.05% FS
Hysteresis	0.05% FS
Non-Repeatability	0.05% FS
Creep (per 30 minutes)	0.1% FS
Temperature Effect on Zero (per 10°C)	0.05% FS
Temperature Effect on Span (per 10°C)	0.05% FS
Zero Balance	±1.5% FS
Input Impedance	1130±10 Ohm
Output Impedance	1000±10 Ohm
Insulation Resistance (Under 50VDC)	≥5000 MOhm
Excitation Voltage	5 VDC
Compensated Temperature Range	-10 to ~+40°C
Operating Temperature Range	-20 to ~+55°C
Safe Overload	120% Capacity
Ultimate Overload	150% Capacity

Appendix G: Figures of Grippers from review papers

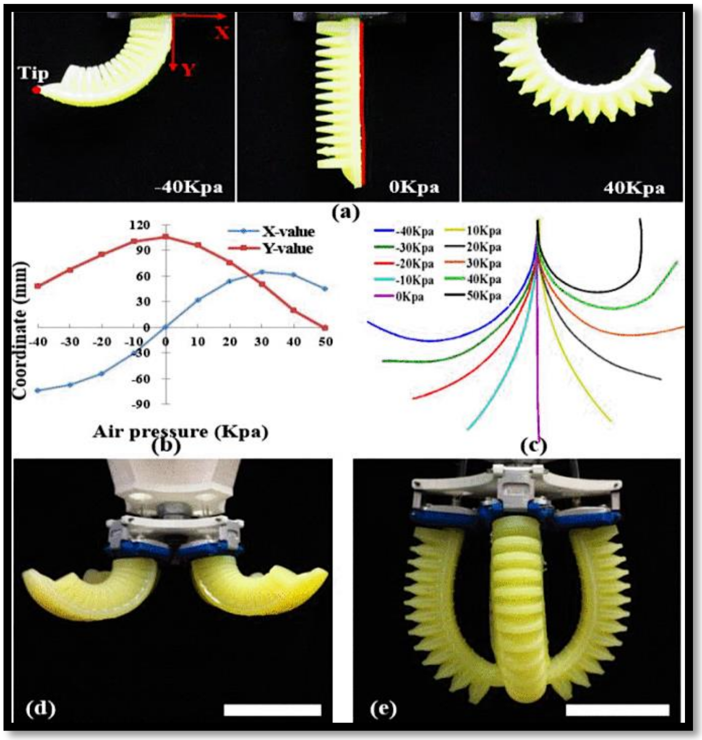

Figure 1: Kinematics of a single soft finger and the soft gripper exhibition deformation under different air pressure [12]

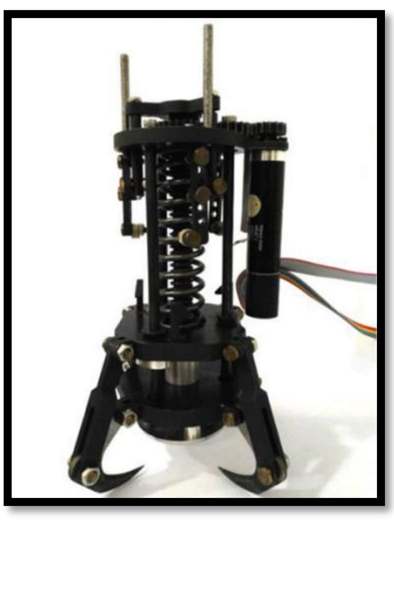

Figure 37: Prototype of the space debris removal gripper [13]

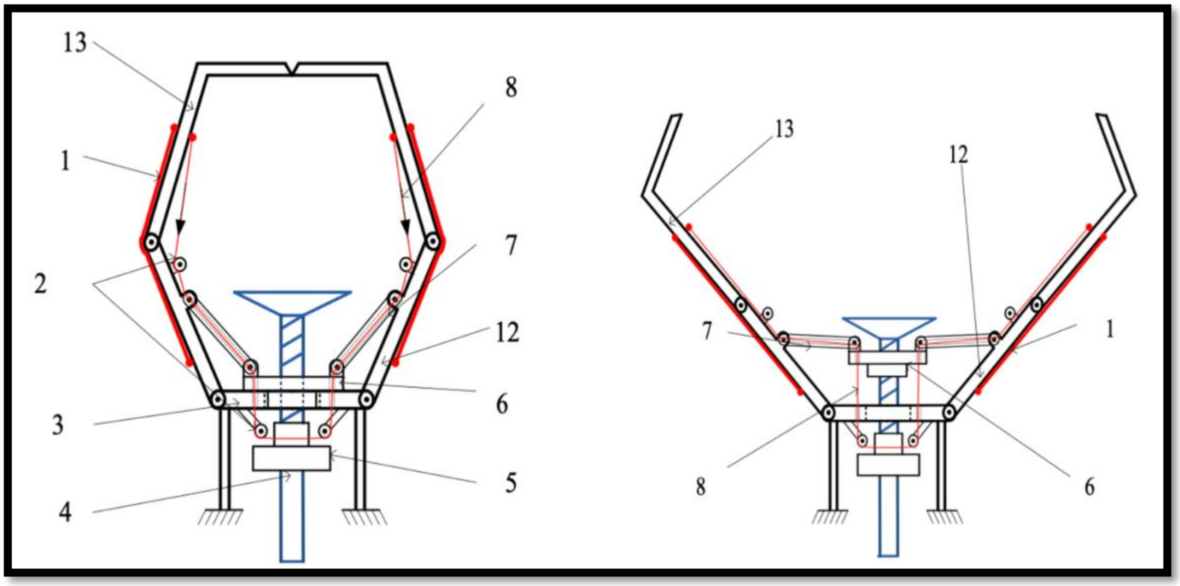

Figure 38: Closed (left) and Open (Right) state of the cable-driven mechanical gripper.

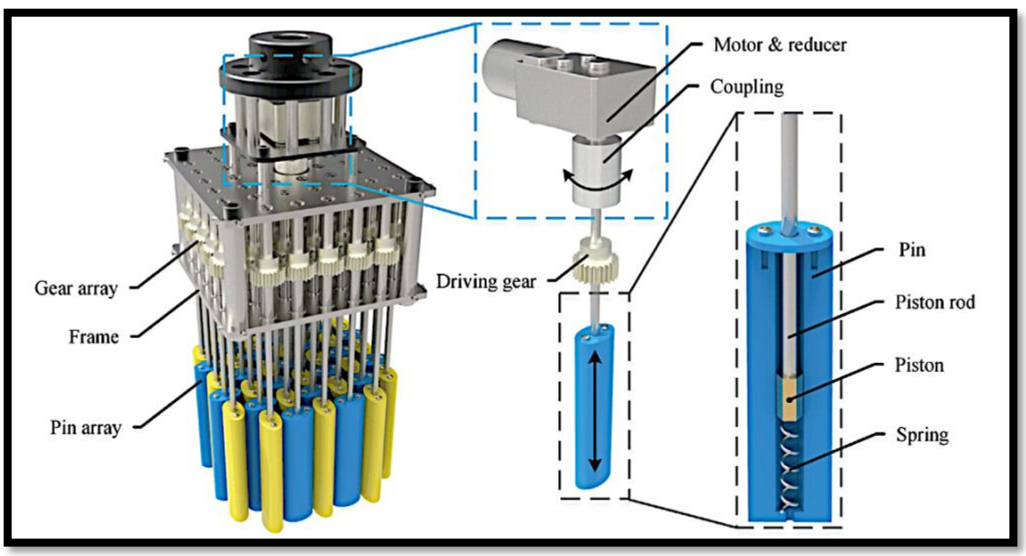

Figure 39: Meshed pin array gripper mechanism [15]

Figure 40: Grasp experiment on different objects [15]

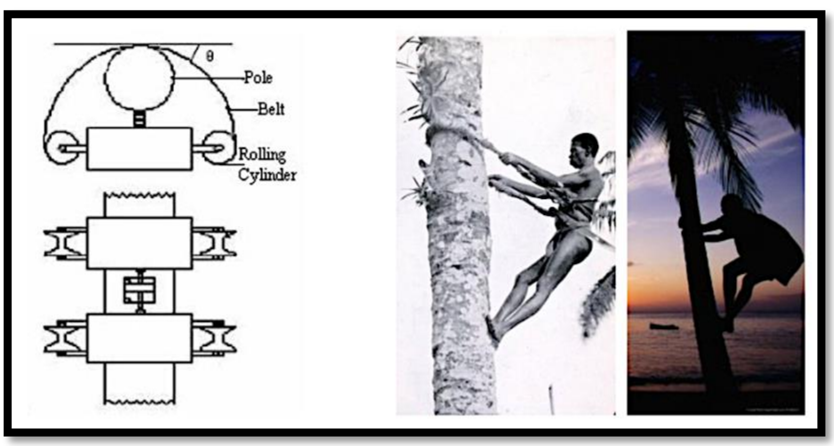

Figure 41: Gripper design (left), and inspiration from pole climbing technique (right) [1]

Appendix H: Figures of Kinematic Background

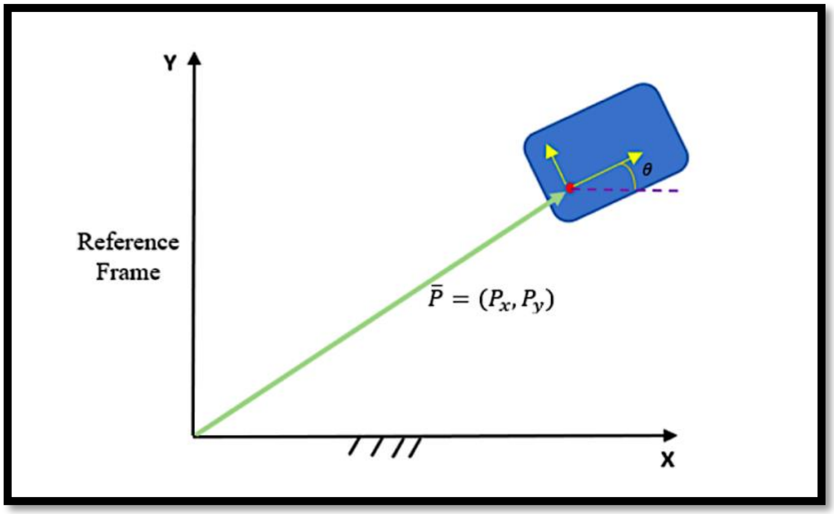

Figure 7: Rigid body in the reference frame

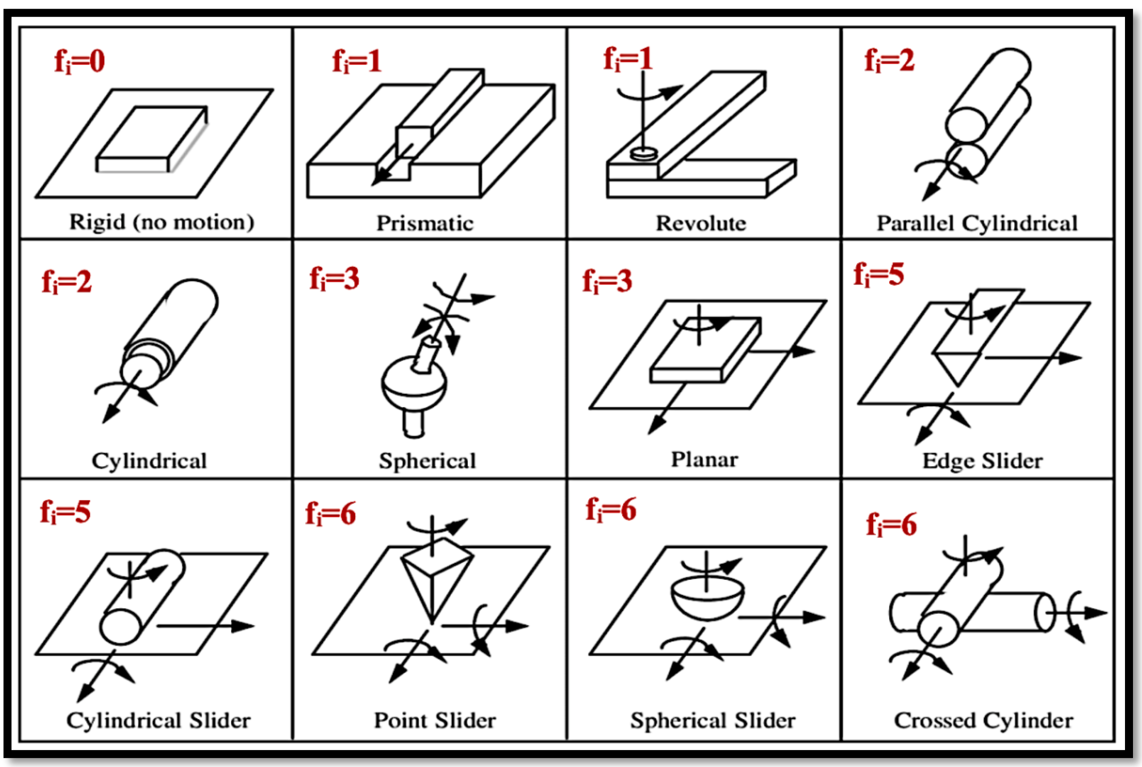

Figure 8: Joints and their Degrees of freedoms

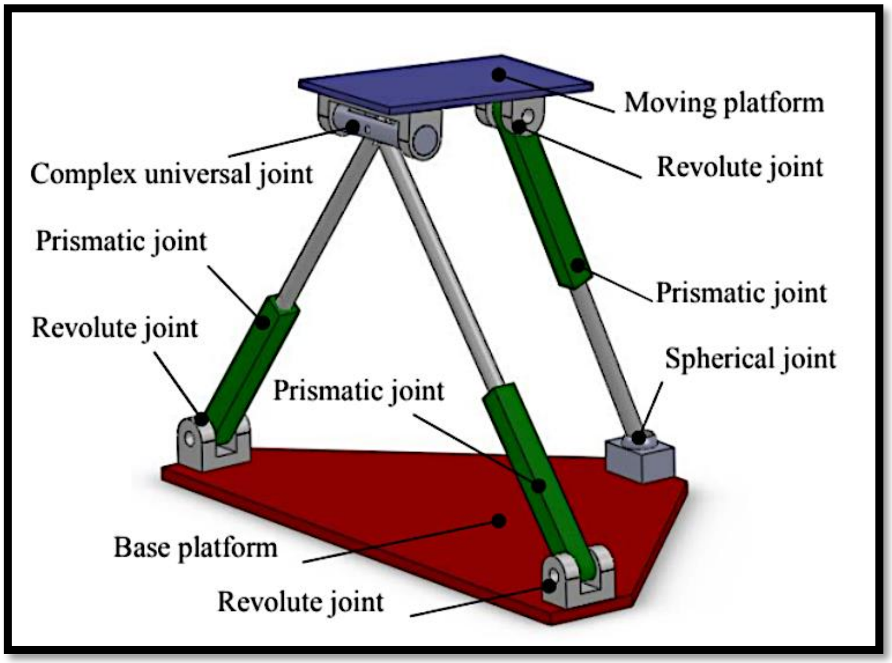

Figure 9: 3-DOF SPM 2-RPU&SPR over-constrained mechanism [27]

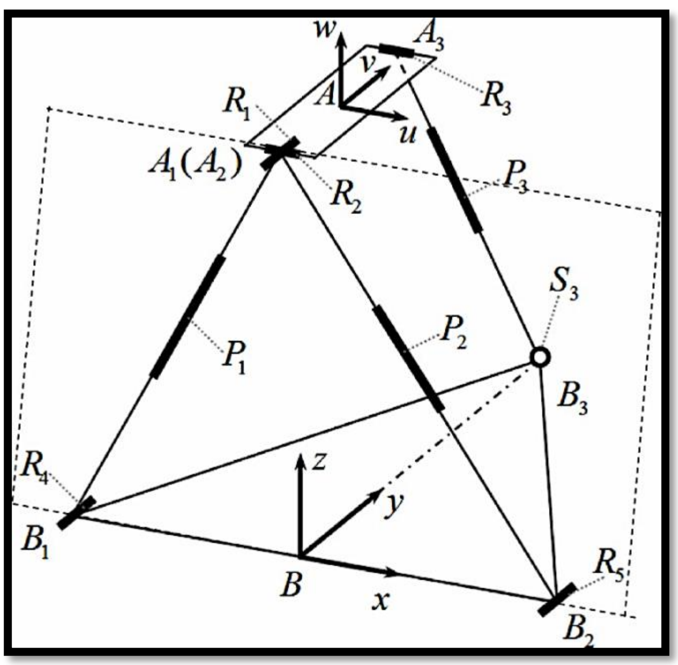

Figure 10: Kinematic sketch of 3-DOF SPM 2-RPU&SPR over-constrained mechanism [27]

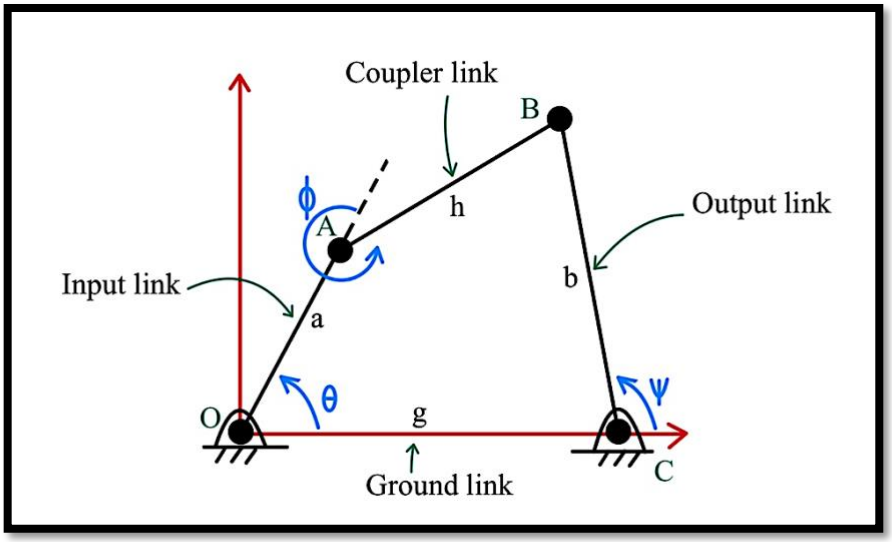

Figure 11: Conventional 4-bar linkage

Appendix I: Figures from novel grasping mechanism design

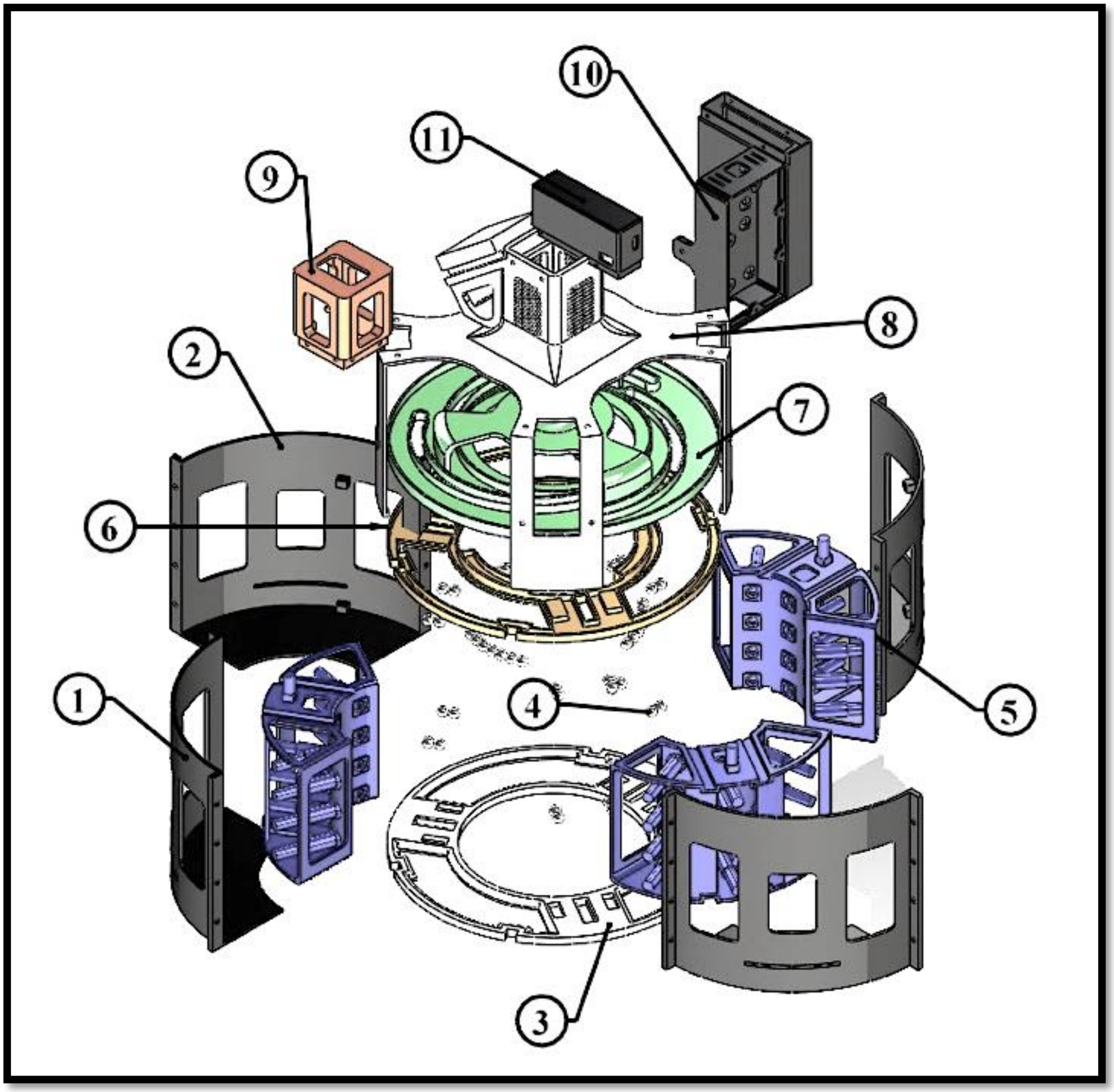

Figure 12: Exploded view of the assembly with part number

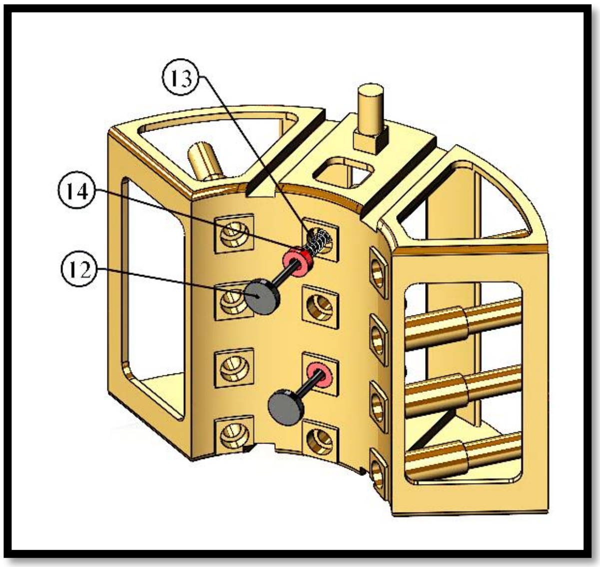

Figure 13: Shutter CAD model referencing TABLE I.

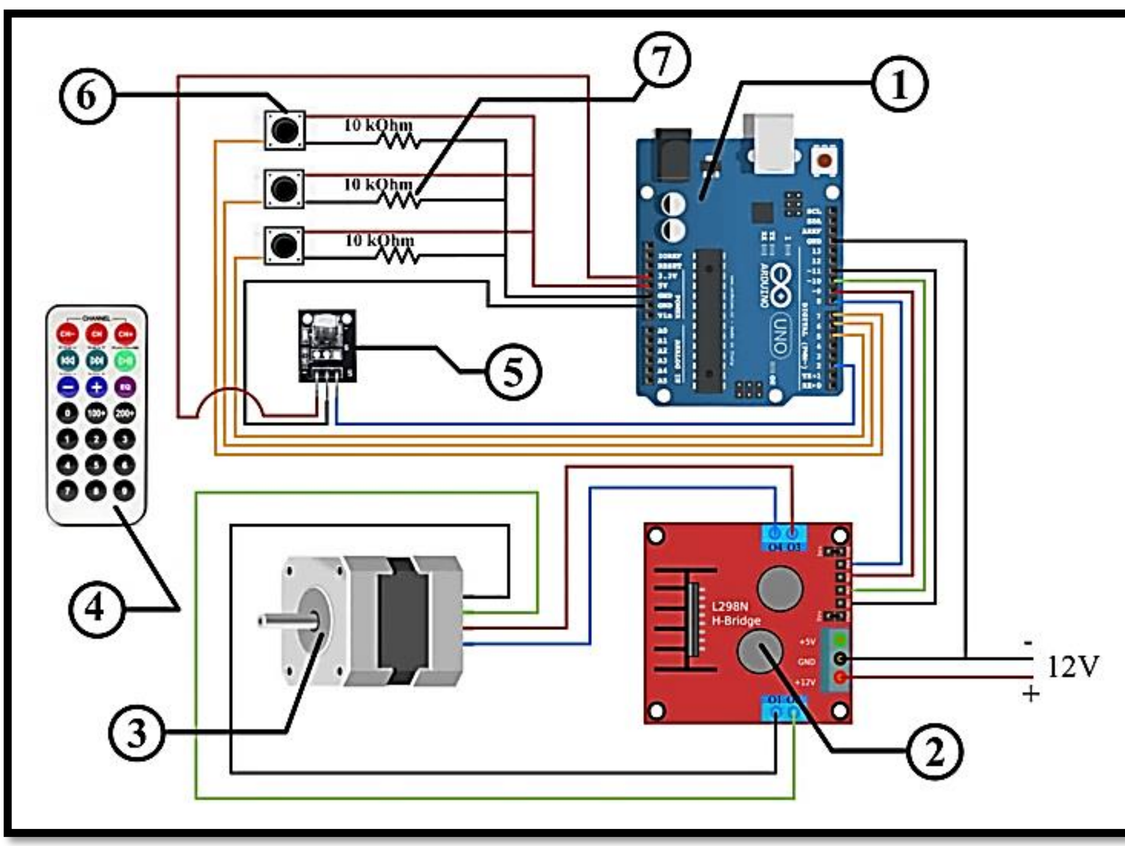

Figure 14: Electric circuit diagram [32][33][34][35]

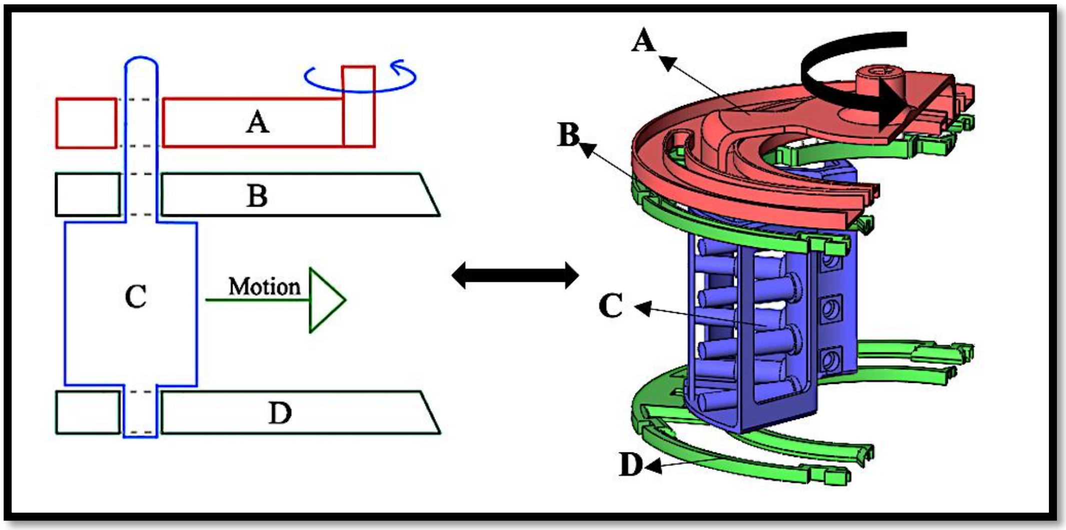

Figure 15: General study of motion (side views)

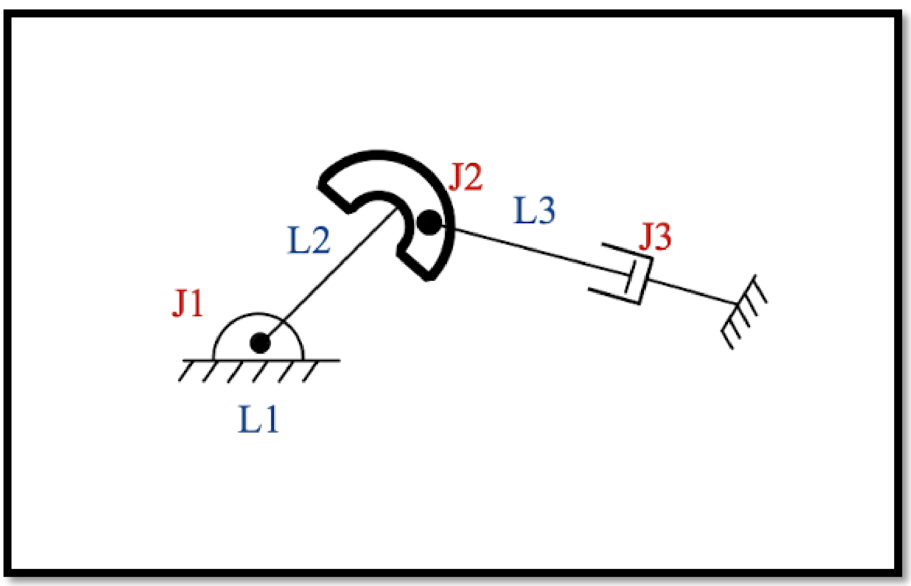

Figure 16: Kinematic sketch of the mechanism.

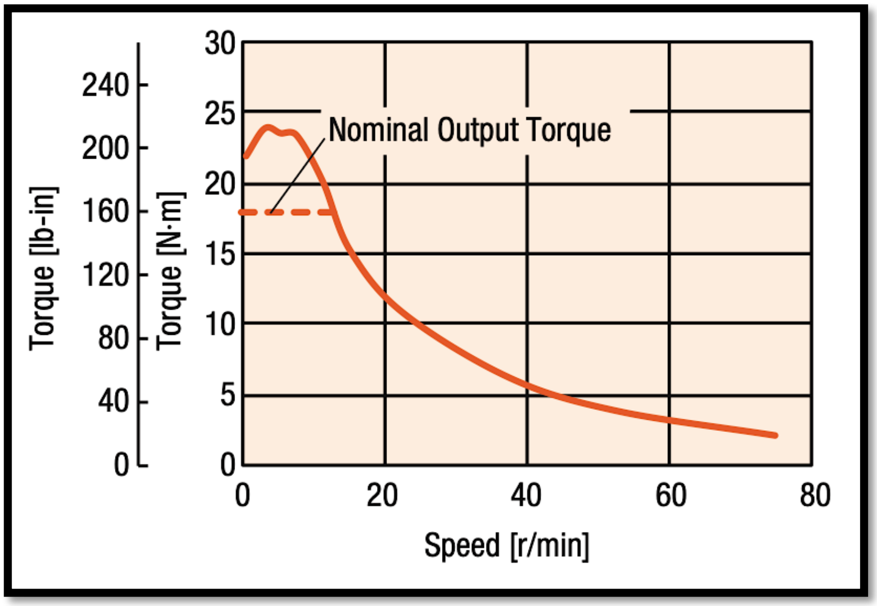

Figure 17: Speed (rpm) vs Torque (N-mm) chart for the motor [29].

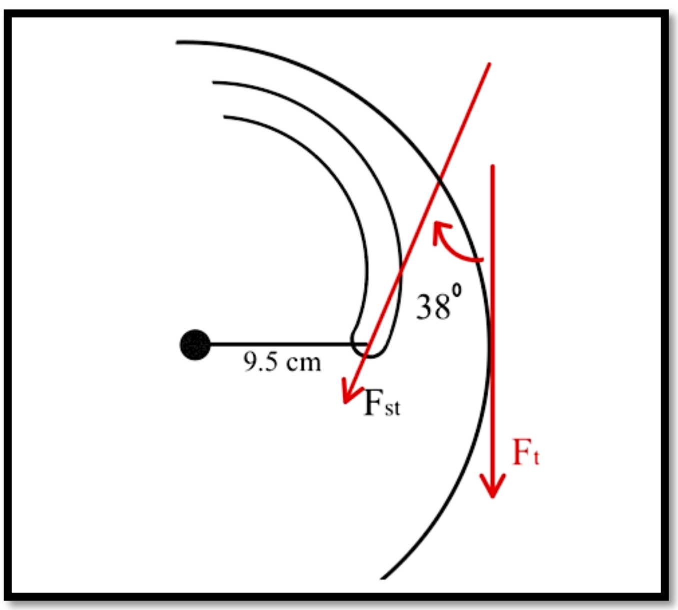

Figure 18: Tangential angle between curve path and motor rotation path.

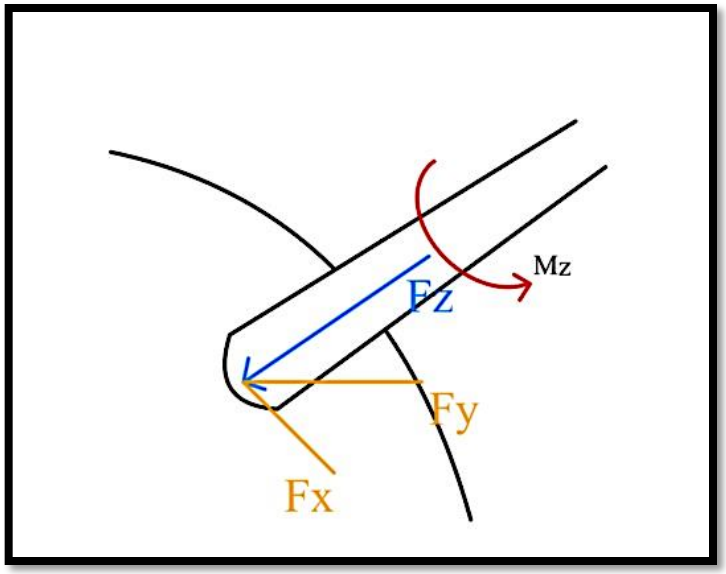

Figure 19: Soft finger & forces related.

Appendix J: Stress and motion study results' figure for mechanism parts

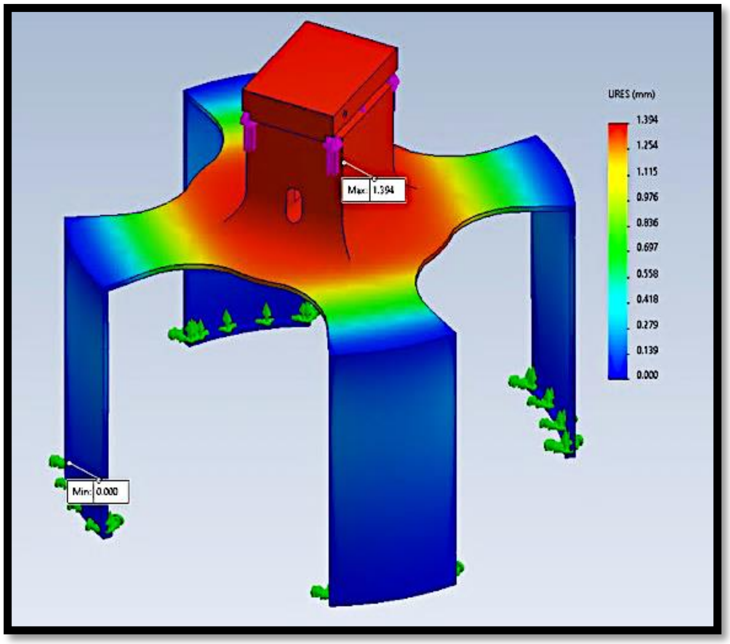

Figure 20: FEA static analysis of the part TOP.

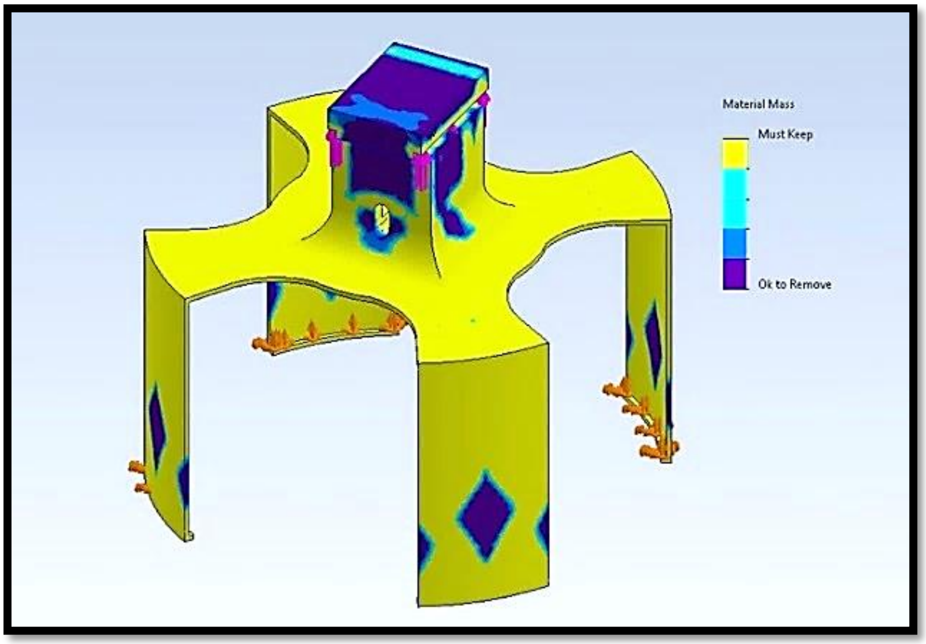

Figure 21: Topology study of the part TOP.

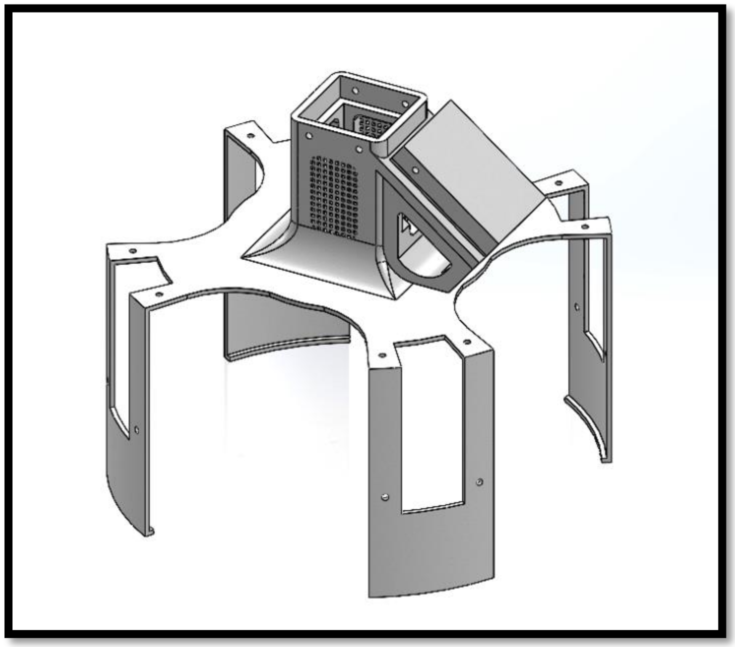

Figure 22: Improved TOP considering analytical studies.

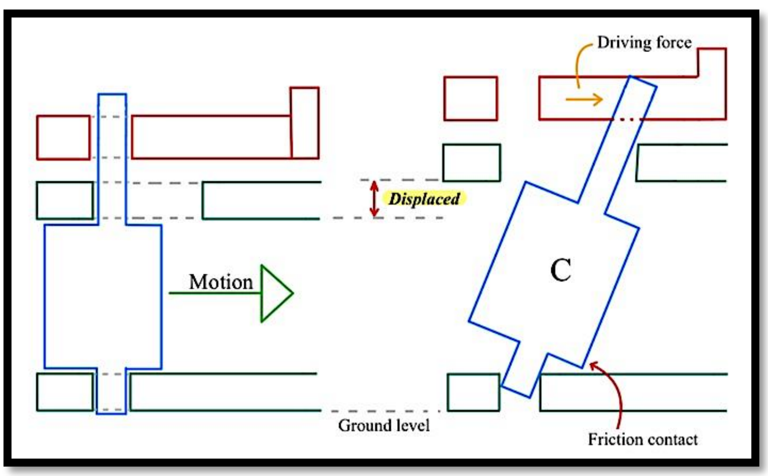

Figure 23: Visual representation of the motion study for non-constrained vertical motion of the curved plate.

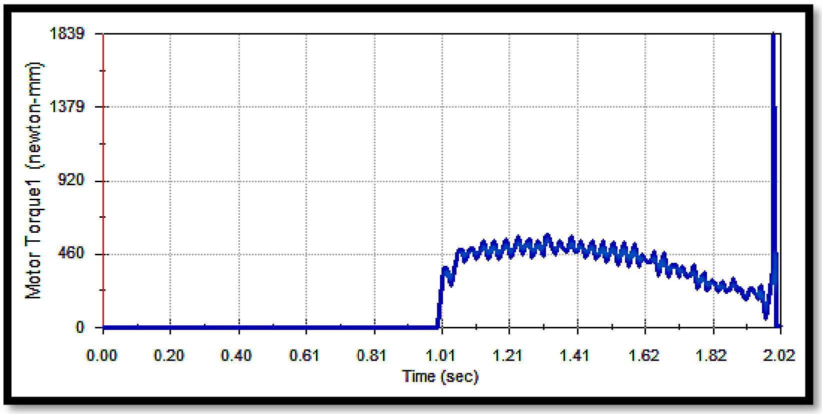

Figure 24: Motion study results for the torque required to actuate the system.

Appendix K: Figures from Smart shelf design process

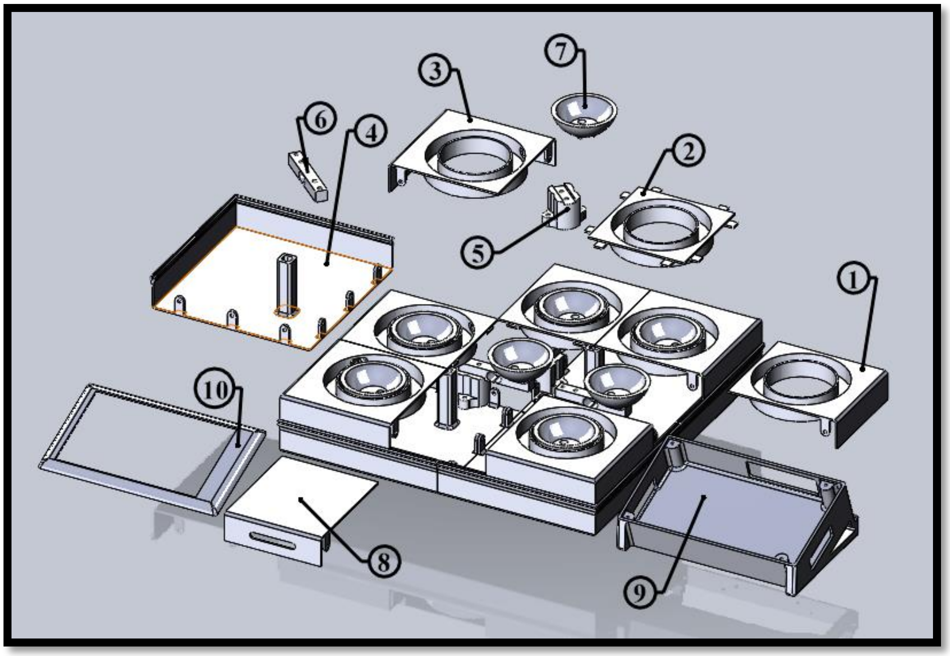

Figure 25: Parts assembly (Exploded view)

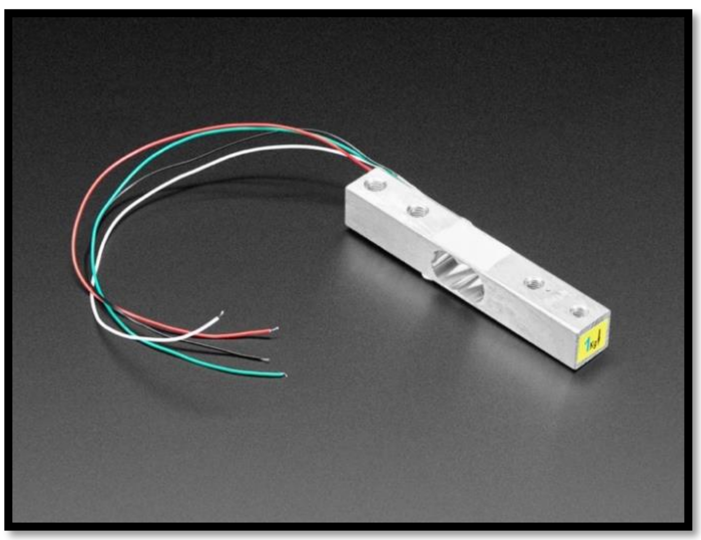

Figure 26: Load cell [38]

Appendix L: Figures from Smart shelf design process

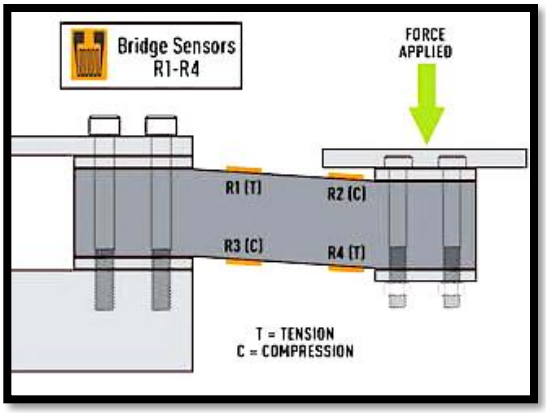

Figure 27: Strain gauge load cell setup [39]

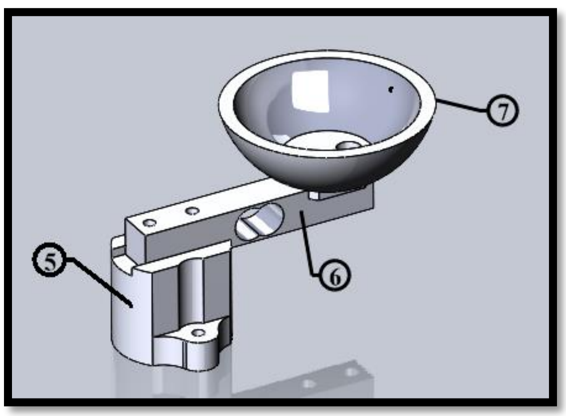

Figure 28: Actual load cell setup

Figure 29: HX711 Amplifier [40]

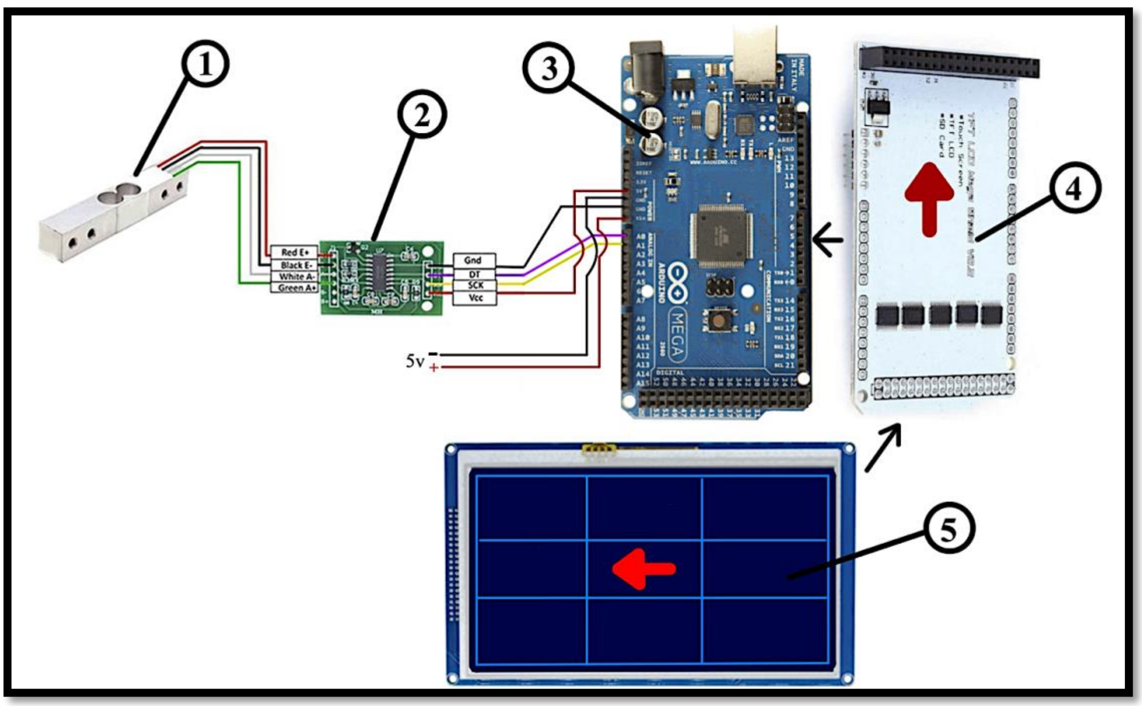

Figure 30: Electrical circuit diagram (only one of the load cells (#1) is shown instead of eight in total) [41][42]

Figure 31: Home screen of the touchscreen interface

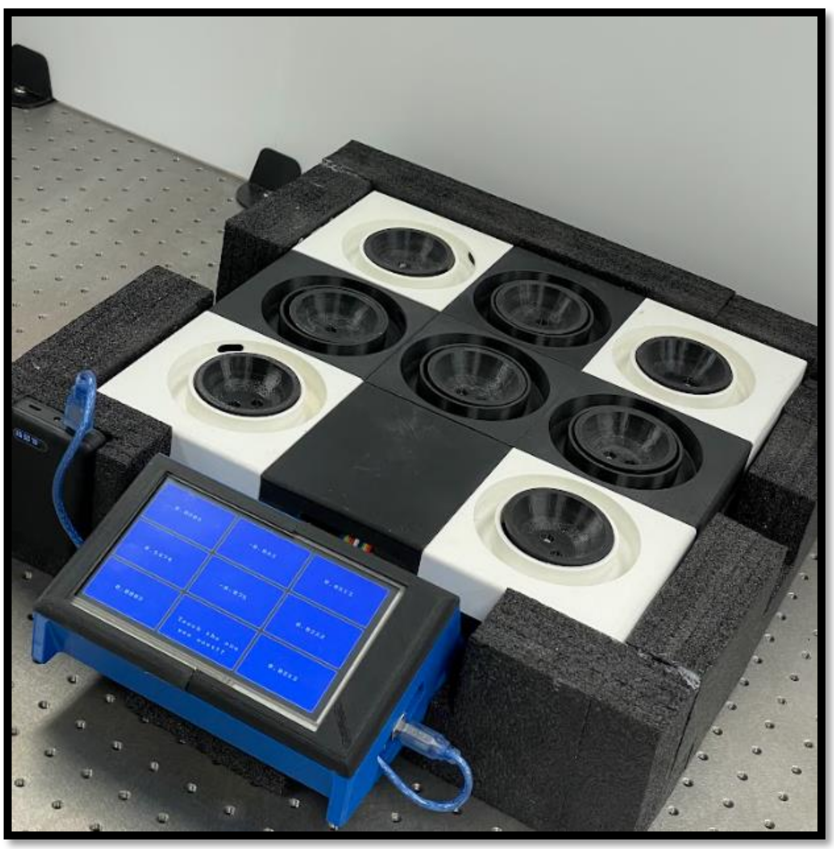

Figure 32: Prototype of the smart shelf

Appendix M: CAD and real-life figures of the prototype

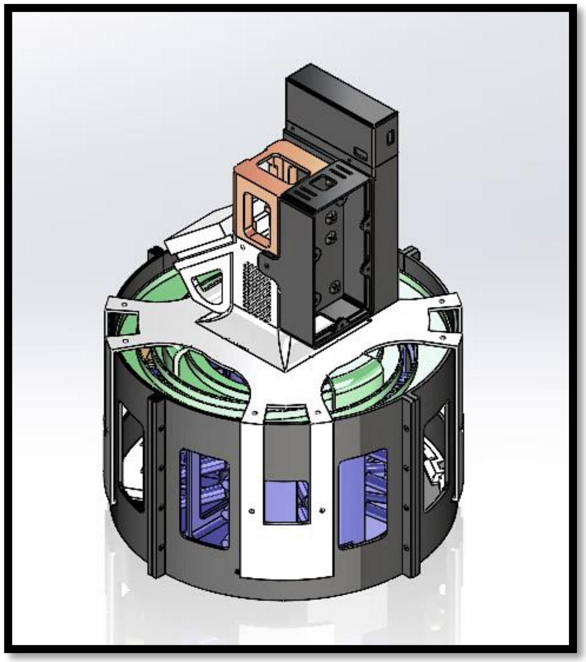

Figure 33: Whole design assembly (Excluding electronics and actuation system).

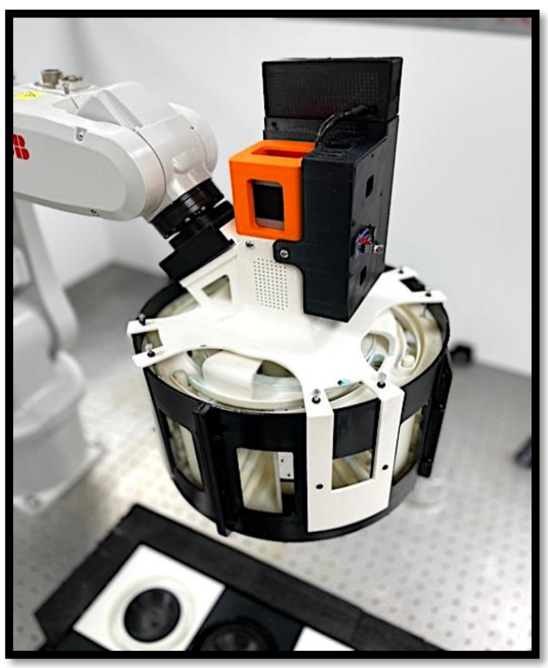

Figure 34: Actual prototype attached to the robotic arm.

Appendix N: Figures from robotic path planning for task execution

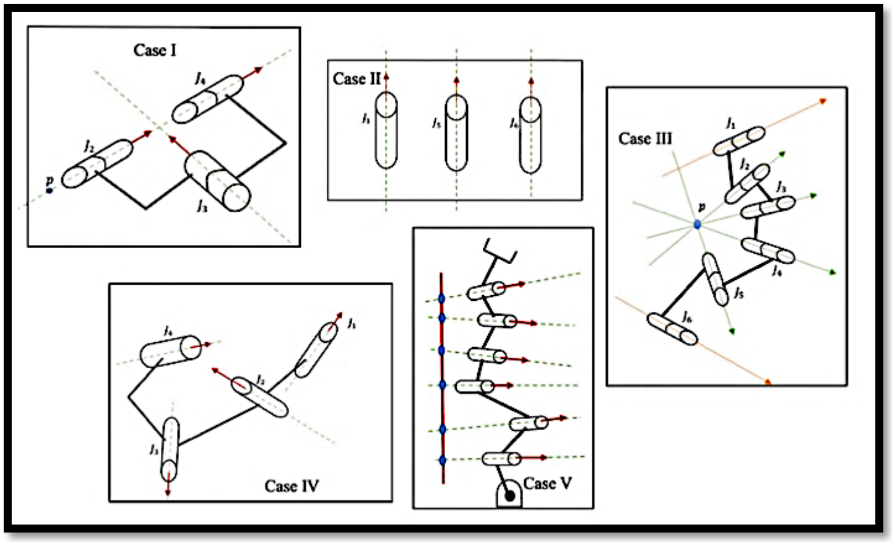

Figure 35: Five cases of singularity for a serial 6-DOF robotic manipulator

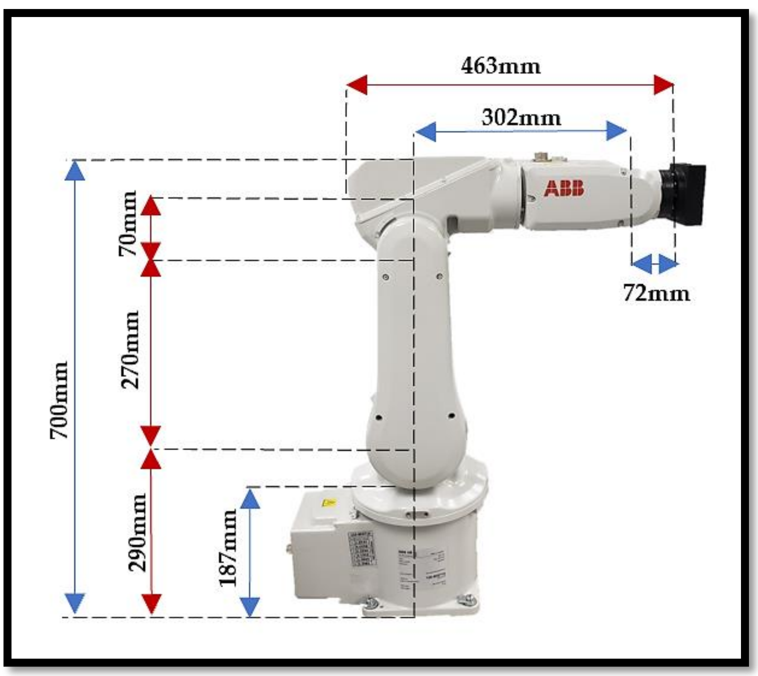

Figure 36: Robotic-arm joint and links breakdown for D-H parameter.

(a) **(b)** **(c)**

Figure 37: Grasping (a) a tomato, (b) a guava, and (c) a hand-sanitizer bottle (all bottom view of the gripper)

Appendix O: Figure of working smart shelf.

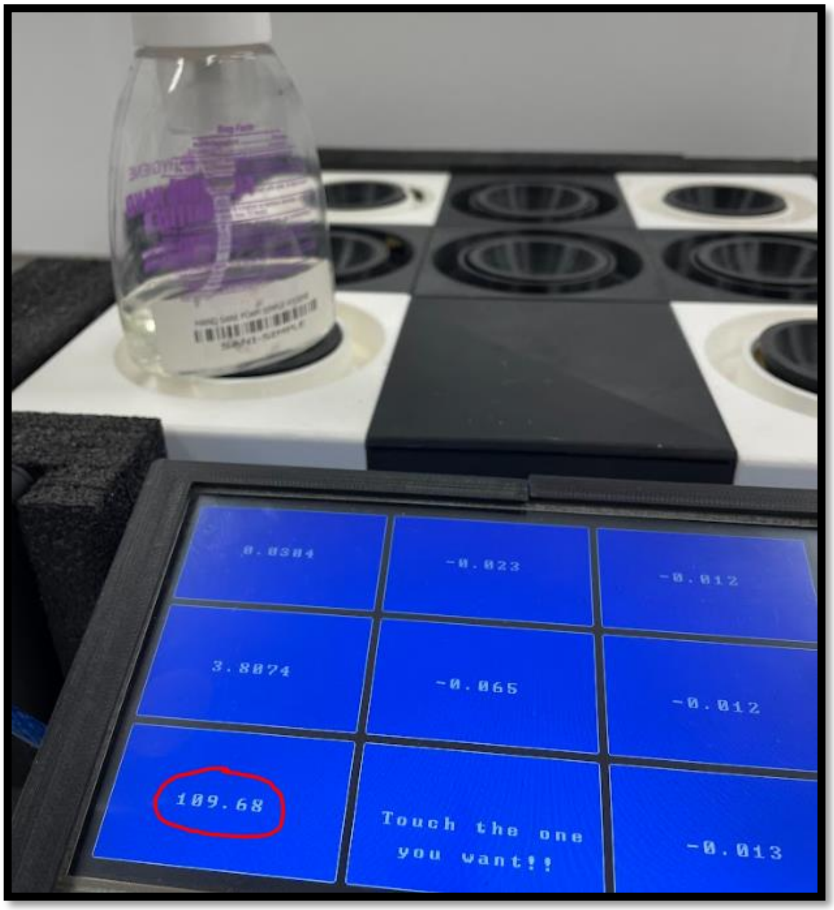

Figure 38: Smart shelf displaying the weight of the hand sanitizer bottle.

Appendix P: Tables from design process

TABLE 1: Designed Parts with Dimensions and Part Numbers (O = outer, R = radius, T = Thickness, H = Heigh

Part	Dimension (cm)	Part No.
Outer Shell A	H = 14.7, OR = 14.3, T = 0.3	1
Outer Shell B	H = 14.7, R = 14.3 T = 0.3	2
Rectangular Slot Plate (Bottom)	OR= 13.9, IR = 8, T = 0.75	3
Bearing Ball	D = 1	4
Shutter	OR = 11, IR= 5, H = 15.25	5
Rectangular Slot Plate (Top)	OR= 13.9, IR = 6.8, T = 0.75	6
Curvilinear Slot Plate	OR= 13.9, IR = 6.8, H = 5.4	7
Top	OR = 14.8, H = 24.6	8
Top cover	6.3 x 6.3 x 7.8	9
Electronics Box	10.2 x 10.275 x 14.7	10
Wire Cap	10.2 x 3.075 x 5.19	11
Piston	R = 0.15, H = 6	12
Spring	R = 0.5, T = 0.05, H = 2.5	13
Piston Blocker	OR = 0.6, IR = 0.25, H = 0.4	14

TABLE 2: Material Properties Comparison

Properties	Aluminum Alloy 6061	ABS
Yield Strength	276 MPa	29.6 MPa
Ultimate Tensile Strength	310 MPa	40 MPa
Elastic Modulus	69000 MPa	2000 MPa
Poisson’s Ratio	0.33	0.394
Mass Density	2700 kg/m3	1020 kg/m3
Shear Modulus	26000 MPa	318.9 MPa

TABLE 3: Electrical Components

Electrical components	Quantity	Component No.
Arduino Uno R3	1	1
L298N Motor Driver Module	1	2
PKP Series 2-Phase Stepper Motor	1	3
Remote Control Module	1	4
HX1838 VS1838 NEC IR Receiver	1	5
6mm x 6mm x 5mm Tactile Push Button	3	6
10 kΩ Resistor	3	7

TABLE 4: Parts, Dimensions, Part Numbers, and Quantities.

Parts	Dimensions (cm)	Part Number	Quantity
Middle Top	12 x 12 x 2.9	1	3
Center Top	12 x 12 x 2.9	2	1
Corner Top	12 x 12 x 2.9	3	4
Base	18 x 18 x 2.9	4	4
Load Cell Stand	1.85 x 4.65 x 3.26	5	8
Load Cells	8 x 1.27 x 1.27	6	8
Object Platform	6.68 x 6.68 x 2.72	7	8
Closed Top	12 x 12 x 2.9	8	1
Screen Base	20.4 x 13.9 x 8	9	1
Screen Cover	20.4 x 11.78 x 1	10	1

TABLE 5 Electronics, their Quantities, and Sources

Component	Quantity	Component No.
1 Kg Strain Gauge Load Cell	8	1
HX711 Amplifier	8	2
Arduino Mega 2560 Rev3	1	3
TFT LCD Mega Shield V2.2	1	4
7” TFT LCD Screen 800x480	1	5

Appendix Q: Table of determinant calculation

TABLE 6: Determinant (Det.) & Rank of the Jacobian from MATLAB®

Joint Angle Orientation: q1, q2, q3, q4, q5, q6 in degrees	**Det.**	**Rank**
1.98, 3.10, -9.94, -3.12, 56.79, 6.58	-0.0196	6
-26.19, 20.20, -27.12, 17.75, 59.85, -26.26	-0.0198	6
-26.19, 18.38, 6.15, 30.32, 31.47, -43.63	-0.0152	6
-26.19, 22.05, 12.92, 42.40, 43.01, -57.16	-0.0186	6
-26.19, 19.09, 8.08, 32.67, 29.24, -46.35	-0.0143	6
-26.19, 18.49, -17.33, 19.31, 52.86, -29.06	-0.0118	6
15.60, 12.09, -8.52, 15.09, 48.65, 25.56	-0.0199	6
39.66, 35.63, -39.88, -28.25, 64.97, 48.83	-0.0144	6
39.66, 34.93, -6.41, -44.15, 38.01, 73.47	-0.0172	6
39.66, 38.77, -2.22, -52.66, 32.66, 83.87	-0.0159	6